

# Open ocean nutrient sampling in Faroese water 2013-2020

Tórshavn · March 2022



**H. Hátún**

**K. M. H. Larsen**

**S. Jacobsen**

**I. Salter**

**E. Gaard**

# Open ocean nutrient sampling in Faroese water 2013-2020

---

Hjálmar Hátún, Karin M.H. Larsen, Sólvá Jacobsen, Ian Salter and Eilif Gaard.

## 1 Contents

|          |   |           |
|----------|---|-----------|
| <b>2</b> | <b>INTRODUCTION.....</b>  | <b>4</b>  |
| <b>3</b> | <b>DATA MATERIAL.....</b>   | <b>9</b>  |
| 3.1      | Nutrient observations at FAMRI standard hydrographic stations. ....           | 9         |
| 3.2      | Coastal station Skopun.....   | 9         |
| 3.3      | The primary production index (PPI).....                                       | 9         |
| 3.4      | Observational campaigns in 1986 and 1995 .....                                | 9         |
| 3.5      | Nutrient observations south of Iceland and in the Faroe-Shetland Channel..... | 11        |
| <b>4</b> | <b>CONTEXT BASED ON PREVIOUS NUTRIENT OBSERVATIONS.....</b>                   | <b>11</b> |
| 4.1      | Open ocean nutrients and primary production on the Faroe shelf .....          | 12        |
| 4.2      | Nutrients in the open ocean and at coastal station Skopun.....                | 13        |
| 4.2.1    | Nutrient data quality.....  | 13        |
| 4.3      | A comprehensive nutrient section in June 1986 .....                           | 14        |
| 4.3.1    | Hydrography (Temperature and salinity).....                                   | 14        |
| 4.3.2    | Upper ocean nutrients .....   | 15        |
| 4.3.3    | Nutrients in the deeper layers .....  | 16        |
| 4.3.4    | MNAW nutrients .....  | 18        |
| 4.4      | Nutrient sections in 1995 .....   | 20        |
| 4.4.1    | Combined section V-N.....   | 22        |
| 4.4.2    | Combined section R-E .....  | 23        |
| <b>5</b> | <b>REGULAR OPEN OCEAN NUTRIENT SAMPLING STARTING IN 2013.....</b>             | <b>24</b> |
| 5.1      | Nutrient sampling and analysis .....  | 24        |
| 5.1.1    | Sampling and preservation .....   | 24        |
| 5.1.2    | Nutrient analysis .....   | 24        |

|            |   |           |
|------------|---|-----------|
| 5.1.3      | Nutrient data comparability.....  | 25        |
| 5.1.4      | Error flagging.....   | 25        |
| <b>5.2</b> | <b>Data structure – in TS-space .....</b>   | <b>26</b> |
| 5.2.1      | TS-nutrients diagrams .....   | 26        |
| 5.2.2      | Nutrients vs. temperature plots.....  | 27        |
| <b>5.3</b> | <b>Oceanographic overview and nutrient data – during three seasons .....</b>        | <b>28</b> |
| 5.3.1      | Stations N04 and N05 – the Faroe Current (FC).....                                  | 28        |
| 5.3.2      | Stations N13 and N14 – north of the Iceland-Faroe Front (IFF).....                  | 31        |
| 5.3.3      | Station V06 – the Faroe Bank Channel (FBC) .....                                    | 31        |
| 5.3.4      | Station R08 – the Iceland Faroe ridge (IFR).....                                    | 33        |
| 5.3.5      | Station S08 – the southern Faroe-Shetland Channel (FSC) .....                       | 34        |
| <b>5.4</b> | <b>Pre-bloom nutrient content in MNAW .....</b>                                     | <b>35</b> |
| 5.4.1      | Seasonal silicate statistics .....  | 36        |
| 5.4.2      | Interannual variability .....   | 36        |
| 5.4.3      | Nitrate and phosphate .....   | 39        |
| 5.4.4      | Comparison with previous $S_{AW}$ and $N_{AW}$ estimates .....                      | 40        |
| 5.4.5      | Conclusions and suggestions regarding the monitoring of $S_{AW}$ and $N_{AW}$ ..... | 41        |
| <b>5.5</b> | <b>Seasonal nutrient drawdown .....</b>   | <b>41</b> |
| 5.5.1      | Silicate .....  | 42        |
| 5.5.2      | Nitrate .....   | 44        |
| 5.5.3      | Pre- and post-bloom nutrient concentrations and the PPI .....                       | 44        |
| 5.5.4      | Conclusion and suggestions regarding drawdown.....                                  | 45        |
| <b>5.6</b> | <b>Nutrients at depth.....</b>  | <b>46</b> |
| 5.6.1      | Conclusions and recommendations regarding deep nutrients .....                      | 48        |
| <b>5.7</b> | <b>Comparison of preservation treatments .....</b>                                  | <b>48</b> |
| <b>6</b>   | <b>DISCUSSION .....</b>   | <b>49</b> |
| <b>6.1</b> | <b>Recommendations .....</b>  | <b>53</b> |
| <b>7</b>   | <b>ACKNOWLEDGEMENTS.....</b>  | <b>53</b> |
| <b>8</b>   | <b>REFERENCES.....</b>  | <b>54</b> |
| <b>9</b>   | <b>APPENDIX FIGURES .....</b>   | <b>59</b> |
| <b>9.1</b> | <b>Setion R-S.....</b>  | <b>69</b> |

## List of figures

|   |    |
|---|----|
| Figure 1 Overview over the study region.....  | 5  |
| Figure 2 Distribution of the main water masses at Section N .....                                   | 8  |
| Figure 3 Open ocean pre-bloom nutrients and primary production of the Faroe shelf.....              | 12 |
| Figure 4 Open ocean pre-bloom nutrients and nutrients at coastal station Skopun. ....               | 13 |
| Figure 5 Hydrography approximately along Section N during June 1986 (MH86). ....                    | 15 |
| Figure 6 Upper nutrient and oxygen concentrations along Section N during June 1986 (MH86).....      | 16 |
| Figure 7 Deep layer nutrient and oxygen concentrations along Section N, June 1986 (MH86).....       | 17 |
| Figure 8 Latitudinal silicate profiles at depths between 400 m and 900 m.....                       | 18 |
| Figure 9 Nutrient profiles along Section N (from MH86).....   | 19 |
| Figure 10 Upper layer nutrients and temperature along Section N in June 1986 (MH86).....            | 20 |
| Figure 11 Combined section V-N during late May, 1995. ....  | 21 |
| Figure 12 Section N during 1-2 September, 1995.....   | 21 |
| Figure 13 Section R-E during May 1995 .....   | 23 |
| Figure 14 Temperature-Salinity (T-S) diagrams, with nutrients (2013-2020).....                      | 26 |
| Figure 15 Nutrient concentrations vs. temperature scatter plots (2013-2020) .....                   | 27 |
| Figure 16 Combined section V-N, February average (2013-2018).....                                   | 29 |
| Figure 17 Combined section V-N, May/June average (2013-2018). ....                                  | 30 |
| Figure 18 Combined section V-N, Aug/Sept average (2013-2018). ....                                  | 30 |
| Figure 19 Combined section R-S, February average (2013-2018). ....                                  | 32 |
| Figure 20 Combined section R-S, May/June average (2013-2018).....                                   | 32 |
| Figure 21 Combined section R-S, Aug/Sept average (2013-2018).....                                   | 34 |
| Figure 22 Individual profiles from standard station N05 during the years 2013-2020. ....            | 35 |
| Figure 23 Boxplots for silicate samples taken at station N05.....                                   | 37 |
| Figure 24 Estimates of the pre-bloom silicate content in Atlantic water ( $S_{AW}$ ). ....          | 38 |
| Figure 25 Pre-bloom nitrate (upper) and phosphate (lower) ( $N_{AW}$ and $P_{AW}$ ).....            | 40 |
| Figure 26 Sketch of nutrient drawdown parameters .....  | 42 |
| Figure 27 Averaged silicate drawdown parameters. ....   | 43 |
| Figure 28 Open ocean silicate and the primary production index for the Faroe shelf (PPI, red). .... | 45 |
| Figure 29 A principal nutrient signal at depth .....  | 47 |

## List of Tables

|   |    |
|---|----|
| Table 1 List of acronyms, arranged alphabetically.....  | 6  |
| Table 2 Hydrographic characteristics of water masses discussed in this report. ....   | 8  |
| Table 3 Error flagged data.....   | 25 |
| Table 4 Average (2013-2020) Atlantic water ( $6.5^{\circ}\text{C} < T < 9^{\circ}\text{C}$ ) silicate concentrations for each season and at each standard station. .... | 36 |
| Table 5 Average silicate drawdown .....   | 43 |
| Table 6 Average nitrate drawdown .....  | 44 |
| Table 7 Location from where deep nutrient records are available. ....   | 46 |

## 2 Introduction

The subpolar North Atlantic is characterized by intense spring blooms (Longhurst, 2007; Mahadevan et al., 2012). These generally ensue after positive air-sea heat fluxes stratify the near-surface layer around April-May, although several other hypotheses for the bloom initiation have been proposed (Chiswell et al., 2015 – and references therein). The spring blooms consist primarily of diatoms, which are fast-growing algae that, in addition to phosphate and nitrate, require silicate to sustain their growth (Allen et al., 2005; Henson et al., 2006a). Macronutrients are quickly drawn out of the shallow summer mixed layer, and in the North Atlantic, silicate typically becomes the limiting nutrient for diatom growth (Allen et al., 2005; Egge and Aksnes, 1992) - occasionally confounded by seasonal iron limitation (Nielsdottir et al., 2009). Although nutrient limitation of primary production at lower latitudes is ‘textbook knowledge’ (Lalli and Parsons, 1993), the oceanographic community has often overlooked the likely importance of this fundamental ecosystem driver in boreal/subarctic parts of the North Atlantic Ocean.

It is now well established that pre-bloom nutrient concentrations in the open ocean north-eastern (NE) Atlantic and in the waters along the European slope, impact nutrient onwelling to the European shelf, which in turn fuels primary production in a large part of the North Sea (Groeger et al., 2013; Holt et al., 2012; Pätsch and Kühn, 2008; Steinacher et al., 2010). Furthermore, one of the ‘virtually certain’ model projections in the IPCC climate reports is that global warming will lead to reduced winter convection and thus reduced upwelling of nutrients (Pörtner et al., 2019). Particularly pronounced nutrient upwelling is expected in the NE Atlantic (Steinacher et al., 2010), and because of this the total primary production in the North Sea is projected to decline by up to 50% during the next century (Groeger et al., 2013). In order to monitor such possible and critical changes, the Faroe Marine Research Institute (FAMRI) initiated an open ocean nutrient sampling program in 2013. The present report is the first thorough presentation of the obtained data.

Similar monitoring was started earlier in neighbouring waters. Rey (2012) demonstrated declined silicate concentrations in Atlantic water (AW, abbreviations are summarized in Table 1 and water mass properties are presented in Table 2) along the Norwegian slope during period 1990 to 2010, and linked this trend to a declined size and circulation strength of the subpolar gyre (SPG). Under project SPACE (SubPolar Atlantic - Climate and Ecosystem), nutrient data from the Rockall region – which previously were only available in fragmentary form in the British Oceanographic Data Center (BODC) – were compiled and structured by Toby Sherwin. Based on these data, Johnson et al. (2013) reported declining nutrient concentrations (especially nitrate and phosphate) in the Rockall Trough, and, like Rey (2012), ascribed this to the weakening SPG. On a broader scale, Hátún et al. (2017a) compiled silicate data from the Labrador Sea, the northern Irminger Sea, the Iceland Basin, the Faroe shelf, the southern Bay of Biscay, the Porcupine Abyssal Plain and updated data along the Norwegian slope, and analyzed these data together with output from the marine biogeochemistry model HAMOCC (Hamburg Ocean Carbon Cycle Model) (Marsland et al., 2003). This study revealed a broad silicate decline from the Labrador Sea in west towards the Barents Sea opening in the north since 1990. Like Rey (2012) and Johnson et al. (2013), Hátún et al. (2017a) concluded that the trends were

linked to the dynamics of the SPG, and that the observed signal was introduced at the southern entrance to the Rockall Trough.

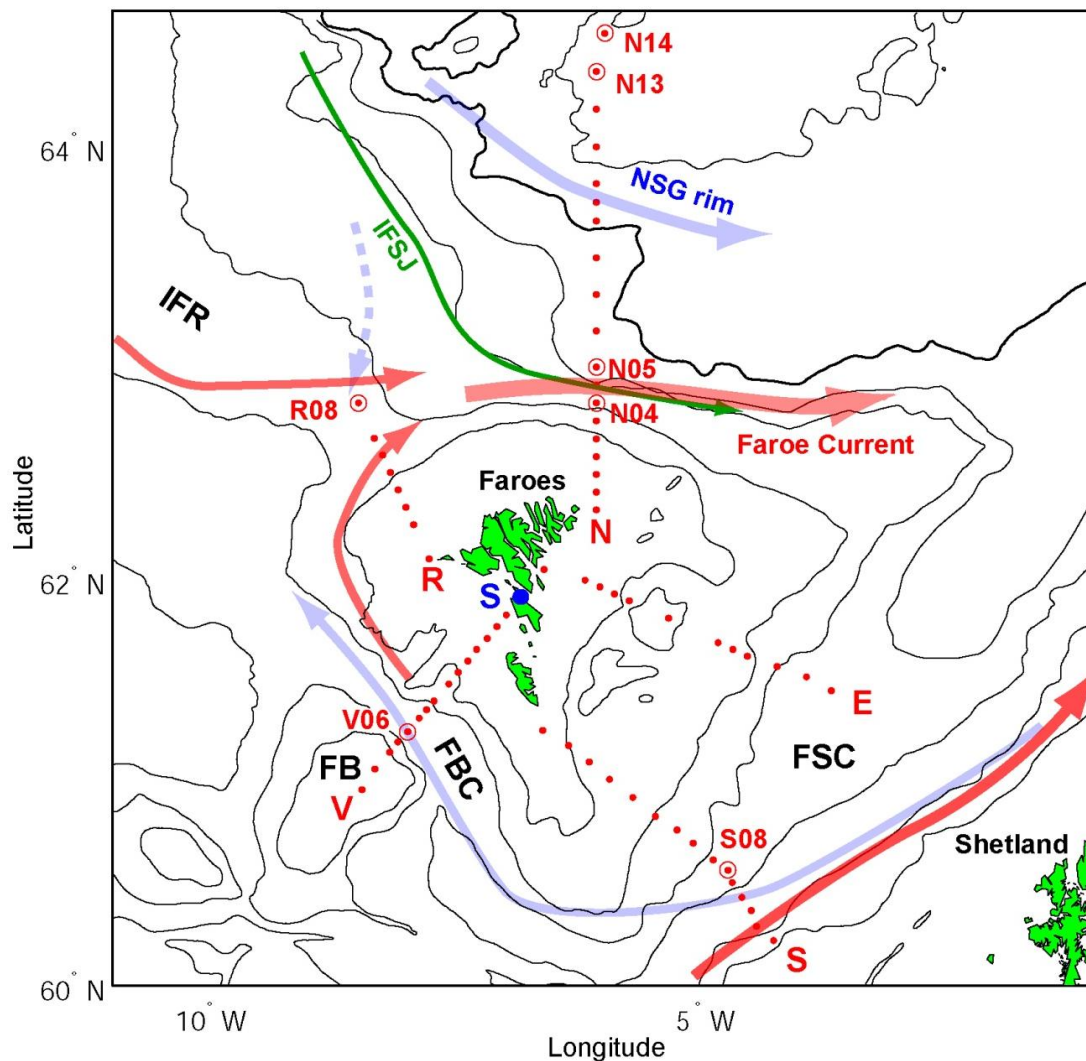


**Figure 1 Overview over the study region**

The hydrographic stations along standard section (N, R, V, S and E) are shown as red dots, with the standard nutrient stations (N04, N05, N13, N14, R08, V06 and S08) encircled. Red arrows show warm and saline Atlantic inflow current branches and blue arrows show deep cold/dense currents. The Iceland-Faroe Slope Jet (IFSJ, Semper et al., 2020) is shown as a narrow green arrow, the Norwegian Sea Gyre rim (NSG rim; Hátún et al., 2021a) is shown with a broader blue arrow and coastal station Skopun (S) is marked with a blue dot. The other abbreviations are written out in Table 1.

In addition to this trend Pätsch et al. (2020) emphasized strong interannual fluctuations in the nutrient concentration in the Faroe Shetland Channel (FSC), derived from data in a biogeochemical North Sea Climatology (NSBC,) (Hinrichs et al., 2017). This shorter term variability was linked both to the northward advection of SPG-induced hydrographic anomalies from the Rockall region, and to regional atmospheric forcing north of Shetland. Eliassen et al. (2017b) discussed inter-annual synchrony between spatio-temporal phytoplankton patterns (based on satellite Ocean Color data)

along the European continental shelf and around the Faroe shelf. The same authors furthermore discussed the importance of nutrient onwelling for the primary production on the Faroe shelf.

**Table 1 List of acronyms, arranged alphabetically**

| Acronym | Name  |
|---------|---|
| AW      | Atlantic Water                              |
| AMOC    | Atlantic Meridional Overturning Circulation |
| FBC     | Faroe Bank Channel                          |
| FC      | Faroe Current                               |
| Fl      | Fluorescence                                |
| FSC     | Faroe-Shetland Channel                      |
| HM86    | Håkon Mosby (cruise in 1986)                |
| IFF     | Iceland-Faroe Front                         |
| IFR     | Iceland-Faroe Ridge                         |
| IFSJ    | Iceland-Faroe Slope Jet                     |
| MEIW    | Modified East Icelandic Water               |
| MH86    | Magnus Heinason (cruise in 1986)            |
| MH95    | Magnus Heinason (cruises in 1995)           |
| MNAW    | Modified North Atlantic Water               |
| NEAW    | North East Atlantic Water                   |
| NNAW    | Norwegian North Atlantic Water              |
| NSAIW   | Norwegian Sea Arctic Intermediate Water     |
| NSDW    | Norwegian Sea Deep Water                    |
| NSG     | Norwegian Sea Gyre                          |
| PPI     | Primary Production Index                    |
| Si      | Silicate                                    |
| SPG     | Subpolar gyre                               |

Moving a step up the food web, Jacobsen et al. (2019) discussed concurrency between nutrient pulses southwest and southeast of Iceland, north of the Faroe slope (actually the first utilization of the data presented in the present report), and pronounced peaks in the total abundance of fish juveniles on the Faroe shelf. In the open ocean pelagic system, Pacariz et al. (2016) discussed the major post-2006 westward expansion of the mackerel stock in the context of the reported silicate decline. These authors concluded that increasingly severe oligotrophy along the eastern margin

increased the incentive/necessity of large pelagic fish stocks to seek western waters, which are richer in nutrients.

Such pieces of evidence for impacts of oceanographic processes on nutrient concentrations ecosystem processes in the NE Atlantic have recently been reviewed in a book chapter by Hátún et al. (2021b). This is a detailed story on how the variable SPG dynamics and variable winter convection activity regulate nutrient (primarily silicate) concentrations in the NE Atlantic, and how major anomalies are being advected polewards by the Atlantic inflows and impact adjacent shelves along the way. Recent studies highlight an additional impact of variable southeastward fluxes of nutrient and zooplankton rich East Icelandic Water into the southern Norwegian Sea, which at its approach towards northern slopes of the Faroe plateau becomes termed Modified East Atlantic Water (MEIW)(Read and Pollard, 1992; Kristiansen et al., 2019, 2016) (Skagseth et al., 2022). For these waters, it has also been argued that inclusion of nutrients as tracers for deep dense overflow waters - the Norwegian Sea Arctic Intermediate Water (NSAIW) and Norwegian Sea Deep Water (NSDW) - (in addition to the traditionally used temperature and salinity), is a pre-requisite for understanding the origins of these waters (Jeansson et al., 2017), which constituted the lower limb of the presently much discussed Atlantic Meridional Overturning Circulation (AMOC) (Chafik et al., 2020; Semper et al., 2020).

The water mass concept is based on the fact that large volumes of water in the oceans have similar characteristics (e.g. temperature and salinity), which do not change much over time. These water masses can therefore be identified by specific values of temperature and salinity and other 'tracers'. Five of the main water masses discussed in this report (MNAW, Norwegian North Atlantic Water [NNAW], MEIW, NSAIW and NSDW) are monitored along Section N, and illustrated in Figure 2 (reproduced from Hátún et al., 2021a). The hydrographic and nutrient/oxygen characteristics of these water masses, together with the warmer North Eastern Atlantic Water (NEAW) (Fogelquist et al., 2003) are summarized in Table 2. This table gives the impression of relatively well defined nutrient levels in the discussed water masses. Findings in the present report show, however, that the nutrient values change, both over time and spatially, especially near the deep currents jets – the Iceland-Faroe Slope Jet (IFSJ, Semper et al., 2020) and the Norwegian Sea Gyre (NSG) rim (Hátún et al., 2021a). The general view of rather quiescent deep waters with homogenous biogeochemical properties might therefore need revision.

The present report will therefore focus on silicate, although nitrate and phosphate will also be discussed. Four of the seven standard stations, from where nutrient samples are made, are part of Section N. Signal and processes along this section, which crosses the Faroe Current (FC) will therefore receive much attention. In addition to putting the present sampling in a larger context and to optimize the sampling, the aim of this report is also to evaluate the quality of the recent data.

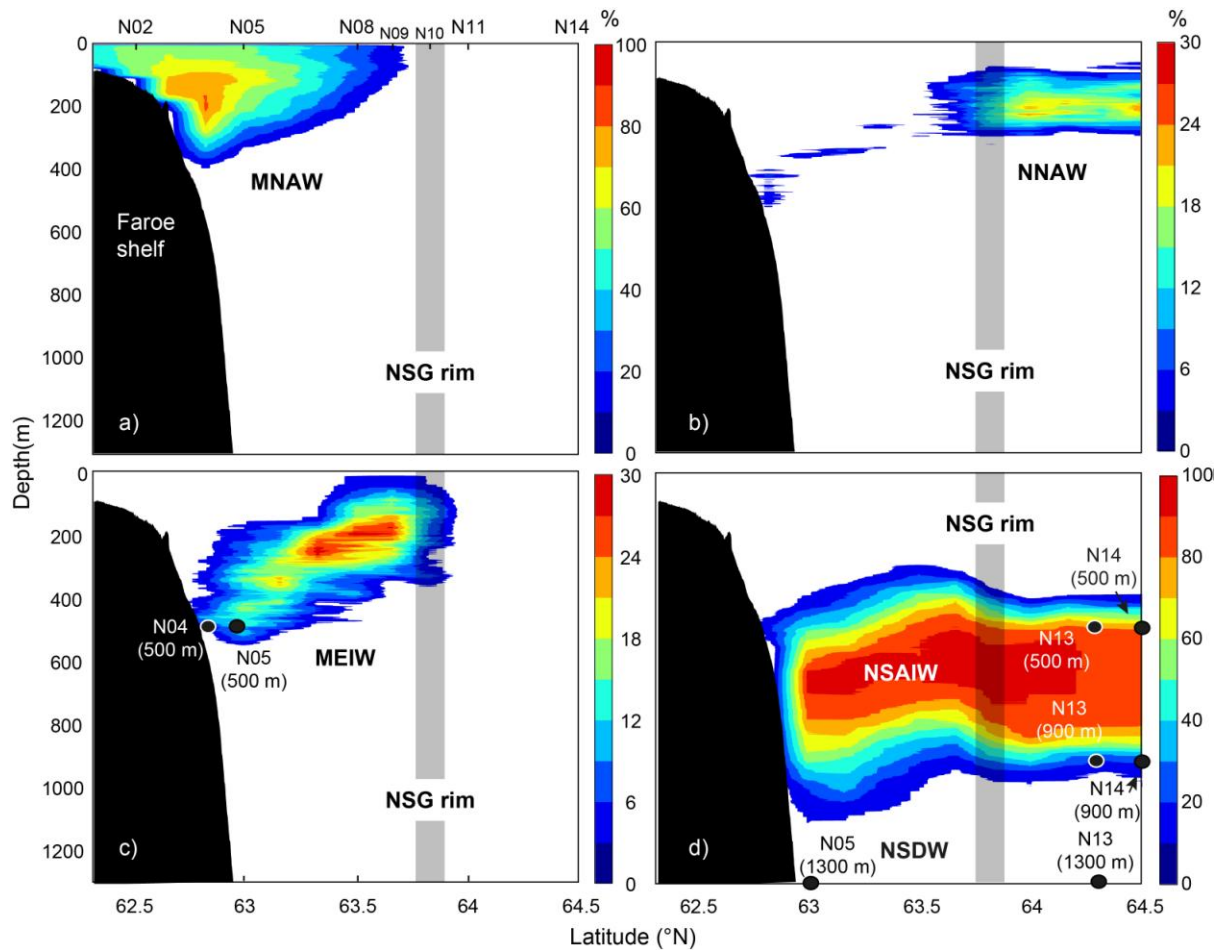


**Figure 2 Distribution of the main water masses at Section N**

Percentages of 103 complete transects between 1988 and 2019 that each latitude-depth data pixel meets the source water mass temperature and salinity criteria in Table 2). Water mass abbreviations are written in full in Table 1. The approximate location of the Norwegian Sea Gyre (NSG) rim is emphasized with grey bars, and the position of selected standard hydrographic stations are shown in panel (a). The positions of the deep nutrient records (see Section 5.6) are shown with black dots.

**Table 2 Hydrographic characteristics of water masses discussed in this report.**

These are taken from the literature; (a) Fogelqvist et al., 2003; (b) Glindø, 2018; (c) Hansen and Østerhus, 2000; (d) Jeansson et al., 2017; (e) Tanhua et al., 2005 and (f) Van Aken and Deboer, 1995.

| Water Mass | $\theta$  | S  | Si  | $\text{NO}_3$   | $\text{O}_2$   |
|------------|---|--|---|---|--|
|            | $^{\circ}\text{C}$  |  | $\mu\text{M}$   | $\mu\text{M}$   | $\mu\text{mol kg}^{-1}$  |
| NEAW       | 8-10 <sup>a</sup>   | ~35.3 <sup>a</sup>   | 3-6 <sup>a</sup> ,  | 12.5-13.5 <sup>a</sup>  | 265-270 <sup>a</sup>   |
| MNAW       | 7-8.5 <sup>c</sup> ; 8.35 <sup>b</sup>                            | 35.10-35.30 <sup>c</sup> ; 35.27 <sup>b</sup>                      | 5.4 <sup>b</sup> , 6.3 <sup>f</sup>   | 13.2 <sup>b</sup>   | 271 <sup>b</sup>   |
| NNAW       | 3.0   | 34.98  | -   | -   | -  |
| MEIW       | 1-3 <sup>a</sup> ; 1.78 <sup>b</sup>                              | 34.60-34.90 <sup>a</sup> ; 34.81 <sup>b</sup>                      | 6-7 <sup>a</sup> ; 6.5 <sup>b</sup>   | 13.1-13.6 <sup>a</sup> ; 13.1 <sup>b</sup>  | ~300 <sup>a</sup> ; 311 <sup>b</sup>                             |
| NSAIW      | -0.5...0.5 <sup>a</sup> ; -0.17 <sup>b</sup> ; -0.16 <sup>e</sup> | 34.87-34.90 <sup>a</sup> ; 34.89 <sup>b</sup> ; 34.88 <sup>e</sup> | 7.0-8.4 <sup>a</sup> ; 7.3 <sup>b</sup> ; 7.0-8.1 <sup>d</sup> ; 7.5 <sup>e</sup> ; | 14.1-14.5 <sup>a</sup> ; 14.1 <sup>b</sup> ; 13.9-14.5 <sup>d</sup> ; 13.8 <sup>e</sup> ; | 294-302 <sup>a</sup> ; 305 <sup>b</sup> ; 300-305 <sup>d</sup> ; |
| NSDW       | ~ -1.03 <sup>a</sup> ; -0.98 <sup>b</sup> ; < -0.5 <sup>c</sup>   | ~ 34.91 <sup>a,b</sup>   | ~ 13 <sup>a</sup> ; 12.6 <sup>b</sup>   | 15.0-15.6 <sup>a</sup> ; 15.3 <sup>b</sup>  | 297-299 <sup>a</sup> ; 297 <sup>b</sup>                          |

### **3 Data Material**

Nutrient observations from the FAMRI standard sections constitute the main data material in this report. In order to look at a broader picture from neighbouring waters to the Faroe shelf, we complement these by data obtained at coastal station Skopun, south of Iceland, in the FSC and previous data obtained in Faroese waters. A short description of each of these data sets is given below.

#### **3.1 Nutrient observations at FAMRI standard hydrographic stations.**

FAMRI is presently maintaining six standard hydrographic sections, whereof five are shown in Figure 1. Section N, V and E were initiated in 1988, section S in 1994, while section R was initiated in 2012. In 2013 FAMRI initiated a sampling programme for nutrient analysis at selected stations on these hydrographic sections (Figure 1). The stations were selected such that they represented specific water masses, such as AW in the FC and overflow in the Faroe Bank Channel (FBC). Preselected sampling depths at each station were also determined in order to sample various water masses at the different stations. Depending on relevance, samples are collected for nutrients, carbon and phytoplankton analysis, but only the nutrient data are discussed here.

#### **3.2 Coastal station Skopun**

Since 1995, FAMRI has maintained a coastal sampling station at a fish farm facility in Skopun. At the sea water intake, temperature is continuously measured and water is sampled for various analyses. Samples are collected for nutrient and salinity analysis twice a week (on average), while samples for phytoplankton analysis are collected once a week during the spring and summer season and every other week for the rest of the year.

#### **3.3 The primary production index (PPI)**

The primary production index (PPI) for the inner Faroe shelf is based on nitrate samples from two stations (stations W and N, Gaard et al., 1998) located near the shallowest stations at Section V and N, respectively during late June. This index represents the “nitrate loss” in the shelf water during spring, and is roughly calculated as the difference between a “typical winter nitrate concentration of 12  $\mu\text{M}$  and the late summer concentrations (Gaard et al., 1998).

#### **3.4 Observational campaigns in 1986 and 1995**

The only available complete nutrient sections in the open ocean water around the Faroe plateau were (to the authors knowledge) made during an observation campaign during June 1986, involving R/S Magnus Heinason (MH86) and R/S Håkon Mosby (HM86) (Hansen et al., 1987; Liljeblad et al., 1987) and by MH during 1995 (MH95).

The historical data from the 1986 observational campaign have been digitized from paper reports (Hansen et al., 1987; Liljeblad et al., 1987) for utilization in the present report (Figure 3 and Figure 4). In response to an ICES resolution of 1985, oceanographers from Tórshavn and Bergen decided to join an investigation of hydrography and currents of the IFR region, using the Faroese R/V Magnus Heinason and the Norwegian R/V Håkon Mosby in June 1986. The project, supported by the Nordic Council for Physical Oceanography may be regarded as a first stage of a more extensive ICES-venture trying to monitor the Atlantic inflow over the whole Greenland-Scotland ridge.

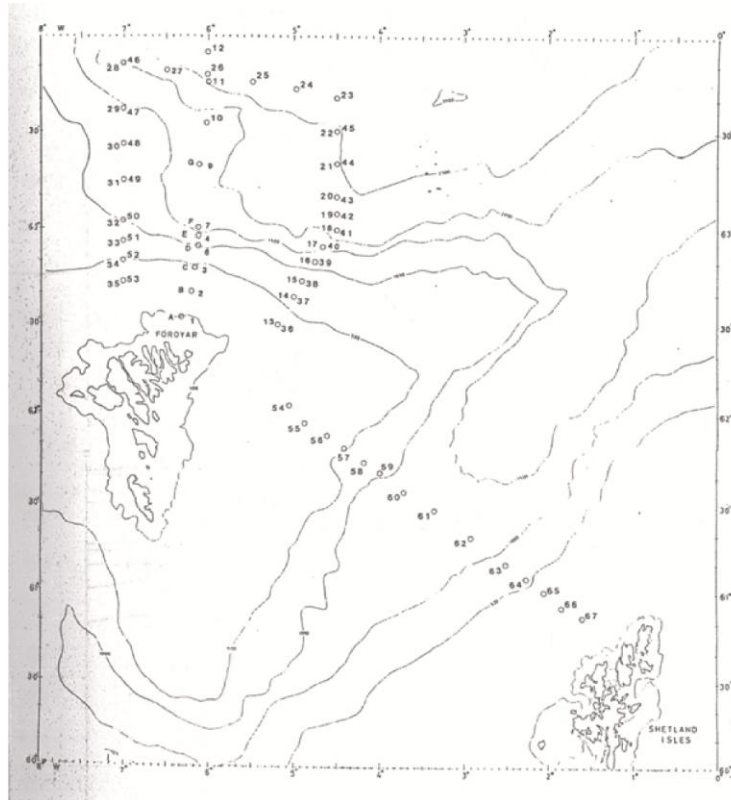


Figure 3 Stations made by R/V Håkon Mosby during June 1986 (Figure 1 in Liljeblad et al., 1987)

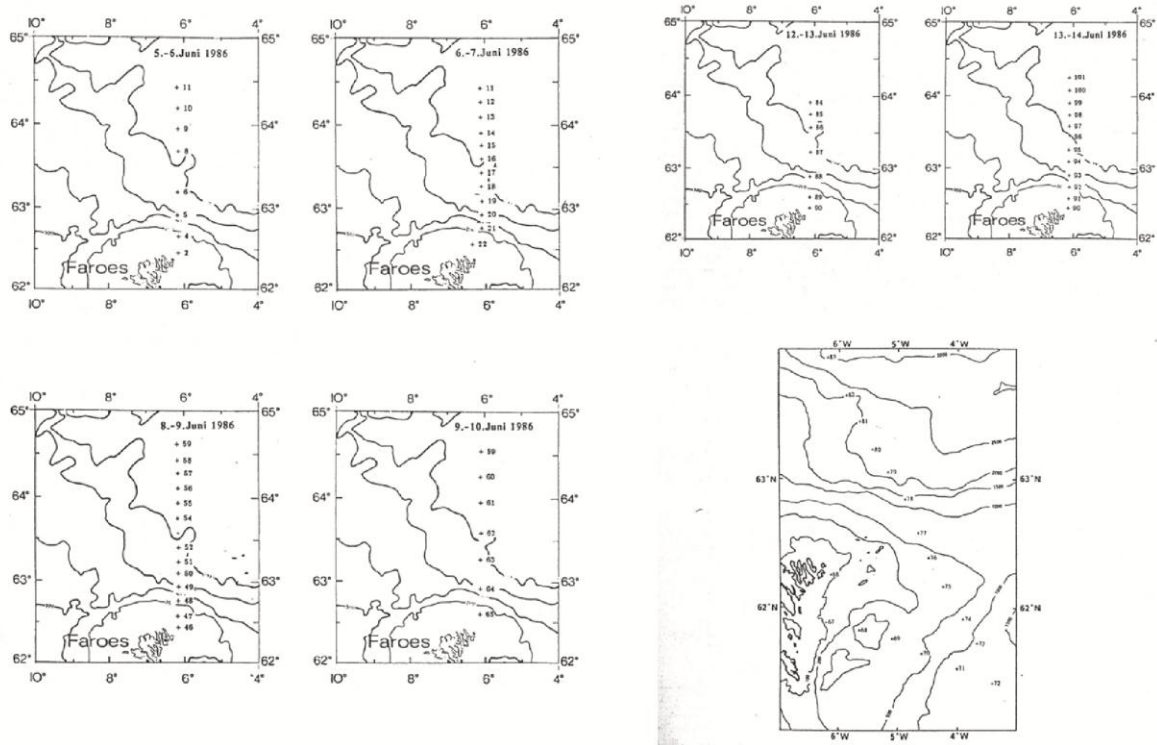


Figure 4 Stations made R/V Magnus Heinason during June 1986 (Figures 1 (left four panels) and 2 (right three panels) in Hansen et al., 1987)

The MH section from 1995 followed roughly the present day section R (was not termed R at that time) and section E. (Gaard, 2000, 1996)

Data from the campaigns during 1986 and 1995 provide valuable spatial context for our assessment of the newer (2013-2020) data along Section N and are discussed in Sections 4.3 and 4.4, respectively.

### **3.5 Nutrient observations south of Iceland and in the Faroe-Shetland Channel**

We complement the presentation of the FAMRI data with nutrient data from the northern Irminger Sea (Faxaflói station 9, FX9 hereafter, Hátún et al. 2017a; Jacobsen et al., 2019) and from the FSC, obtained by averaging December-February data from a biogeochemical North Sea Climatology over the geographic box [1°W-3°E, 59-61°N] (from Pätsch et al., 2020).

## **4 Context based on previous nutrient observations**

One motivation for initiating the FAMRI open ocean nutrient sampling program was to improve our understanding of the highly variable primary production dynamics on the Faroe shelf – evident in the PPI (Gaard et al., 1998). Before scrutinizing the new (2013-2020) open ocean nutrient samples (Section 5), the previously published open ocean pre-bloom nutrient concentrations from south Iceland waters (Hátún et al., 2017a; Jacobsen et al. 2019) and the FSC (Pätsch et al., 2020) are compared to both the PPI proxy record (Section 3.3) and the twice weekly nutrient samples from coastal station Skopun (Section 3.2).

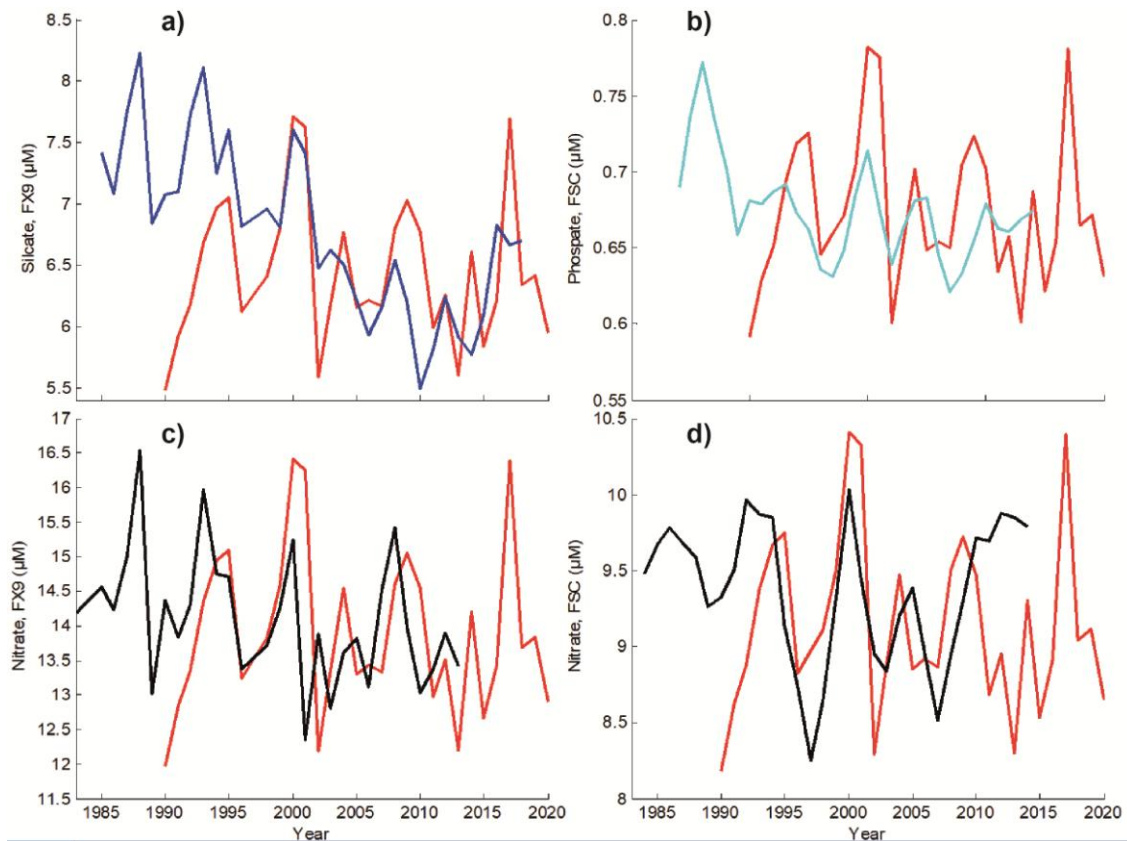


**Figure 5 Open ocean pre-bloom nutrients and primary production of the Faroe shelf.**

The primary production is represented by the primary production index (PPI, red) (Gaard et al., 1998, Section 3.3). Panels (a) and (c) show silicate (blue) and nitrate (black), respectively, in the northern Irminger Sea ( $S_{FX9}$  and  $N_{FX9}$ ). Panels (b) and (d) show phosphate (light blue) and nitrate (black) in the FSC.

#### 4.1 Open ocean nutrients and primary production on the Faroe shelf

The PPI is characterized by having multi-annual variability with large peaks in the productive years. These peaks appear to coincide with peaks in pre-bloom nutrient concentrations, both in the waters south of Iceland (FX9, Figure 5a,c) and in the FSC Figure 5b,d. All PPI peaks have a corresponding silicate peak south of Iceland ( $S_{FX9}$ ), except the moderate peak in 2014 (Figure 5a). Marked nitrate spikes south of Iceland ( $N_{FX9}$ ) do likewise coincide with rapid increases in the PPI (e.g. 1993, 2000 and 2008, Figure 5c). The apparent nitrate-PPI link was, however, less clear during the years 2001-2003. These concurrent peaks lead to a significant correlation between the PPI and the nutrients south of Iceland (on a 1% level); after these records have been linearly detrended  $R(PPI, Si_{FX9}) = 0.47$  and  $R(PPI, Ni_{FX9}) = 0.50$ . The correlations between the PPI and nitrate and phosphate records from the FSC are, however, not statistically significant;  $R(PPI, Ni_{FSC}) = 0.33$  and  $R(PPI, Ph_{FSC}) = 0.22$ .

As previously described, the pre-bloom silicate concentrations have declined by about  $0.60 \mu\text{M}$  pr. decade throughout the entire subpolar Atlantic since the 1980s (Hátún et al. 2017a) (Figure 5a). We here show that nitrate has also declined (Figure 5c), although more gradually ( $0.39 \mu\text{M}/\text{decade}$ ). The pre-bloom phosphate record from the FSC likewise suggest a decline (Figure 5b), while no trend is evident in the nitrate data from the FSC (Figure 5d). The difference in magnitude between Si and Ni and Ni and P indicate that both Si:N and N:P ratios have changed over this period (not shown).

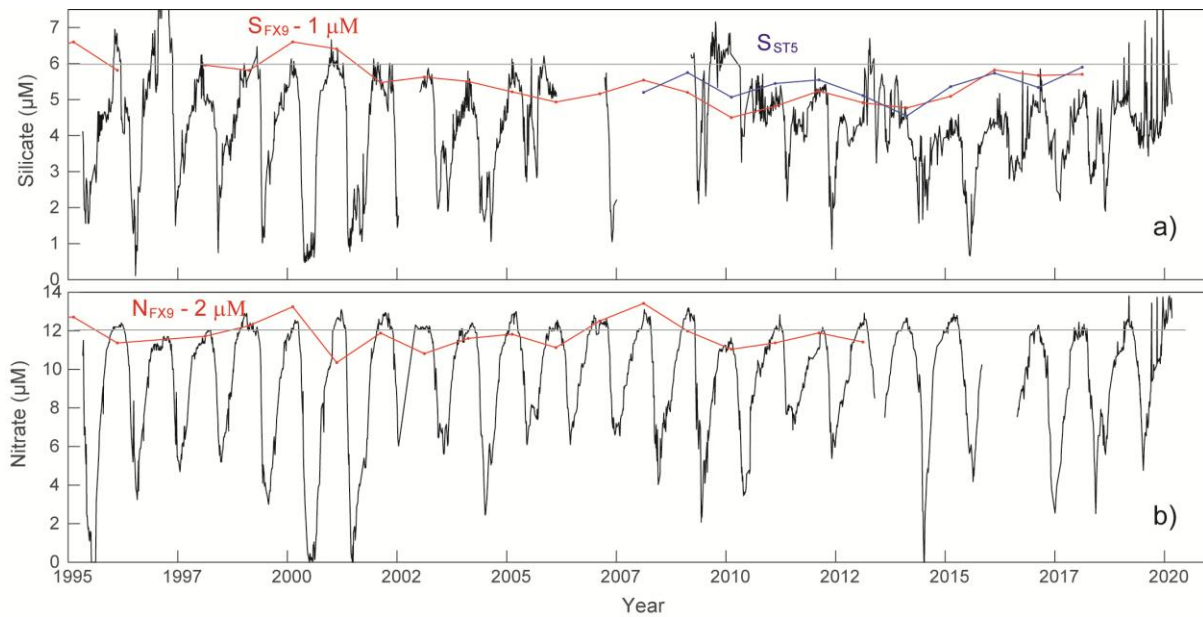


**Figure 6 Pre-bloom nutrients south of Iceland and nutrients at coastal station Skopun.**

a) Silicate and b) Nitrate. The open ocean pre-bloom nutrient records from the northern Irminger Sea ( $S_{FX9}$  and  $N_{FX9}$ , red) and from the northern Iceland Basin ( $S_{ST5}$ , blue, see Section 5.4.2) have been utilized. To better enable comparison with the other records, the FX9 records have been by  $1 \mu\text{M}$  (silicate) and  $2 \mu\text{M}$  (nitrate), respectively. The assumed “typical winter nitrate concentration” of  $12 \mu\text{M}$  (see Gaard et al., 1998 and Section 3.3) is illustrated with a gray horizontal line in panel b. The typical winter silicate concentration of  $6 \mu\text{M}$  (during the late 1990s) is also emphasized with a gray horizontal line (a).

## 4.2 Nutrients in the open ocean and at coastal station Skopun

The broad pre-bloom silicate decline is also evident in the 25-years long record from coastal station Skopun (Hátún et al., 2017a)(Figure 6a). In addition to the decreasing trend, all oceanic records (Irminger Sea, Iceland Basin, FSC and likely north of the Faroe slope) also reveal characteristic interannual fluctuations, which are generally in phase (Figure 5). Although less clearly, the high-temporal-resolution record from Skopun shows similar interannual variability, which however appears to lag the oceanic conditions by about one year. Cooper (1955) argued for a similar time lag between oceanic influxes and biogeochemical and biological conditions on a shelf, by considering lateral influx of nutrients (he used phosphate) onto the English shelf, enriching bottom deposit after and increase subsequent re-suspension back to the water column. This apparent lagged relation should merely be regarded as a curious tentative observation which, however, warrants closer scrutiny. The nitrate series from Skopun does not suggest that the Faroe shelf has experienced nitrate decline which corresponds to the nitrate decline in south Iceland waters (cf. Figure 5c and Figure 6b).

### 4.2.1 Nutrient data quality

The silicate record at Skopun shows pronounced seasonal draw-down during years before 2006 and a noisier signal after a gap in the record (2006-2009), where after the seasonal variability become less clear (Figure 6a) (also described in Eliassen et al., 2017a). This suggests that either has the system changed character – markedly – after 2009, or has the data quality deteriorated (apparently after that data gap). Evidence for erroneous silicate data is, without doubt, evident in 2019 and 2020.

For the nitrate data, there is no marked shift in the seasonal dynamics/data characteristics after ~2009, and the only indications of increased noise in the nitrate data are a few spikes in 2019-2020 (Figure 6b).

We therefore suggest that the silicate data should be used with care, while quality of the nitrate data is more robust (see Section 5.1).

### **4.3 A comprehensive nutrient section in June 1986**

In the observational campaign in 1986 Section N was comprehensively covered several times by MH86 during the days June 5.-14 (Figure 4). We have here treated the sections, from where nutrient data were available (between June 8 and June 14, stations 46-57, and 90-100), as a single section.

#### **4.3.1 Hydrography (Temperature and salinity)**

The warm and saline wedge of Modified North Atlantic Water (MNAW) was relatively broad during these days (Figure 7), compare with several of the newer sections Figure 18-20), and eastward flow of low-saline MEIW (Read and Pollard, 1992) is evident immediately under this wedge ( $S < 34.9$ , bluish colors in Figure 7b). At large depths ( $> 800$  m), two cores with low temperatures (and thus high density) are evident, one just south of  $63^\circ\text{N}$  and one just north of  $63.5^\circ\text{N}$  (Figure 7a,c). These are thus in the zones of the Iceland-Faroe Slope Jet (IFSJ) (Semper et al., 2020) and the even deeper Norwegian Sea Gyre (NSG) rim farther north (Hátún et al., 2021a), respectively. Semper et al. (2020) suggest that the IFSJ is intensified during so-called 'Elevated isopycnal states', which is when dense water ( $\sigma_\theta > 28.03 \text{ kg m}^{-3}$ ) is present at station N04 ( $62.83^\circ\text{N}$ ). During 8-14 June 1986, the isopycnals seem somewhat elevated (Figure 7c), but since station N04 was not occupied at that time (this was before the establishment of the standard stations along Section N), we cannot ascertain whether or not the system was in an elevated isopycnal state/strong IFSJ during June 1986.

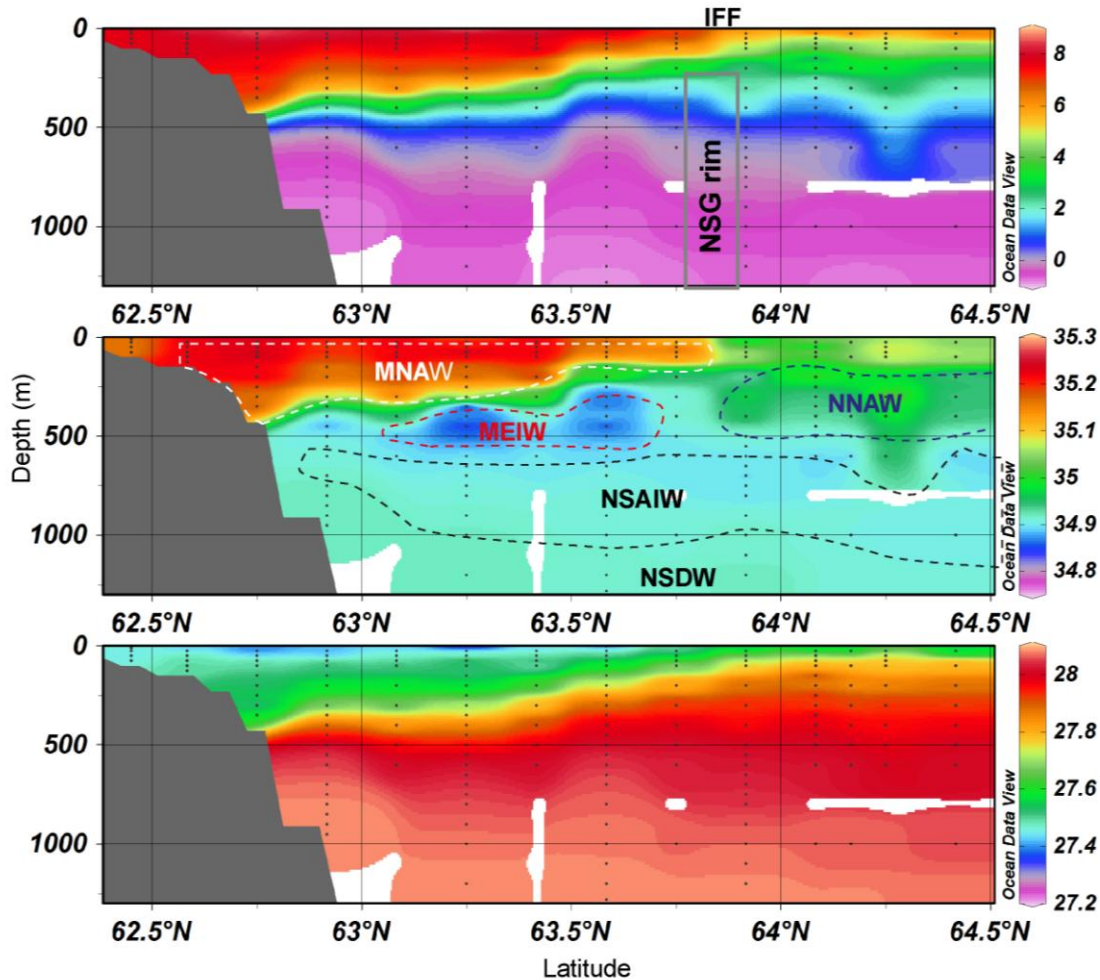


**Figure 7 Hydrography approximately along Section N during June 1986 (MH86).** Upper: temperature ( $^{\circ}\text{C}$ ), middle: salinity and lower: potential density ( $\sigma_{\theta}$ ). The approximate distribution of the main water masses (see Figure 2 and Table 2) is outlined, and abbreviations are provided in Table 1.

#### 4.3.2 Upper ocean nutrients

The upper layer water column (0-300 m) was characterized by relatively high concentrations of silicate ( $6\text{-}7\ \mu\text{M}$ ) and nitrate ( $13\text{-}14\ \mu\text{M}$ ) in the FC zone - bounded by the  $\sim 200\ \text{m}$  isobaths to the south, the *NSG rim* (Hátún et al., 2021a) to the north, and the mixed layer above ( $\sim 50\ \text{m}$  depths) (Figure 8). Silicate was exhausted in the mixed layer over the FC core (Figure 8a), while nitrate was most reduced – although not reaching growth limiting concentrations – in the *NSG rim* zone ( $63.5\text{-}64.2^{\circ}\text{N}$ ) (Figure 8b). A strong meridional near-surface nutrient gradient is evident at  $\sim 62.5^{\circ}\text{N}$ , which likely is the Faroe shelf tidal front (Larsen, 2009). Silicate and nitrate concentrations were, respectively,  $0.54\ \mu\text{M}$ ,  $7.63\ \mu\text{M}$  north of the tidal front and  $5.21\ \mu\text{M}$ ,  $10.49\ \mu\text{M}$  south of the front.

Low oxygen content, or high apparent oxygen utilization (AOU) is related to time since the water parcel last was in contact with the atmosphere (Sarmiento and Gruber, 2019). Low oxygen content clearly outlines the AW body of the FC, which demonstrates that AW is an ‘older water mass’, while the recently ventilated subarctic water masses are ‘younger’. The oxygen distribution suggests that the FC consisted of two cores during June 1986 (Figure 8c), which is in line with recent findings by

Hátún et al. (2021a), who showed that this typically occurs when the NSG circulation is weak and the AW wedge is wide (northward extended). The AW slab appears to be well defined by  $[O_2] < 6.25 \text{ ml L}^{-1}$  (corresponds to  $8.31 \text{ mg L}^{-1}$ ) and temperatures between 6 and  $8^\circ\text{C}$  (which is slightly lower than the present-day MNAW temperature interval, see Section 5.4). Oxygen concentrations are elevated in the mixed layer, partly due to primary production (Richardson et al., 2000), especially in the NSG rim region (Figure 8c), where the nitrate concentrations are most reduced (Figure 8b). The oxygen data furthermore clearly capture the presence of a tidal front at  $62.5^\circ\text{N}$ , with low  $O_2$  in the oceanic lower layer, high  $O_2$  in the oceanic mixed layer and intermediate concentration in the vertically mixed shelf water (Figure 8c).

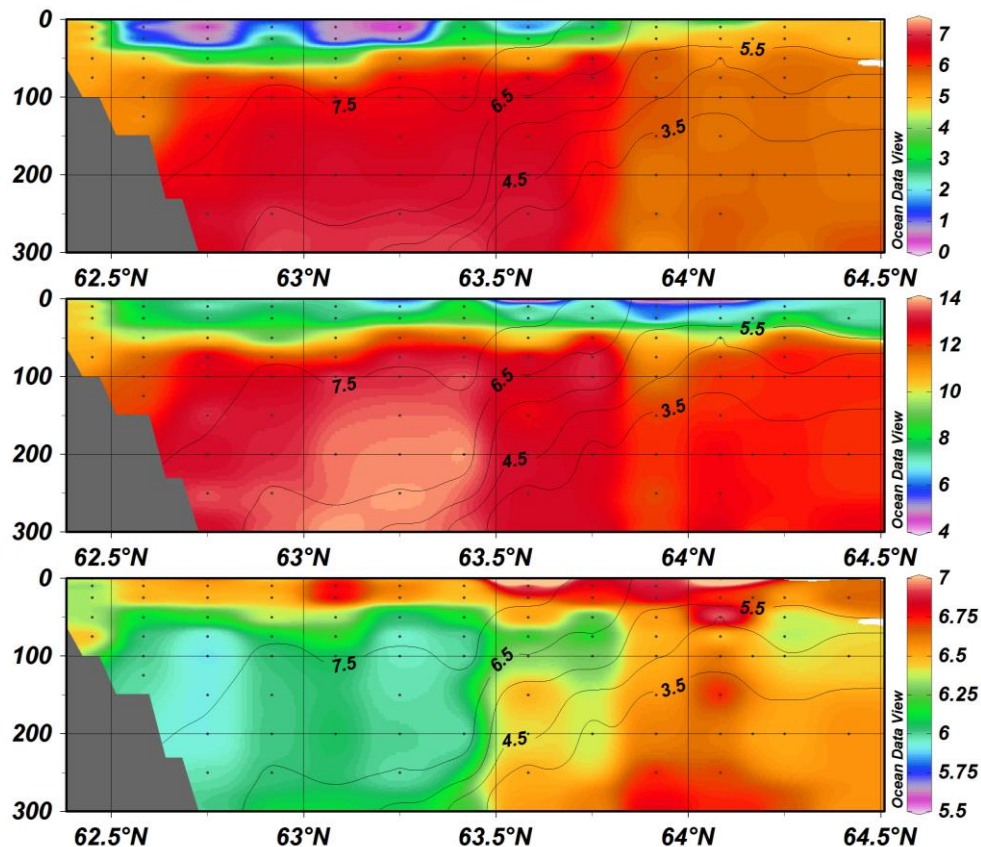


**Figure 8 Upper nutrient and oxygen concentrations along Section N during June 1986 (MH86).** Upper: silicate ( $\mu\text{M}$ ), middle: nitrate ( $\mu\text{M}$ ), and lower: oxygen ( $\text{ml L}^{-1}$ ). The black lines represent isotherms ( $^\circ\text{C}$ ).

### 4.3.3 Nutrients in the deeper layers

In the deeper layers, silicate resembles the temperature/density distribution (cf. Figure 7a,c and Figure 9c). The two dense cores mentioned above clearly have slightly higher silicate content, compared to the waters between these cores (at the same depths). High silicate concentrations are also observed north of the NSG rim ( $\sim 64.2^\circ\text{N}$ ), and the oxygen concentration is slightly reduced in these deep cores (Figure 9c). Nitrate is also high below 1000 m ( $> 14 \mu\text{M}$ ), but the structure of the dense cores is less articulated in the nitrate concentrations (Figure 9b).

R/S Håkon Mosby (HM86) also made a transect roughly following Section N during June 1-4 (Figure 3). These data are spatially coarser than the presented MH86 data, and this transect only reached

north to 63.92°N. The silicate distribution from HM86 (Appendix Fig. A1a) is basically the same as from the MH86 data, with elevated concentrations near the two aforementioned dense cores. The HM86 data reach deeper than the MH86 data, and show that the silicate concentration in the cores increases all the way towards the seafloor. Both datasets show strong lateral silicate gradients at the depths of the deep cores. At 1000 m depths, HM86 observed high silicate concentrations in NSG rim zone (10.01  $\mu\text{M}$  at 63.60°N, 10.58  $\mu\text{M}$  at 63.75°N and 7.19  $\mu\text{M}$  immediately north of this (63.92°N)). About one week later, MH86 observed 9.36  $\mu\text{M}$  at 63.60°N, 10.23  $\mu\text{M}$  at 63.75°N and 8.71  $\mu\text{M}$  at 63.92°N (same locations). Oxygen data from HM86 (Fig. A1c) are comparable to those from the MH86 transects, while the nitrate concentrations are much lower and more random (Fig. A1b). Our judgment is that the HM86 nitrate data are unreliable, and the reasons for this are not known by the authors.

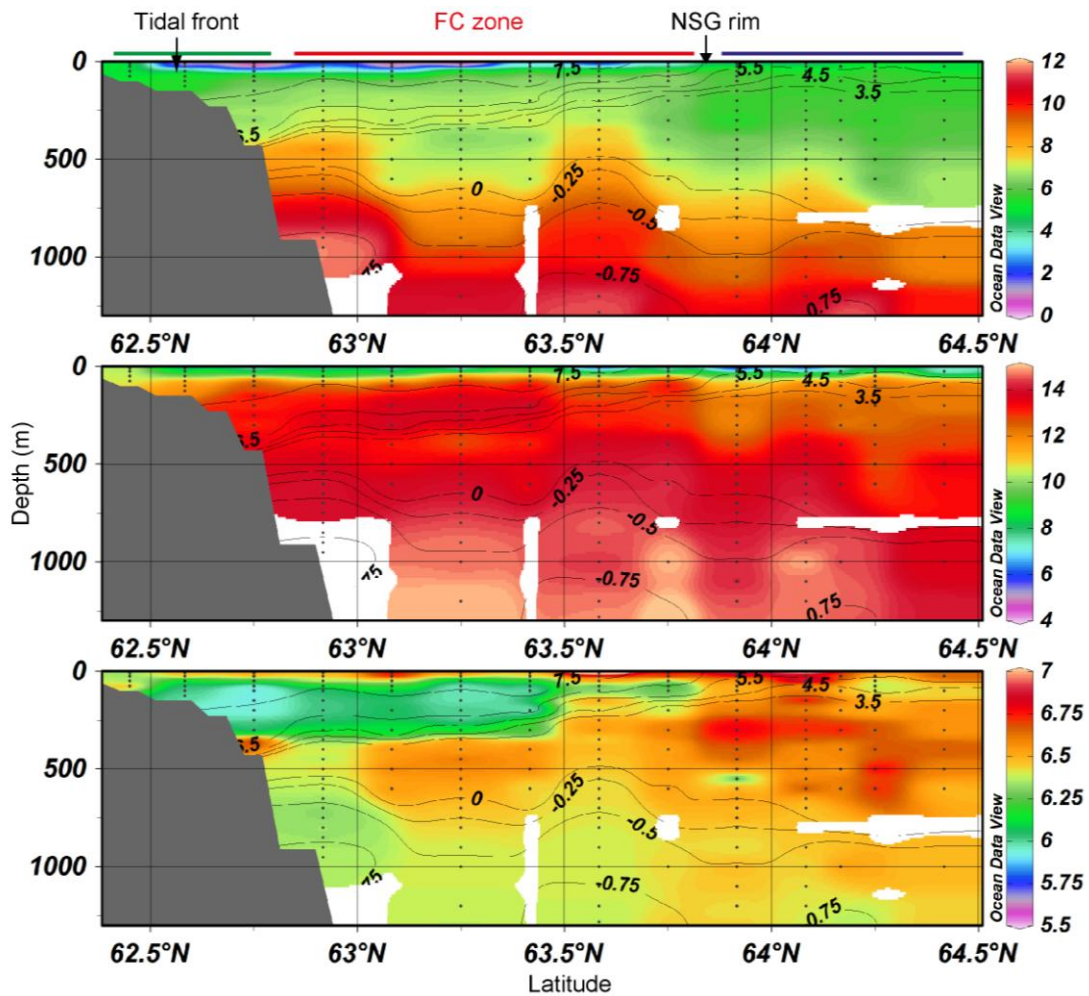


**Figure 9** Deep layer nutrient and oxygen concentrations along Section N, June 1986 (MH86). Upper: silicate ( $\mu\text{M}$ ), middle: nitrate ( $\mu\text{M}$ ), and lower: oxygen ( $\text{ml L}^{-1}$ ). The black lines represent isotherms ( $^{\circ}\text{C}$ ). The colored overlying lines refer to the segregation in Figure 11.

To provide a clearer picture of these silicate cores, the MH86 data have been structured into a matrix composed of all available depth levels by all available latitudes. At locations where sampling has been repeated during early June 1986 (same depth and same latitude), the values have been averaged. Each depth level is then plotted as a function of latitude (Figure 10). This shows a coherent pattern at all depths below  $\sim 400$  m, with silicate peaks in the vicinity of the IFSJ (just south

of 63°N, and thus near standard stations N04 and N05) and at the southern flank of the average position of the NSG rim (which is ~ 63.75°N). The repeated stations at 63.58°N and 63.93°N demonstrated relatively large changes in silicate concentrations during the few days separating them. Difference of up to 1  $\mu\text{M}$  characterized the depth levels of 200-600 m, with a more than 2  $\mu\text{M}$  difference at 400 m at each of the two locations. Below 600 m, the differences did not exceed 0.5  $\mu\text{M}$ .

This suggests *i*) that the silicate data probably are reliable, *ii*) that the silicate concentration at depth can easily vary 3-4  $\mu\text{M}$  over relatively short distances in this regions and *iii*) that the silicate concentration at depth (at a given location) changes rapidly, likely associated with lateral movement of the NSG rim.

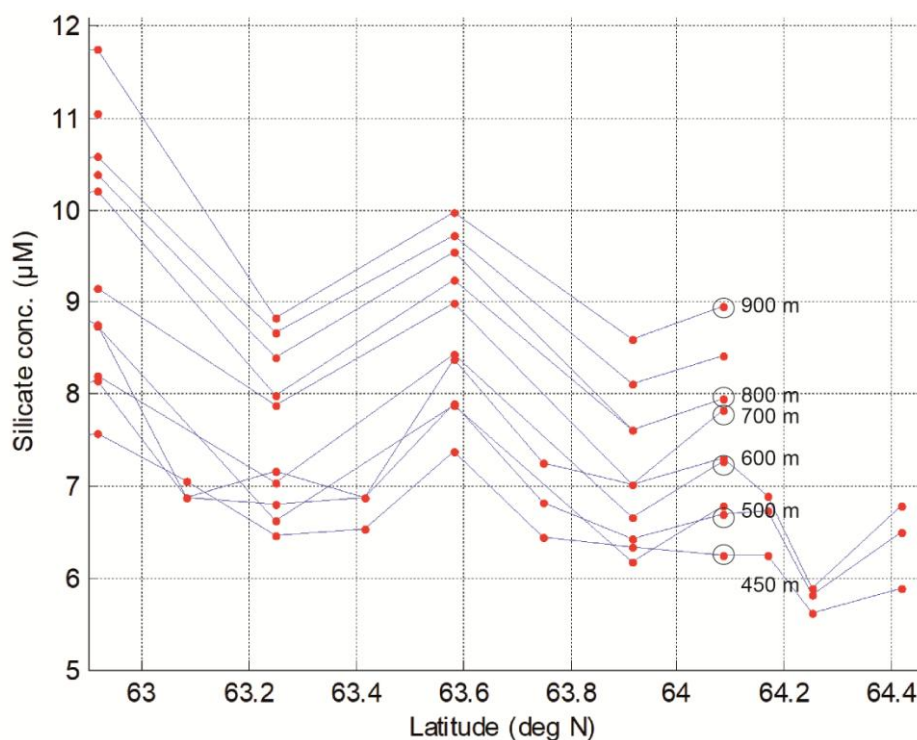


**Figure 10** Latitudinal silicate profiles at depths between 450 m and 900 m.

#### 4.3.4 MNAW nutrients

Silicate and nitrate data from MH86 are in Figure 11 plotted as profiles, divided into three zones: near-slope (green), FC (red) and in – and north of – the NSG rim (blue). The FC profiles are relatively homogenous in the 100-300 m layer (under the mixed layer), both vertically and horizontally. The profiles in/north of the NSG are also relatively homogenous, but cluster at lower concentrations, compared to the FC. At depth (500-600 m), the NSG rim profiles can reach concentrations comparable to the FC zone. The increased spread in nutrient concentrations at these depths probably reflects the previously discussed strong lateral nutrient gradients.

A lateral perspective of the sub-mixed layer silicate and nitrate concentrations in June 1986 is provided by plotting the 100-300 m depth-averages at each station as a function of latitude (Figure

12). Both silicate and nitrate increase steeply from the shelf and north to  $\sim 63^\circ\text{N}$ , while the temperature decreases slightly along this stretch. This shows that the present standard stations N04 ( $62.83^\circ\text{N}$ ) and N05 ( $63.00^\circ\text{N}$ ) can experience slightly different water types, and thus nutrient concentrations. Silicate continues to increase out the  $\sim 63.6^\circ\text{N}$  (near the NSG rim) and drops abruptly north of  $63.8^\circ\text{N}$ . The highest nitrate concentrations were observed at  $\sim 63.1^\circ\text{N}$ , and decline northward from this – more gently than silicate did. By averaging these data over the  $62.8\text{--}63.5^\circ\text{N}$ ,  $100\text{--}300\text{ m}$  window (depth criterion, like used by Jacobsen et al., 2019), we estimate the 1986 silicate concentration representative for the MNAW ( $S_{\text{AW}}$ ) to  $6.75 \pm 0.24\ \mu\text{M}$  and the nitrate ( $N_{\text{AW}}$ ) to  $13.60 \pm 0.36\ \mu\text{M}$ .

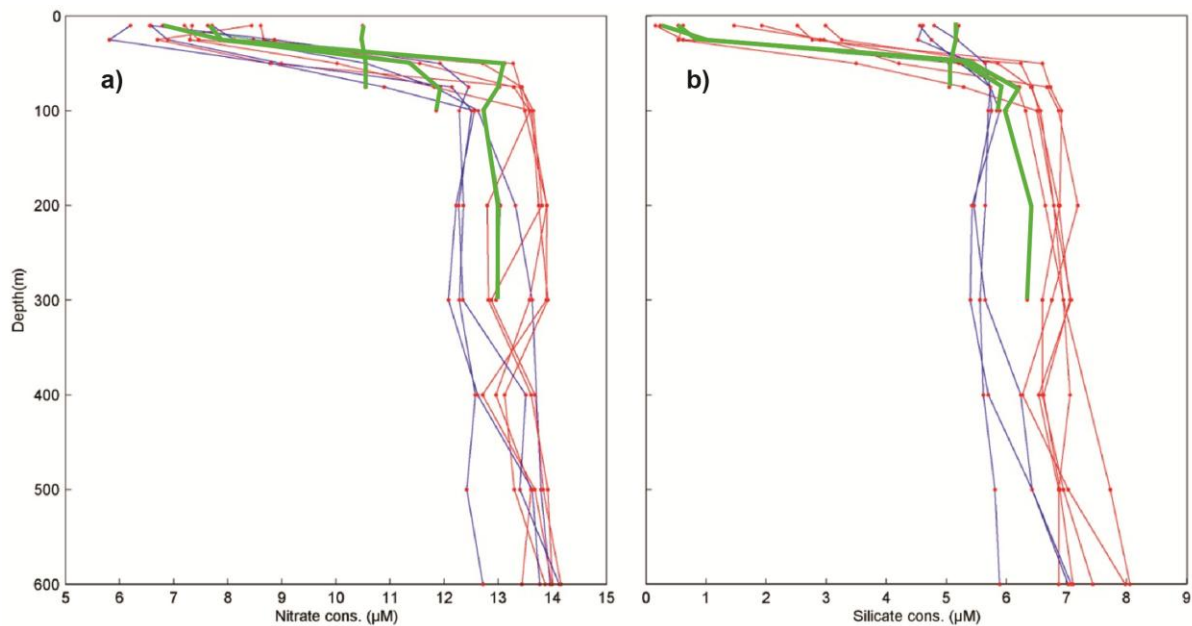


**Figure 11 Nutrient profiles along Section N (from MH86).**

a) Nitrate and b) silicate. Green profiles are near the shelf, red are in the FC zone and blue are north of the NSG rim (see Figure 9).

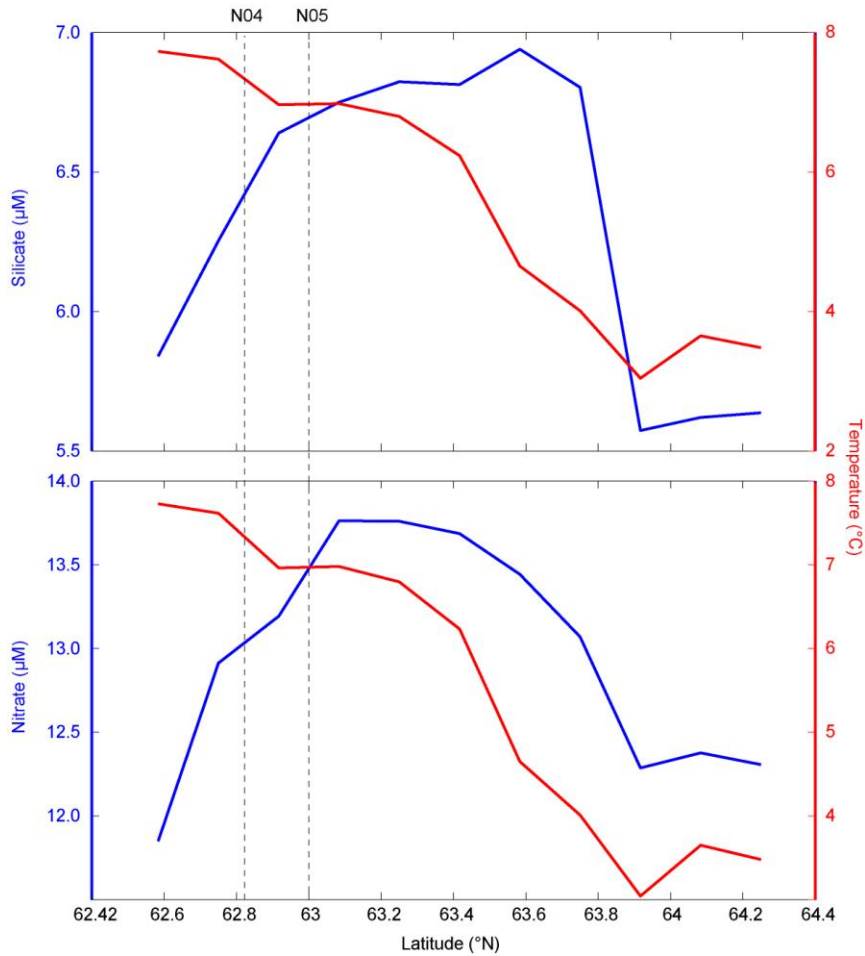


**Figure 12 Upper layer nutrients and temperature along Section N in June 1986 (MH86).**

Upper: Silicate and lower: nitrate concentrations. Temperatures (red) are vertically averaged over 100-300 m (sub-mixed layer, see Figure 8). The latitudinal positions of modern standard stations N04 and N05, respectively, are shown with black dashed lines.

#### 4.4 Nutrient sections in 1995

Several hydrographic sections, radiating out from the Faroe shelf, were made in May 1995 (MH95) (Section 3.4) (Gaard, 1996). In addition, Section N was also occupied in early September this year. Samples for nutrient analysis were made at 5, 20, 40, 60 and 100 m at all sections, with 200 m added to Sections R and N, and 2000 m added to Section N.

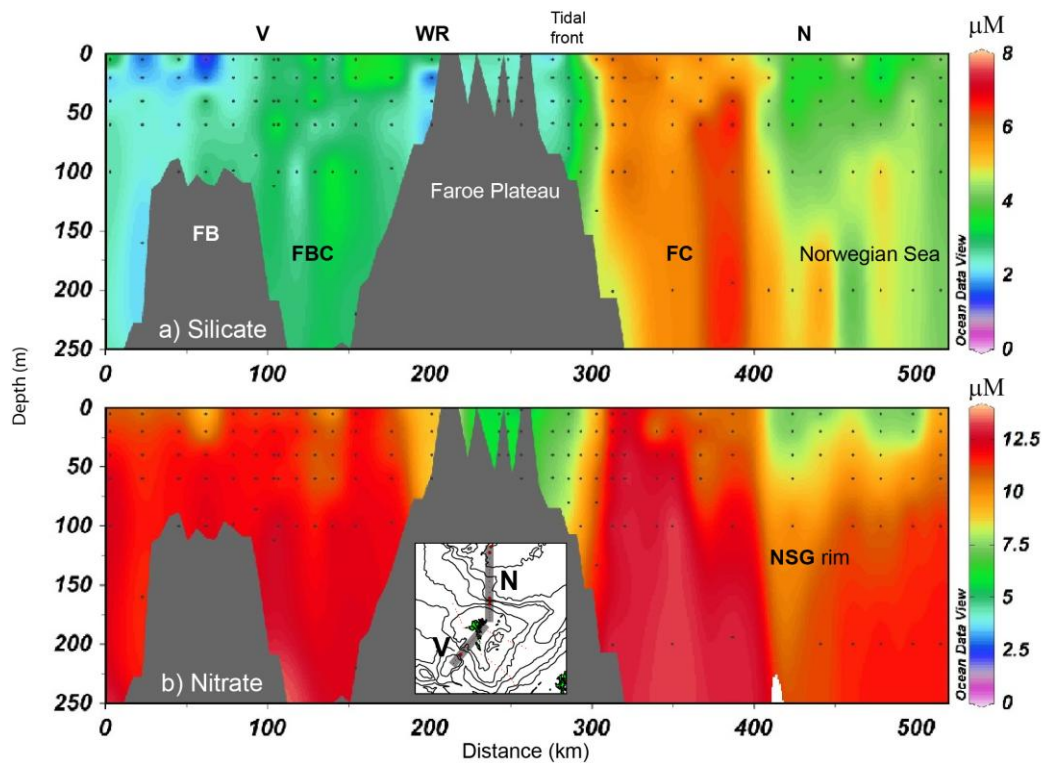


**Figure 13 Combined section V-N during late May, 1995.**

From west of the Faroe Bank (left), across the Faroe Plateau (middle) and north along Section N (right). Upper: silicate and lower: nitrate (both in  $\mu\text{M}$ ).

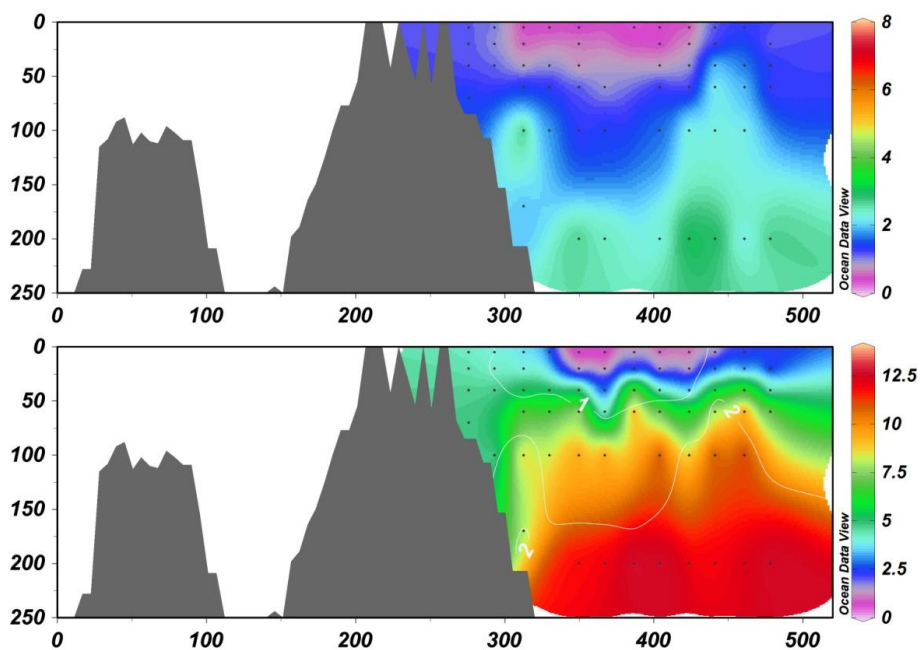


**Figure 14 Section N during 1-2 September, 1995.**

Upper: silicate and lower: nitrate (both in  $\mu\text{M}$ ). No data available along Section V in September. Axis and panels labels and some annotations are provided in Figure 13 Combined section V-N during late May, 1995. The white contour lines in the lower panel represent the  $1\mu\text{M}$  and  $2\mu\text{M}$  levels of silicate.

#### 4.4.1 Combined section V-N

The data from standard Sections V and N have been illustrated as one transect from west of the Faroe Bank, across the Faroe Plateau and north along Section N (Figure 1, Figure 13 and Figure 14). This shows that near limiting silicate concentrations were observed on the Faroe Bank and in the Western Region (WR) on the Faroe shelf (Eliassen et al., 2017a; Hátún et al., 2013), already in May (Figure 13a). There is a strong contrast between relatively high silicate concentrations in the FC zone and much lower concentrations in the FBC. The silicate content decreased again in and north of the NSG rim (about 420-450 km in this section), and there is a strong lateral gradient between the FC and south onto the Faroe shelf – probably associated with the tidal front (Larsen, 2009). For the 60-200 m water column in the FC, we estimate  $S_{AW}$  for May 1995 to  $6.06 \pm 0.40 \mu\text{M}$ . Nitrate was also reduced on the Faroe shelf and over the NSG rim, but not to limiting concentrations in May (Figure 13b). Nitrate was higher in the FC than in the FBC, but the contrast was much smaller than the silicate contrast. There was also a strong lateral nitrate gradient from the FC and onto the Faroe shelf. We estimate  $N_{AW}$  in the FC (May 1995) to  $13.10 \pm 0.29 \mu\text{M}$ .

During the summer there had been strong drawdown of silicate, leading to limiting concentrations ( $< 2 \mu\text{M}$ ) throughout the upper  $\sim 100$  m along the entire Section N in early September 1995 (Figure 14). Nitrate also reached limiting concentrations, although only in the upper  $\sim 30$  m. This implies a large decrease in silicate below the nitracline, which could be due to resting spore formation of dominant diatom species, as has been observed in other systems (Rey and Skjoldal, 1987).

Opposed to the MH86 data (Figure A1), the samples taken at 1300 m were much lower and showed very small lateral silicate changes. The value was  $7.92 \mu\text{M}$  at the stations at  $63^\circ\text{N}$ ,  $63.17^\circ\text{N}$ ,  $63.34^\circ\text{N}$ ,  $63.67^\circ\text{N}$  and  $64^\circ\text{N}$ ,  $7.53 \mu\text{M}$  at  $63.54^\circ\text{N}$  and  $7.85 \mu\text{M}$  at  $64.33^\circ\text{N}$  (not shown). This very different character of the deep silicate samples from both periods is puzzling, and requires further scrutiny (See Section 4.3.3).

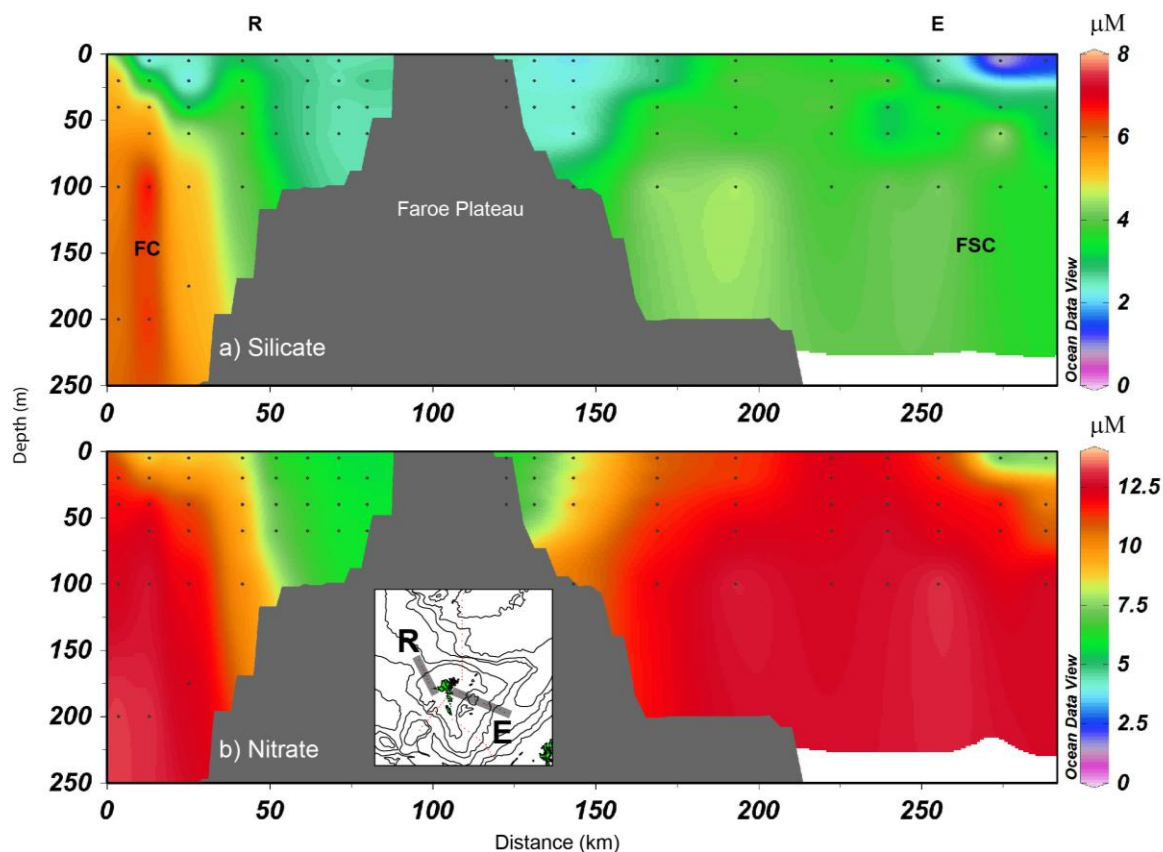


**Figure 15 Section R-E during May 1995**

a) Silicate and b) nitrate. Abbreviations are presented in Table 1.

#### 4.4.2 Combined section R-E

A NW-to-SE nutrient transect across the Faroe plateau was also obtained for May 1995, by combining data from roughly present day section R and section E (Figure 15) (This is the only utilization of data from standard hydrographic Section E in the present report). This also demonstrates strong silicate reduction on the Faroe shelf, and silicate limitation in the upper ~25 m in the FSC (Figure 15a). There is a strong contrast between relatively high silicate in the AW current, which hugs the NW edge of the Faroe plateau, and the concentrations southeast of the plateau. This lateral contrast is not evident in nitrate. Strong slanting nutriclines extend from the Faroe slope seafloor towards the surface at the NW end of Section R. Strong lateral silicate gradients are evident near this AW current core.

The comprehensive transects from MH86, HM86 and MH95 have provided spatial context for the assessment of the new nutrient samples along Section N, which is laterally limited to the four standard stations – N04, N05, N13 and N14.

## 5 Regular open ocean nutrient sampling starting in 2013

In this section, we present the recently acquired dataset, which constitutes the basis of the present report.

### 5.1 Nutrient sampling and analysis

The following sections provide details on sampling, preservation and analysis of the inorganic nutrients nitrate ( $\text{NO}_3^-$ ) + nitrite ( $\text{NO}_2^-$ ), referred to as 'nitrate', phosphate ( $\text{PO}_4^{3-}$ ) and silicic acid ( $\text{Si(OH)}_4$ ), referred to as 'silicate'.

#### 5.1.1 Sampling and preservation

Onboard the research vessel the samples were collected with Niskin bottles mounted on the CTD rosette. Immediately after sampling the water was transferred into clean plastic (polyethylene) bottles. The bottles and caps were rinsed three times with sampling water before filling. The samples were then preserved with 12 drops of chloroform per 100 ml of sample, stored in refrigerator and analysed usually within 10-90 days. Occasionally, the samples were analyzed at sea. In those instances, the samples were not preserved, but stored dark and cold until analysis, which was done the same day or the next day after sampling.

The coastal samples were collected at the land based station 'Skopun'. This station pumps large amounts of seawater (about 15 tonnes per minute) from 18 m depth in Skopunarfjörður through a sub-sea tunnel (diameter  $\sim 0.8$  m) into a land based station. The seawater was pumped into a pond from which the nutrient samples were collected. The samples were transferred into pre-rinsed plastic bottles and preserved with 12 drops chloroform per 100 ml of sample and analysed usually within 10-90 days. The tidal currents are extremely strong in this area which results in periodically strong turbulence and most likely also strong resuspension of sediment materials, interrupted by periods with weaker tidal currents. Two such tidal cycles occur daily.

#### 5.1.2 Nutrient analysis

The methods behind the nutrient analyses are based on colorimetric reactions.

Until 2009 the nitrate + nitrite was analysed on an analog 1-channel autoanalyzer using methods described in (Grasshoff, 1983). Reduction of nitrate to nitrite was according to Stainton (1974). The nitrate + nitrite analysis (calibrants and samples) were recorded on a paper plotter and further calculations of concentrations were done manually (Gaard, 1991). Silicate was analysed manually using method by Strickland and Parsons (1972). Disodium-hexafluoro-silicate ( $\text{Na}_2\text{SiF}_6$ ) was used to make standard stock solution. The absorbance was measured at 812 nm in 1 cm cuvettes, after a reduction time of 2-3 hours (Gaard, 1999).

From 2009 and onwards, nitrate + nitrite, silicate and phosphate were analysed on an Auto Analyzer 3 (three channel gas-segmented flow analyzer), produced by SEAL Analytical. The analytical methods were according to producers manual, however with the difference that the disodium-hexafluoro-silicate (instead of sodium meta-silicate) was used to make the standard stock solution. Potassium-dihydrogen-phosphate ( $\text{KH}_2\text{PO}_4$ ) was used to make the standard stock for the phosphate analyses. All nutrients were analysed simultaneously. The nitrate absorbance was measured at 550 nm, the phosphate absorbance at 880 nm and the silicate absorbance at 820 nm. Working standards were prepared fresh every day of analysis. The analyses were not commenced before a regular bubble

pattern and stable baseline were established. Analytical software provided by SEAL Analytical calculated the concentrations in the samples, based on the absorbance-concentration relationship of the working standards. Baseline drift and carryover samples were included in each run. Peak markers were checked by the analyst after each run and corrected for spikes and other anomalies if necessary.

### 5.1.3 Nutrient data comparability

FAMRI has participated in inter-laboratory comparison studies using reference material. In 2014/2015 and 2017/2018 the International Ocean Carbon Coordination Project (IOCCP) and Japan Agency for Marine-Earth Science and Technology (JAMSTEC) conducted inter-laboratory comparison studies of nutrient certified reference materials in seawater, which FAMRI took part in (Aoyama, 2018, 2015).

Recommendations for best practices of future nutrient analyses at FAMRI:

- 1) Collect samples into acid (10% HCl) washed containers that fit directly onto the AA3 analyzer.
- 2) Time from sampling to analysis should be as short as possible (preferable < 2 months).
- 3) Filter samples from near shore (i.e. Skopunarfjörður) with a cellulose acetate 0.2 µm filter or alternatively centrifuge samples prior to analysis.
- 4) Use commercially available nutrient stock standard solutions, e.g. OSIL (<http://osil.com/>), to validate the analyses.
- 5) Ultrasonicate or stir the silicate standard stock solution for a minimum of 5 hours prior to usage.

### 5.1.4 Error flagging

The new nutrient data collection (2013-2020) is relatively disaggregated (geographically, different depth, years, seasons and parameters), with data gaps and some erroneous spikes. These data are therefore initially scrutinized quality controlled using the software Ocean Data View (ODV) (Schlitzer, 2007). Spikes in silicate concentration is one recurrent type of error (Table 3). These samples have been error flagged in ODV, and filtered out before the data are exported from ODV, for further analysis in Matlab.

**Table 3 Error flagged data**

| Station | Date      | Depth (m) | Silicate value (µM) |
|---------|-----------|-----------|---------------------|
| N04     | 17/1-2014 | 61        | 7.33                |
| N04     | 14/5-2015 | 4         | 7.77                |
| N04     | 14/5-2017 | 61        | 8.30                |
| N05     | 14/1-2013 | 19        | 7.91                |
| N05     | 17/1-2014 | 40        | 8.98                |
| N05     | 5/8-2015  | 203       | 16.02               |
| N05     | 14/5-2017 | 59        | 9.20                |
| N05     | 14/5-2018 | 40        | 7.34                |
| V06     | 18/5-2017 | 200       | 11.00               |
| V06     | 10/6-2019 | 40        | 9.50                |

## 5.2 Data structure – in TS-space

The nutrient data (all years and seasons) are here divided into the northern stations (*Northern group*: Sections R and N) and the Faroese channels stations (*Southern group*: Sections V and S, Fig. 1).

### 5.2.1 TS-nutrients diagrams

The northern and southern groups are separately illustrated in TS-diagrams in Figure 16, with the northern group plotted in the upper panel and the southern group in the lower. The colors represent nutrient concentrations - silicate in the left panels and nitrate in the right panels. Principal patterns evident in the silicate data from the northern group (mainly Section N) are: The highest silicate values are sampled in the deep dense waters, NSAIW (see e.g. Hansen and Østerhus (2000) and Table 1 for water mass abbreviations), and NSDW, which are potential source waters for the FBC Overflow. The intermediate density NNAW north of the Iceland-Faroe Front (IFF) holds lower silicate concentrations ( $< 5 \mu\text{M}$ ), while the warmer and lighter MNAW have slightly higher concentrations (5-6  $\mu\text{M}$ ). The intermediate density MEIW is not well sampled by these stations. Very low concentrations (0-2  $\mu\text{M}$ , and thus phytoplankton growth inhibiting (Egge and Aksnes, 1992)), are observed in the near-surface seasonal mixed layer, evident as scattered dark blue dots at high temperatures and/or low salinities.

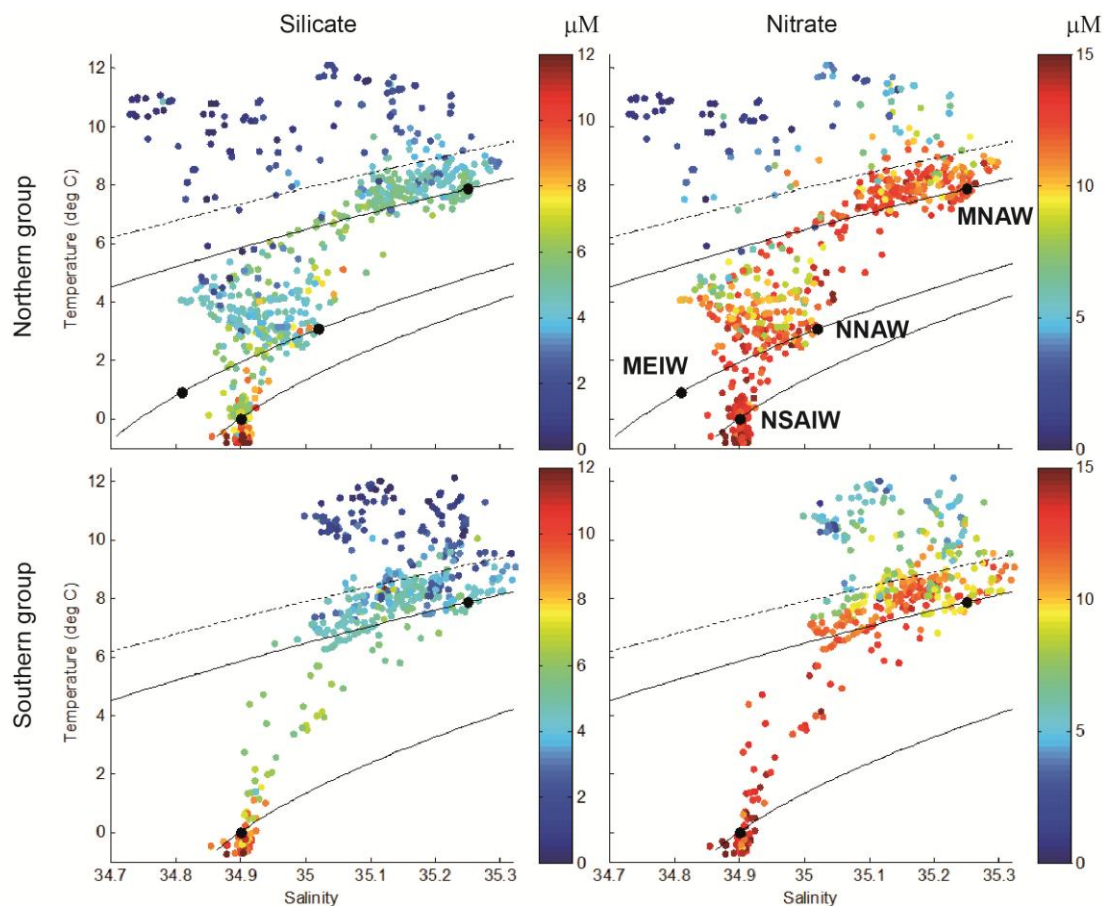


**Figure 16 Temperature-Salinity (T-S) diagrams, with nutrients (2013-2020).**

The colors show nutrient concentrations (in  $\mu\text{M}$ ). Upper panels: Northern group (stations N04, N05, N13, N14 and R08) and lower panel: Southern group (stations V06 and S08). Silicate in left panels and nitrate in the right panels. The black dots illustrated the T-S domains of key water masses, whose abbreviations and properties are provided in Table 1 and Table 2, respectively.

The southern group data points scatter between dense overflow waters in the narrow TS-range  $T < 0^{\circ}\text{C}$  and  $S = 34.9 \pm 0.01$ , and the lighter AW density range  $\sigma_{\theta} < 27.5$  – which has a rather large salinity range (35.00-35-35, Figure 16). Nutrient concentrations generally decrease with increasing temperatures. The summer mixed layer in the southern group consists of a sun-heated layer, with no haline stratification (as opposed to the northern group). The TS-nitrate pattern is similar, maybe less segregated than silicate.

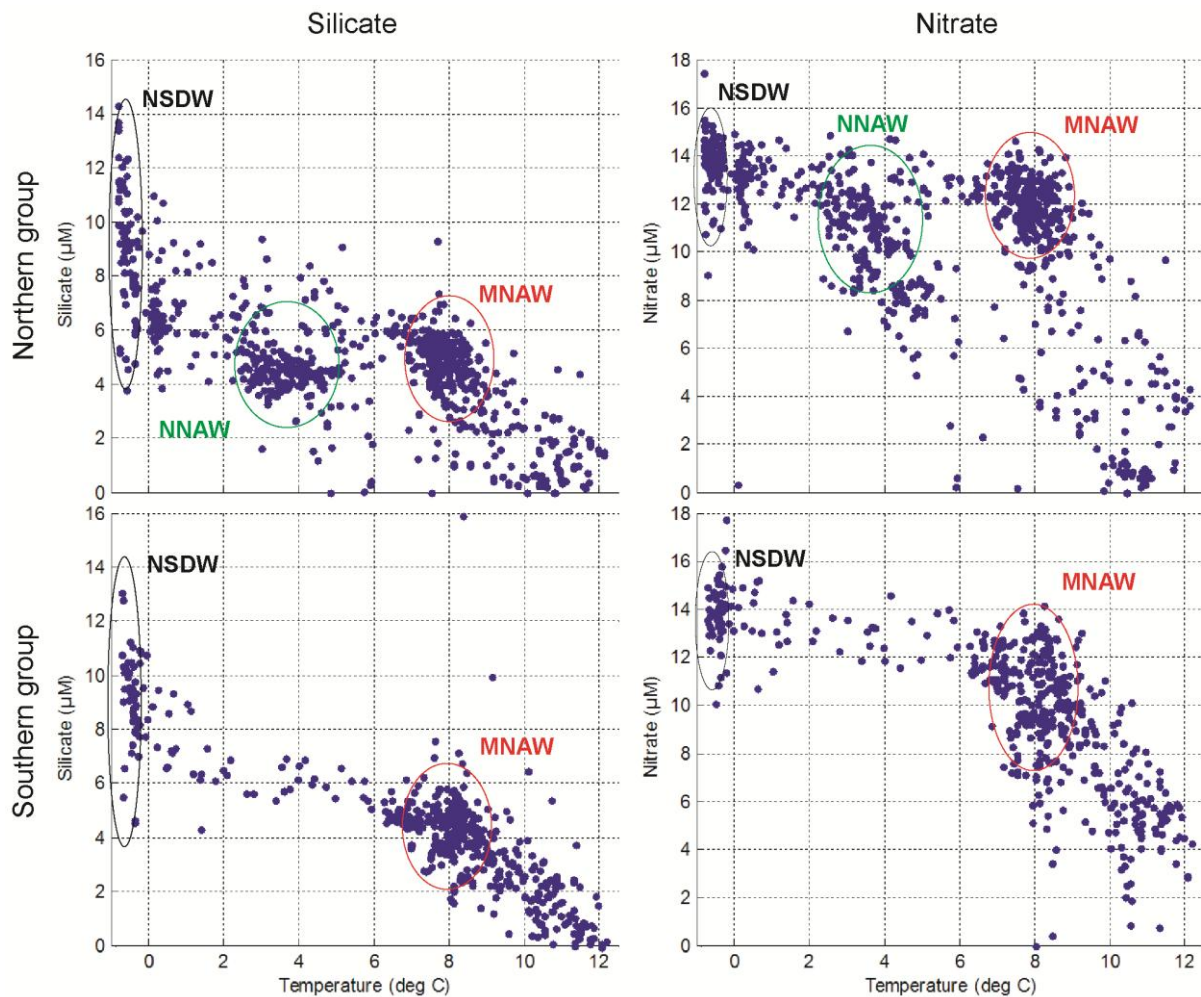


**Figure 17 Nutrient concentrations vs. temperature scatter plots (2013-2020)**

Upper panels: Northern group (stations N04, N05, N13, N14 and R08) and lower panel: Southern group (stations V06 and S08). Silicate in left panels and nitrate in the right panels.

### 5.2.2 Nutrients vs. temperature plots

The basic data structure is, furthermore, illustrated in nutrients vs. temperature scatter plots (Figure 17). The ‘cloud’ of data points in the 7-9°C temperature range - in both groups - reflects MNAW. The additional cloud at 2.5-5°C in the northern group reflects the NNAW and an overlying fresher water mass, located north of the IFF (See Section 5.3.2, below). The very low (growth limiting) values are generally observed for temperatures exceeding 9-10 °C, except from a few samples from the freshwater stratified mixed layer at Section N. There is a wide spread in the silicate concentrations in

the deep (cold,  $< 1\text{ }^{\circ}\text{C}$  and thus dense) large water masses, between  $5\text{ }\mu\text{M}$  and nearly  $15\text{ }\mu\text{M}$  at the northern group. This deep-water spread is less extensive in nitrate (Figure 17) and in phosphate (not shown). The silicate spread is also observed in the overflow water at the southern group, although not as extensive as at Section N. No low-salinity stratification is, as mentioned, observed in the Faroese channels.

Based on the comprehensive and older (MH86, HM86 and MH95) nutrient transects (Sections 4.3 and 4.4) and the above TS-nutrient structure, relevant aspects to further investigate with the new (2013-2020) data are interannual variability in:

**i) Nutrient levels in the Atlantic water (Section 5.4),**

**ii) The seasonal nutrient drawdown (Section 5.5)**

**iii) The deep nutrient variability (Section 0).**

Before this, an overview of the data material is given in Section 5.3.

### **5.3 Oceanographic overview and nutrient data – during three seasons**

Here we provide an overview over the oceanographic conditions at each discussed standard nutrient station (N04, N05, N13, N14, R08, V06 and S08) during the seasons: mid-February, mid-May although occasionally in June, and in the turn of the month August-September. This is done by combining sections V and N into one transect from the Faroe Bank, across the Faroe Plateau and northward into the central Norwegian Sea, and combining section R and S into one transect from the eastern side of the Iceland-Faroe Ridge (IFR), across the Faroe Plateau and across the southern part of the FSC and onto the Scottish slope. These are presented both as averaged sections for T,S, oxygen ( $\text{O}_2$ ), and fluorescence (FI) over the years 2013-2018 (data are available for the most recent years, but these have not been utilized yet), Figure 18-23 and as individual transects (Figs. A2-A36). In addition to the complete transects, profiles of silicate, nitrate, temperature and salinity for all years (2013-2020) are plotted for each standard station, divided into the same three seasons. Standard station N05 is shown in Figure 24 and the other stations are shown in the Appendix (Figs. A37-A42). Key patterns observed at each individual station are described below.

#### **5.3.1 Stations N04 and N05 – the Faroe Current (FC)**

The nutrient stations on Section N are located in contrasting environments. The southern stations (N04 and N05) are, on average, penetrating warm and salty AW in the upper 200-300 m water column, which is clearly identified by its relatively low oxygen content ( $< 9\text{ mg L}^{-1}$ ) (Figure 18-20, panel c). Station N04 reaches down to 600 m depth (Fig. A37), and thus to a complex interplay of waters near the location where the main pycnocline between AW and the underlying subarctic waters typically intersects the Faroe slope seafloor (see Figure 2). Vertical undulations of this interface, partly induced by the intermittent presence of the IFSJ, likely induce much variability to the deep layers here. Station N05 reaches deeper under the AW (Figure 2 and Figure 24), and thus through a ‘sandwich’ of respectively MEIW, NSAIW and NSDW.

February is characterized by weak vertical stratification at both N04 and N05 (Figure 24c,d and A37c,d) and a low standing stock of phytoplankton, here proxied by the fluorescence data (Figure 18d).

The near-surface stratification is still weak in May, although enough to sustain increased primary production. The phytoplankton growth is, however, of episodic nature and probably lower than near the Faroe shelf in south and the region north of the IFF (Figure 19d). The near-surface oxygen concentration, which is a more integrated measure of new primary production than the momentaneous phytoplankton stock (aka Fluorescence), has increased in the near-surface (0-100 m) layer (Figure 19c), and nutrient drawdown in the mixed layer is evident in May (Figure 24e,f and A37e,f).

The AW wedge is not always wide and deep in Aug/Sept, and N05 can experience marked rise of the underlying cold subarctic waters (doming of the isotherms/isopycnals, e.g. Figs. A16 and A17). Such events split the FC into two separated salty and oxygen poor AW cores (which also was evident during June 1986, Section 4.3), and bring a thin and low-saline surface layer towards station N05. This makes temporally averaged TS-transects of Section N during Aug/Sept appear more diffuse compared to the earlier seasons - with a northward extended AW wedge and a 'fresh hat' (Figure 20). The near-surface layer is strongly stratified in Aug/Sept (thermally and/or due to the low-saline layer at N05, Figure 24l), with high FI values (chl concentrations) over N05, which decrease towards the Faroe slope (Figure 20). By Aug/Sept, silicate is exhausted at both stations (Figure 24j and A37j), while nitrate is strongly reduced although not completely exhausted at N05 (Figure 24i). We conclude that primary production is probably higher at N05 than at N04 in August.

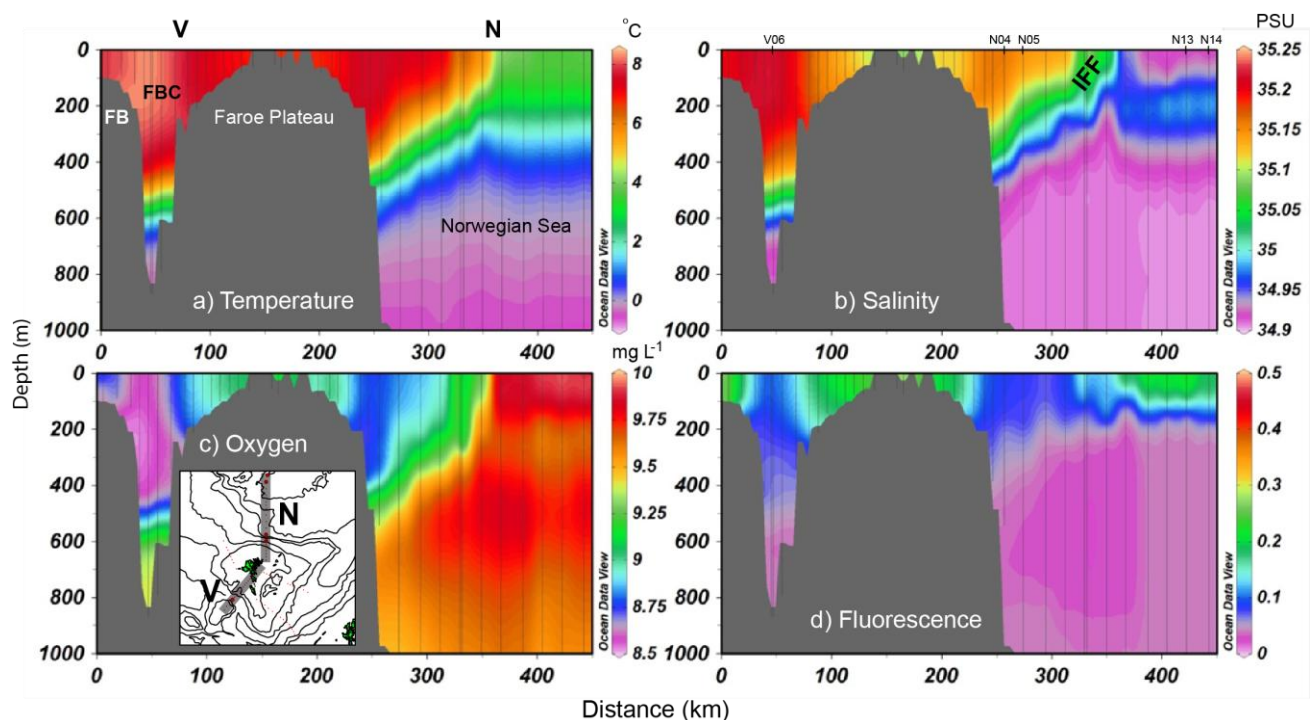


**Figure 18 Combined section V-N, February average (2013-2018).**

(a) Temperature ( $^{\circ}\text{C}$ ), (b) salinity (psu), (c) oxygen concentrations ( $\text{mg L}^{-1}$ ) and (d) fluorescence. The five standard nutrient stations occupied along section V-N (V06, N04, N05, N13 and N14) are shown in b), and abbreviations are provided in Table 1.

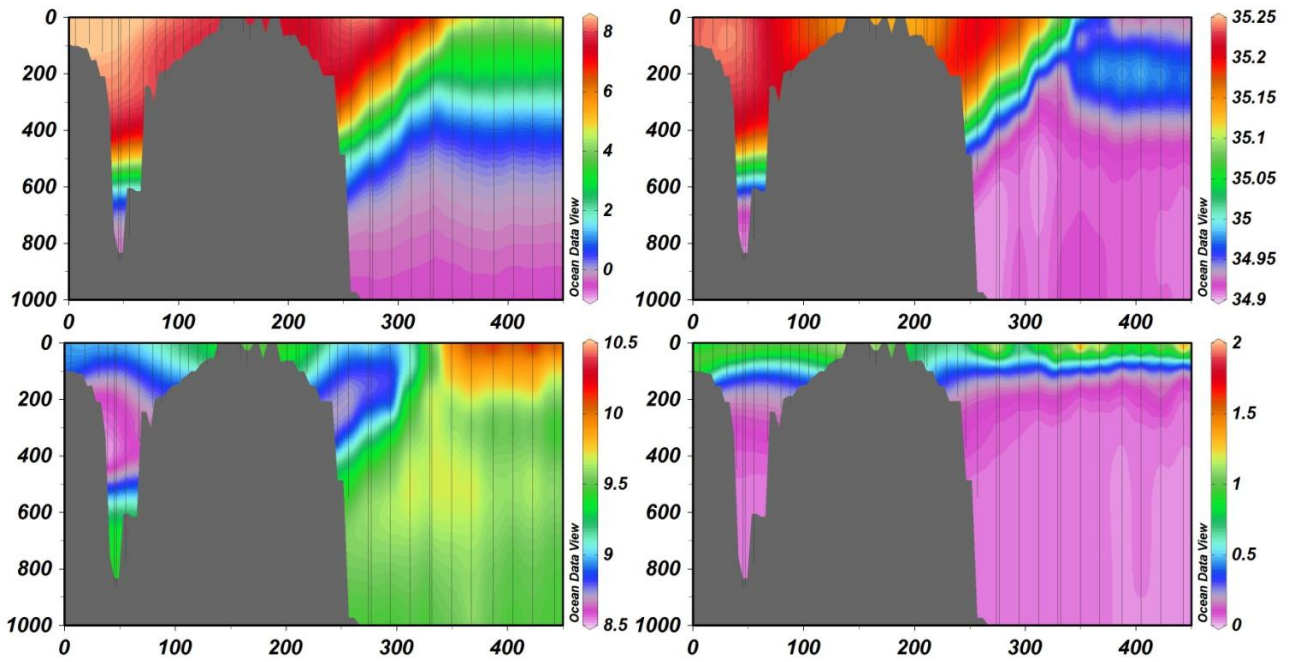


**Figure 19 Combined section V-N, May/June average (2013-2018).**

(a) Temperature ( $^{\circ}\text{C}$ ), (b) salinity (psu), (c) oxygen concentrations ( $\text{mg L}^{-1}$ ) and (d) fluorescence. Axis and panels labels and some annotations are provided in Figure 18. Not that the oxygen colorscale is slightly different from Figure 18, and the colorscale for fluorescence spans wider than in Figure 18d in order to encompass the much higher values during summer.

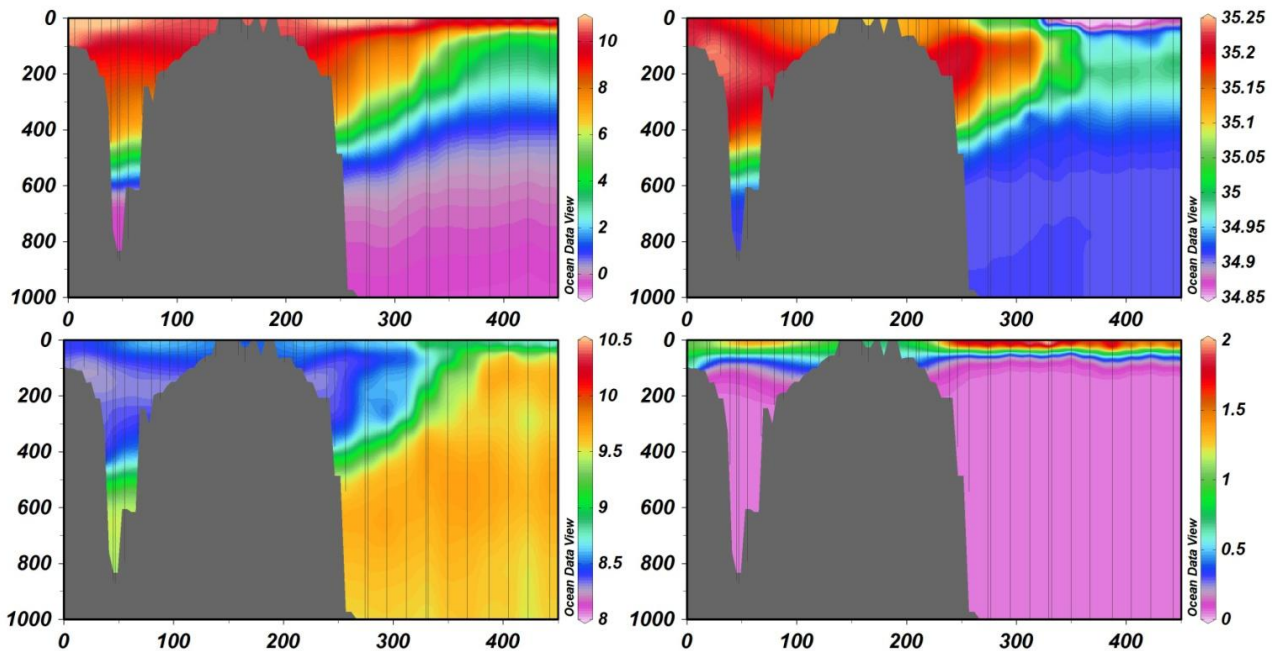


**Figure 20 Combined section V-N, Aug/Sept average (2013-2018).**

(a) Temperature ( $^{\circ}\text{C}$ ), (b) salinity (psu), (c) oxygen concentrations ( $\text{mg L}^{-1}$ ) and (d) fluorescence. Axis and panels labels and some annotations are provided in Figure 18. Not that the oxygen colorscale is slightly different from Figure 18, and the colorscale for fluorescence spans wider than in Figure 18d in order to encompass the much higher values during summer.

### 5.3.2 Stations N13 and N14 – north of the Iceland-Faroe Front (IFF)

These stations are located north of the IFF, which on average is located at 63.6-63.8°N (~ 350 km on the distance-depth sections (Figure 18-20). NNAW occupies the 100-300 m depth layer here, with NSAIW and NSDW constitute the body of the NSG below. A relatively low-saline type of water occupies the 0-100 m layer during all seasons, and the authors are not aware of any formal definition (name and acronym) for this water type. The water column is stratified (haline stratification), even in February (relatively shallow winter mixed layer, Figs. A38 and A39), which leads to persistent primary production, and the highest oxygen content observed in Faroese waters (Figure 18c). High fluorescence and oxygen levels persist at least until May/June (Figure 19) (Major anomaly in 2017). In Aug/Sept the oxygen concentrations decrease towards the surface north of the IFF, while the oxygen still increases towards the surface south of the front (Figure 20). This suggests that while stratification enhances primary production in the AW in late August, it might impede production farther north due to the more severe nutrient limitation there. Fluorescence values are still high in August, witnessing a remaining biomass of phytoplankton. Nutrient drawdown has started at both stations in May – perhaps more strongly at N14 (Figs. A38-A39e,f) – and by Aug/Sept both stations are completely exhausted of both silicate and nitrate (Figs. A38-A39i,j). The relatively high fluorescence values north of the front, despite the depleted nutrients, suggests potential regenerated production there.

Like at N05, high silicate variability is observed at both stations at 1300 m (Figs. A38-A39b,f,j), where the hydrography is virtually constant. Silicate variability at N14 increases from 1000 m to 2000 m (Fig. A39b,f,j). The nitrate variability at depth is lower than the silicate variability (Figs. A38-A39a,e,i).

### 5.3.3 Station V06 – the Faroe Bank Channel (FBC)

Station V06 is located in the deepest part of the FBC (Figure 1). It penetrates a deep (400-500 m) slab of 'pure' AW, which is warmer, more saline and has lower oxygen content than the AW that surrounds the Faroe plateau (Figure 18-20 and A41). Below the main pycnocline, cold and dense overflow water pours through the channel in a NW direction.

In February, the water column is vertically homogenous deep down into the AW layer, with low primary production (low FI values, Figure 18). FI is slightly increased in May/June, and O<sub>2</sub> increases towards the surface, witnessing active primary production (Figure 19). The phytoplankton stock is, however, highly variable during this mid-summer period, although we have not performed any statistics here, to back up this statement. Relatively weak surface mixed layer has established in Aug/Sept (warm and low-saline), while the vertical temperature gradient tends to increase throughout the AW layer, through the year (Figs. A41k,l). FI in Aug/Sept is higher at station V06 compared to the adjacent Faroe Bank and the vicinity of the Faroe plateau (Figure 20). This is, however, not reflected in correspondingly high O<sub>2</sub>, so the new primary production is probably moderate during late summer. The silicate profiles appear as inverses of the temperature profiles – homogenous in the upper 600 m in February and increased full water column vertical gradient through the season (Figs. A41f,j). Nutrient drawdown has started in May, and silicate is exhausted in Aug/Sept (Fig. A41j). A nitrate residual of about 5 μM, however, remains during fall (Figs A41i).

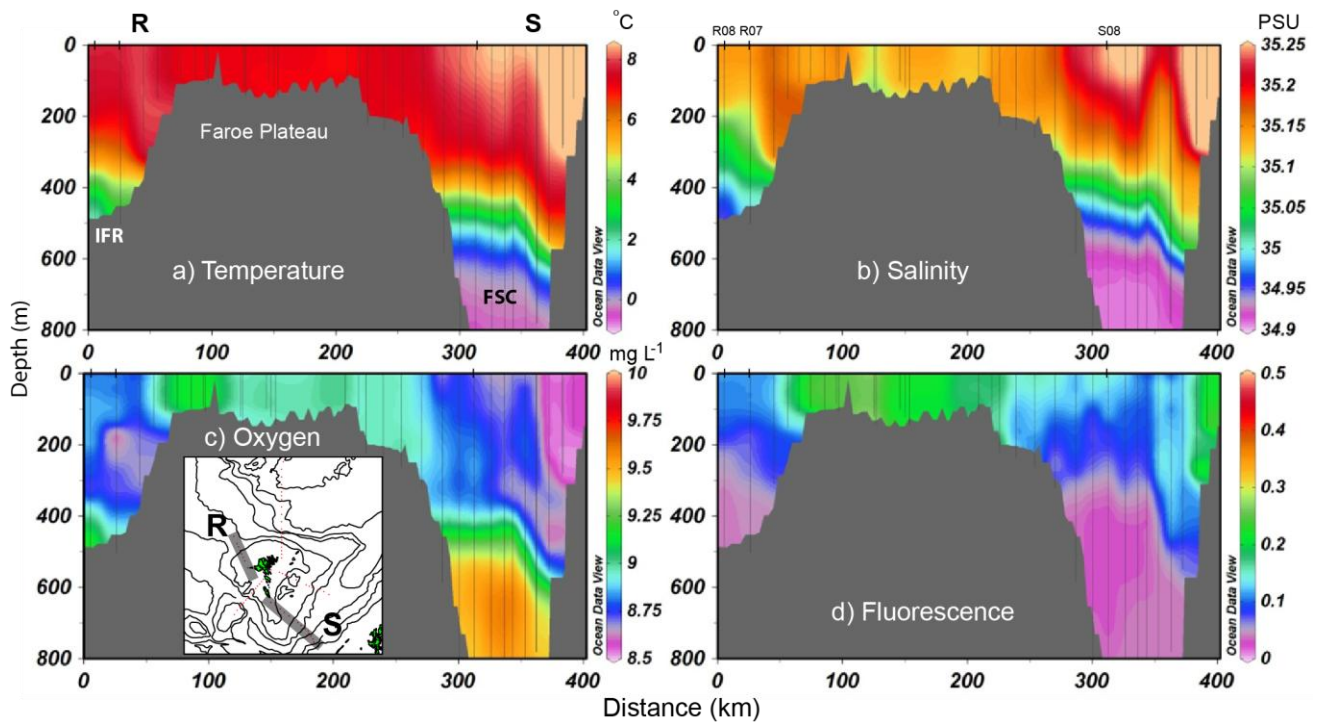


**Figure 21 Combined section R-S, February average (2013-2018).**

(a) Temperature (°C), (b) salinity (psu), (c) oxygen concentrations (mg L<sup>-1</sup>) and (d) fluorescence. The three standard nutrient stations occupied along section R-S (R08, R07 and S08) are shown in b), and abbreviations are provided in Table 1.

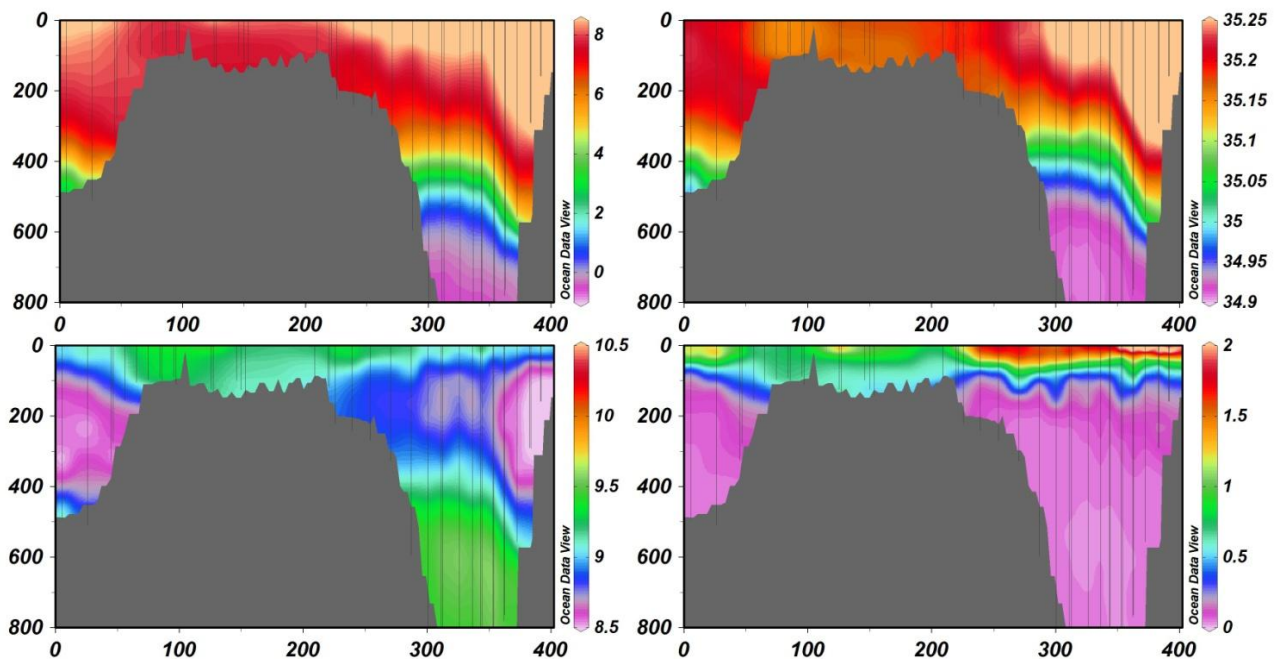


**Figure 22 Combined section R-S, May/June average (2013-2018).**

(a) Temperature (°C), (b) salinity (psu), (c) oxygen concentrations (mg L<sup>-1</sup>) and (d) fluorescence. Axis and panels labels and some annotations are provided in Figure 21. Not that the oxygen colorscale is slightly different from Figure 21, and the colorscale for fluorescence spans wider than in Figure 21d in order to encompass the much higher values during summer.

### 5.3.4 Station R08 – the Iceland Faroe ridge (IFR)

R08 is the off-slope end station on the relatively new (and not always occupied) Section R (Fig. 1). Wedged between near-surface slope-influenced waters to the east, and intermittent overflow type waters (MEIW and/or NSAIW) near the sea-floor in west (Figure 21-23), AW water turns this NW corner of the Faroe plateau towards the FC (Fig. 1). Hydrographic clines rise from the Faroe slope and generally outcrop at the surface near the position of station R08. It is therefore rather ambiguous which waters R08 actually samples.

In February, this station samples a homogenous Atlantic layer in the upper ~ 300 m (Fig. A40), which appears to reside west of a shelf-hugging MNAW current core (high salinity and low oxygen) (Figure 21). Oxygen and FI are generally low during February and the nutrient concentrations are relatively homogenous throughout the near-surface AW (Fig. A40). Oxygen concentrations were, however, elevated in February 2018 when a more than 250 m tall overflow water pulse appears to have enriched even the surface waters with oxygen (Fig. A24). During May/June, the highest salinity on Section R is observed at station R08 (Figure 22), suggesting an off-slope movement of the AW core, and slight thermal and haline stratification appears (Fig. A40). The slanted oxycline is clear during mid-summer, and high FI can be observed at R08 - e.g. during 2015 (Fig. A27) and 2018 (Fig. A30). Stratification is strong in Aug/Sept (Fig. A40), and FI levels are high (Figure 23, however only three sections are available from Aug/Sept). Nutrient drawdown has occurred in Aug/Sept, although weaker than at the Section N stations. Silicate approached limiting concentrations ( $2 \mu\text{M}$ ), while nitrate reaches ca.  $5 \mu\text{M}$  (Figs. A40i,j).

#### 5.3.4.1 Digression on R08 vs. R07

Based on the discussion above, we could expect that station R07, which is located immediately southeast of R08 on Section R, might be closer to a main AW current core. To enable a comparative analysis, both stations were sampled in 2019 (February and August). In February, the upper AW layer at R07 was indeed warmer and saltier than at R08 ( $T = 8.00 \pm 0.01^\circ\text{C}$  vs.  $7.67 \pm 0.01^\circ\text{C}$  and  $S = 35.16 \pm 0.01$  vs.  $35.13 \pm 0.005$ ). The silicate concentration was also higher (and noisier) at R08 ( $\text{Si} = 5.10 \pm 0.47 \mu\text{M}$ ), compared to R07 ( $\text{Si} = 4.72 \pm 0.26 \mu\text{M}$ ) (averages over the 0-200 m depth range  $\pm$  standard deviation). This suggests that R08 is located in a region with strong lateral gradients, likely between northward flow of AW from the FBC, and a slightly different class of AW from the southeast of Iceland. Although data uncertainty was large during February 2019 compared to other years (see Fig. A44), this lateral difference of  $\sim 0.4 \mu\text{M}$  is still relatively large, and on the order of the interannual  $S_{\text{AW}}$  variability derived from the R08 data (Fig. A44). R08 reaches more properly down into intermittent IFR overflow type water than R07 does (see Figure 21-23).

Based on these observations, we suggest that nutrient sampling should continue at R08 (rather than switching to R07) because several years of data exists at R08. And it can, in addition, provide valuable information on the IFR overflow. The strong lateral gradients should (see Figure 15), however, be kept in mind, when interpreting derived estimates of  $S_{\text{AW}}$  from this location (see below). Increased vertical resolution sampling near the seafloor would improve the derived overflow water information.

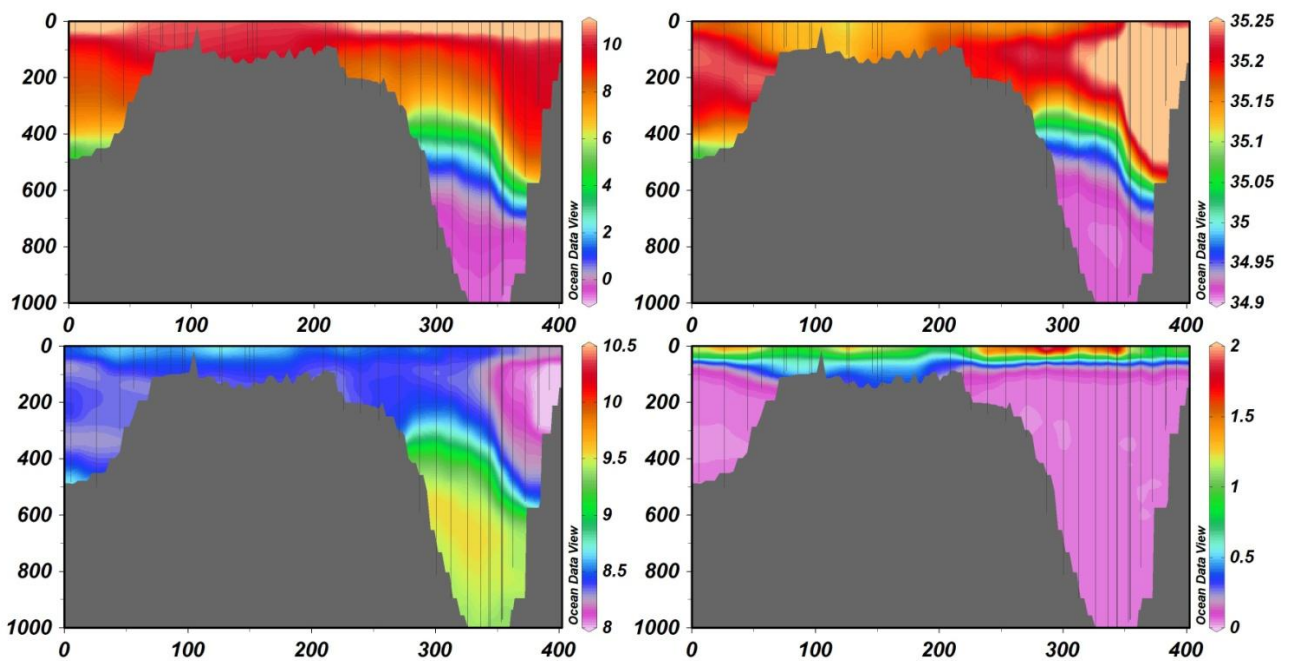


**Figure 23 Combined section R-S, Aug/Sept average (2013-2018).**

(a) Temperature ( $^{\circ}\text{C}$ ), (b) salinity (psu), (c) oxygen concentrations ( $\text{mg L}^{-1}$ ) and (d) fluorescence. Axis and panels labels and some annotations are provided in Figure 21. Note that the oxygen colorscale is slightly different from Figure 21, and the colorscale for fluorescence spans wider than in Figure 21d in order to encompass the much higher values during summer.

### 5.3.5 Station S08 – the southern Faroe-Shetland Channel (FSC)

Station S08 is placed at the deepest location on Section S, which crosses the southern FSC (Figure 1 and Figure 21b). Steep isotherms and isohalines, and a clear oxygen-low blob, show that this station is, on average, located at the off-slope flank of the Slope Current (Berx et al., 2013) (Figure 21-23). This current branch carries true AW (warmer and saltier than the AW discussed in this report, which in reality is MNAW, Hansen and Østerhus, 2000) towards the Norwegian slope (Fig. 1). There can, nevertheless, be large deviations from this average picture; e.g. a wide AW wedge was observed during May 2013 (Fig. A25) and February 2014 (Fig. A21), and a narrow wedge was observed during February 2017 and February 2018 (Figs. A23-A24). Spatial shifts in this major current will strongly influence the samples taken at station S08, which complicates the interpretation of data from this station.

The upper mixed AW layer is relatively shallow in February ( $\sim 250$  m, Fig. A42), and primary production is usually low (low Flu and  $\text{O}_2$ , Figure 21). A temperature gradient throughout the upper 1000 m characterizes this station and its steepness increases through the season (Figs. A42g,k). Primary production has increased much in May/June (Figure 22), and the silicate profiles gradually increase with depth – inversely of the temperature profiles (Fig. A42).

Similar to the above mentioned contrast across the IFF, the overall increased stratification in Aug/Sept leads to increasing  $\text{O}_2$  towards the surface (increased primary production) on the NW part of the Faroe Plateau (Section R), but decreasing near-surface oxygen content near the Scottish slope (Figure 23). The waters north of the Faroe have a higher nutrient content and may benefit from stratification, while the waters north of Scotland/Shetland experience oligotrophy – which enhances with stratification. Station S08 is located in a transition zone between these contrasting regions. The

waters between S08 and the south Faroe slope contain much more near-surface phytoplankton (higher FI), compared to the region between S08 and the Scottish slope (Figure 23). Silicate is depleted in Aug/Sept, while a nitrate residual of about 5  $\mu\text{M}$  remains (Figs. A42i,j).

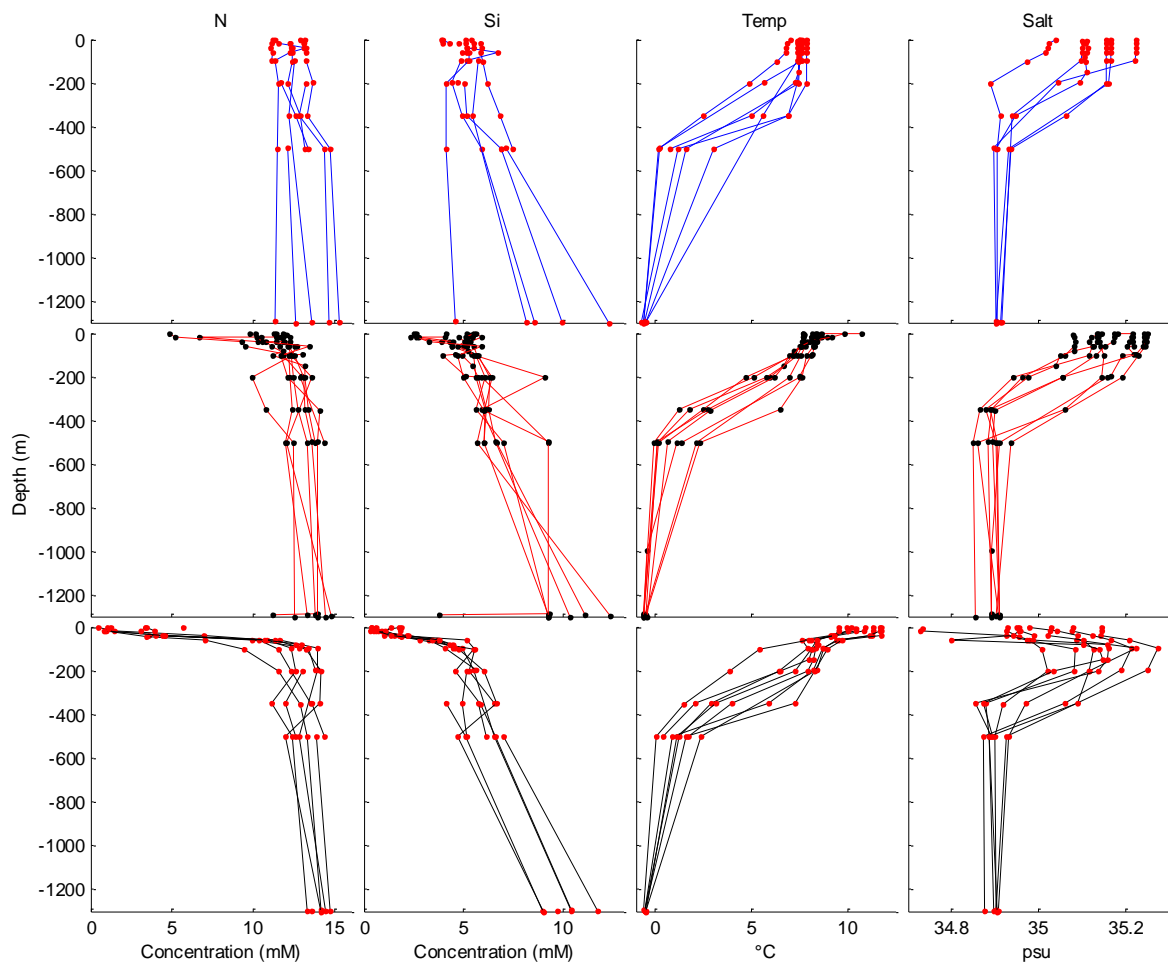


**Figure 24 Individual profiles from standard station N05 during the years 2013-2020.**

nitrate (left, N), silicate (middle left, Si), temperature (middle right) and salinity (right)

Upper row: Mid-February, middle row May-June and lower row: August-September. Corresponding figures for the other standard nutrient stations are shown in the Appendix.

#### 5.4 Pre-bloom nutrient content in MNAW

The potential for generating reliable time series of nutrient concentrations in the poleward flowing Atlantic water is tested by averaging all samples taken in the MNAW temperature range, 6.5-9°C (Hansen and Østerhus, 2000). The cut off at 9°C should minimize the nutrient decreasing influence of samples made in the spring/summer mixed layer. The average (2013-2020) AW nutrient concentrations, average standard deviations and average number of samples underlying these statistics, are in Table 4 provided for each standard station, and each of the three seasons (Feb, May/June, Aug/Sept).

### 5.4.1 Seasonal silicate statistics

The estimates of silicate concentrations in the MNAW ( $S_{AW}$ ) for February are slightly higher than the estimates for May, likely caused by silicate utilization in the AW layer, and/or inclusion of samples in an emerging surface mixed layer (which is difficult to robustly avoid). The difference between the February and May estimates is generally below 0.3  $\mu\text{M}$ , apart from one or two outlier years. This is also reflected in the lower standard deviations in February, compared to May. The  $S_{AW}$  estimates for Aug/Sept are less reliable, with high standard deviations (Std) and low sample numbers ( $N$ ). The standard deviation is, naturally, only calculated for estimates with  $N > 1$ . The availability of only a single sample frequently occurs in August, which is caused by the strong vertical temperature gradient where only few samples fall in the MNAW temperature range ( $6.5^\circ\text{C} < T < 9^\circ\text{C}$ ). The characteristics are different at each station, and the spread in the averaged values of  $S_{AW}$ , std and  $N$  are not provided in Table 4. AW does not reach N13 and N14, and these stations are therefore not included in this table.

**Table 4 Average (2013-2020) Atlantic water ( $6.5^\circ\text{C} < T < 9^\circ\text{C}$ ) silicate concentrations for each season and at each standard station.**

The average number of samples included in the estimates ( $N$ ), and the standard deviations (Std) are also shown. Months with only one sample ( $N = 1$ ) do not contribute to the standard deviation calculation.

| Station | February                           |      |      | May                                |      |      | Aug/Sept                           |      |      |
|---------|------------------------------------|------|------|------------------------------------|------|------|------------------------------------|------|------|
|         | Average $S_{AW}$ ( $\mu\text{M}$ ) | Std  | N    | Average $S_{AW}$ ( $\mu\text{M}$ ) | Std  | N    | Average $S_{AW}$ ( $\mu\text{M}$ ) | Std  | N    |
| N04     | 5.08                               | 0.26 | 3.71 | 5.11                               | 0.55 | 5.71 | 4.49                               | 0.93 | 2.86 |
| N05     | 5.12                               | 0.32 | 4.14 | 4.98                               | 0.55 | 5.5  | 4.52                               | 0.75 | 2.25 |
| R08     | 5.46                               | 0.25 | 4.6  | 4.42                               | 0.96 | 4.5  | 4.98                               | 0.78 | 2.75 |
| V06     | 4.50                               | 0.29 | 6.33 | 4.00                               | 0.83 | 4.43 | 5.32                               | 0.43 | 1.71 |
| S08     | 4.43                               | 0.37 | 3.5  | 3.92                               | 0.62 | 2.5  | 5.01                               | NaN  | 1    |

### 5.4.2 Interannual variability

Details of both seasonal and interannual characteristics, together with statistics for each survey, are shown as boxplots – one for each standard station. The boxplot for station N05 is shown in Figure 25, while those for the other stations are shown in Figs. A43-46. The upper panels in these figures show data from mid-February, the middle panels show May data, and the lower panels show February and May data, combined. In agreement with Table 4, the spread in data (boxes, edged by the 25<sup>th</sup> and 75<sup>th</sup> percentiles) is lowest for the February data. At the most comprehensively sampled stations (N04, N05 and V06) (Figure A43, Figure 25, and A45, respectively), the interannual variability is similar for February and May. The data coverage has been less reliable at station R08 and S08 – some years with only February data, some years with only May data and a few years with both (Figs. A44 and A46).

To enable a comparative discussion on interannual  $S_{AW}$  trends, the medians at each station are summarized for February only (Figure 26a) and February and May combined (Figure 26b). Inclusion of the May data alters some aspects, although the principal patterns remain the same.  $S_{AW}$  is highest, and most interannually variable, at the Section N stations. The concentrations were highest at N05 up to 2017, where after the highest  $S_{AW}$  values are observed at N04.  $S_{AW}$  in the FC was about 5.2-5.5  $\mu\text{M}$  in 2013, dropped to around 4.2  $\mu\text{M}$  in 2014 and 2015, and increased to nearly 6  $\mu\text{M}$  in 2017-

2018. All nutrient stations experienced a  $S_{AW}$  peak in 2018 (N05 peaked in 2017, albeit still high values in 2018), a drop in 2019 followed by a slight increase in 2020.

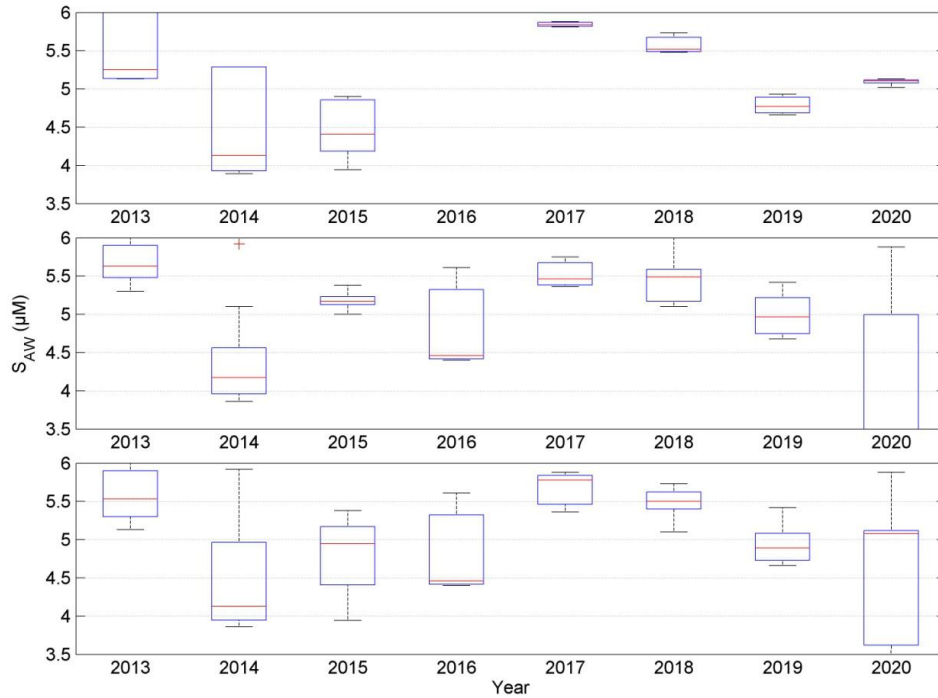


**Figure 25 Boxplots for silicate samples taken at station N05.**

Upper panel: Mid-February, mid-panel: May-June and lower panel: the two seasons combined. The red central mark is the median, the edges of the boxes are the 25th and 75th percentiles, the whiskers extend to the most extreme data points the algorithm considers to be not outliers, and the outliers are plotted individually (from the Boxplot.m routine in Matlab®). Corresponding figures for the other standard nutrient stations are shown in the Appendix (Figures A43-A46).

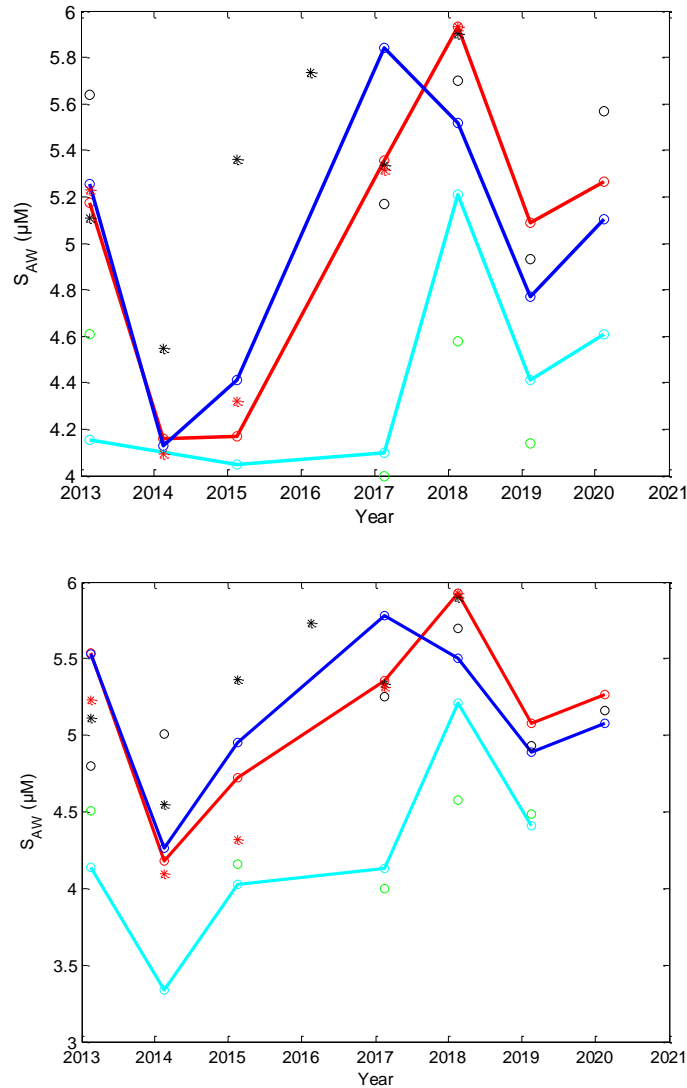


**Figure 26 Estimates of the pre-bloom silicate content in Atlantic water ( $S_{AW}$ ).**

This is shown for the individual standard nutrient stations. N04 (red), N05 (blue), R08 (black circles), V06 (cyan) and S08 (green circles). Upper panel shows February only and lower shows February and May/June combined. The red and black asterix stars show previously published pre-bloom silicate records from, respectively, standard station N04 and a station southeast off the Iceland slope (ST5) (Jacobsen et al., 2019). Note that the scales in the two panels are slightly different.

The February values at IFR station (R08) are at level with the FC stations, while the May values at this station in 2013 and 2014 appear unreliable (see weak statistics, Fig. A44).

Apart from the 2018 peak, the values in the west and south (V06 and S08) lie around 4  $\mu\text{M}$ , and are therefore significantly lower than at the IFR and in the FC (Figure 26). The May 2014 estimate in the FBC (no February data available this year) suggest exceptionally low silicate concentrations this year.

At station N04, our  $S_{AW}$  estimate (based on the temperature envelope of MNAW), is very close to the nutrient series presented by Jacobsen et al. (2019), calculated as an average over the 15-200 m depths, and thus over AW (Figure 26a). While the difference between the February and May estimates are generally below 0.3  $\mu\text{M}$ , there was a large discrepancy at the FC stations in 2015,

when the May estimate was 0.6  $\mu\text{M}$  and 0.8  $\mu\text{M}$  higher than the February estimate for stations N05 and N04, respectively. The combined Feb-May value is therefore lifted (cf. Figure 26a,b), which means that a representative silicate concentration north of the Faroes during spring 2015 might be higher than presented in Jacobsen et al. (2019). This also would be in better compliance with the pre-bloom silicate record off the southeastern Iceland slope (station ST5, Jacobsen et al. 2019) (Figure 26). It is worth mentioning that anomalously deep winter convection took place during the winter 2014-2015, which likely induced large nutrient upwelling in the NE Atlantic (Hátún et al., 2021b). There is an advective time-lag from Icelandic waters to the Faroe Current (Larsen et al., 2012), and it is therefore plausible that enhanced Si concentrations were more evident in Faroese water later in the year.

### 5.4.3 Nitrate and phosphate

Interannual variability is also evident in the AW concentrations in both nitrate ( $N_{\text{AW}}$ ) and phosphate ( $P_{\text{AW}}$ ) (Figure 27). These changes are coherent for both of these nutrients and at all stations. In May, this signal has vanished in nitrate, but appears more robust for phosphate (Figs. A47-A51). Like for  $S_{\text{AW}}$ ,  $N_{\text{AW}}$  is highest at the Section N stations (and the values below refer to these stations), slightly lower at the IFR station (R08) and even lower at V06 and S08.  $N_{\text{AW}}$  was relatively low in 2013 and 2014 ( $\sim 11 \mu\text{M}$ ), increased sharply to a peak in 2015 (13.2-14  $\mu\text{M}$ ), followed by a decline until 2019, and a second, slightly lower peak (13-13.5  $\mu\text{M}$ ), in 2020 (Figure 27a). Phosphate was also high in 2015 (no  $P_{\text{AW}}$  estimate is available for 2013 and 2014), declined until 2019 (although not at N04), followed by a sharp increase in 2020 (Figure 27b). The inter-annual variability in  $N_{\text{AW}}$  differs from  $S_{\text{AW}}$  (Figure 26), which contrasts with the water south of Iceland, where nitrate and silicate generally vary in synchrony (Figure 5). Also note that the interannual variability in  $N_{\text{AW}}$  is higher than the winter concentrations at coastal station Skopun (Figure 6).

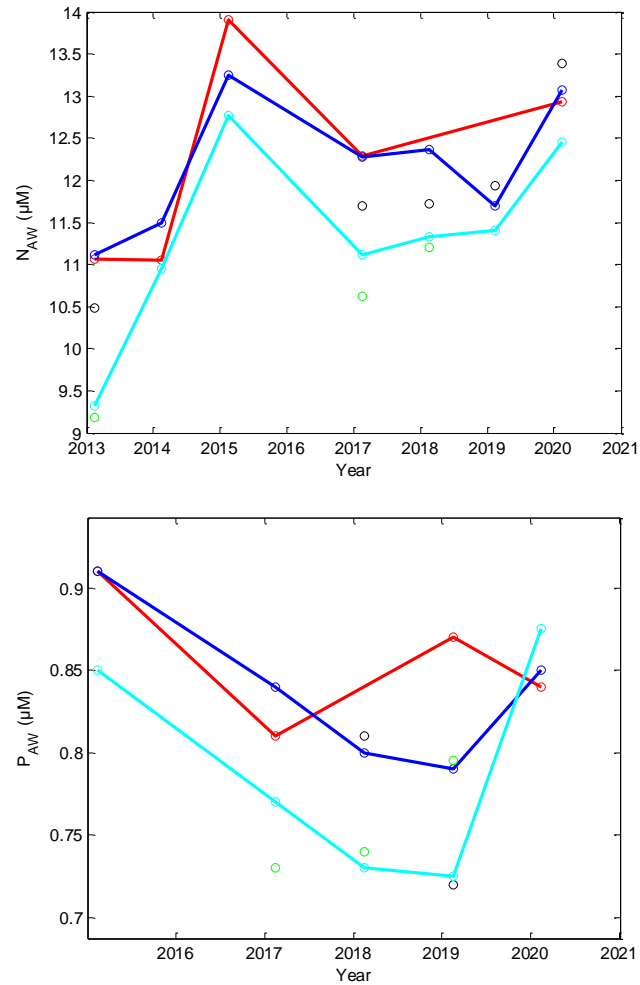


**Figure 27 Pre-bloom nitrate (upper) and phosphate (lower) ( $N_{AW}$  and  $P_{AW}$ ).** This is shown for the individual standard nutrient stations. N04 (red), N05 (blue), R08 (black circles), V06 (cyan) and S08 (green circles). The series are based on February data only.

#### 5.4.4 Comparison with previous $S_{AW}$ and $N_{AW}$ estimates

Comparing with the nutrient samples from June 1986 (Section 4.3.4) we find that the 2013-2020 averaged estimate for  $S_{AW}$  and  $N_{AW}$  have decline by about  $1.7 \mu\text{M}$  ( $6.75$  to  $5.1 \mu\text{M}$  and  $13.6$  to  $11.6 \mu\text{M}$ , see Section 4.3.4) over this roughly 30-years period. This translates to a silicate trend of  $-0.57 \mu\text{M}/\text{decade}$ , and a nitrate trend of about  $-0.66 \mu\text{M}/\text{decade}$ . The  $S_{AW}$  and  $N_{AW}$  for May 1995 ( $6.06 \mu\text{M}$  and  $13.10 \mu\text{M}$ , see Section 4.4) were about  $1 \mu\text{M}$  higher than the 2013-2020 averages, which translates to trends for both parameters of about  $-0.5 \mu\text{M}/\text{decade}$ . These trends are comparable to the previously reported silicate trend of  $-0.60 \mu\text{M}/\text{decade}$  along the Norwegian slope (Hátún et al., 2017a), and they are slightly higher than the observed nitrate trend in the waters south of Iceland ( $-0.39 \mu\text{M}/\text{decade}$ , Figure 5). Although data from single years is not sufficient for verifying a multi-decadal trend, it should be mentioned that the nutrient concentrations south of Iceland in 1986 and 1995 were not on one of the marked peaks, which ride on the declining trend. These decline rates should therefore not be overestimates. The 1986 appear more uniform (less noisy) than the newer data, but the standard deviation associated with the old and new  $S_{AW}$  and  $N_{AW}$  estimates are still comparable (see Section 4.3.4 and Table 4).

#### 5.4.5 Conclusions and suggestions regarding the monitoring of $S_{AW}$ and $N_{AW}$

We conclude that despite some uncertainties regarding the silicate sample quality (see Section 4.2.1), meaningful/reliable multi-year time series of  $S_{AW}$  can be derived from these data.  $S_{AW}$  in February is most reliable, while the May estimate can be used to support the February estimate or to complement this for years when no February data are available. The data from Aug/Sept should not be used for estimating  $S_{AW}$ .

All stations should be thoroughly sampled in the Atlantic layer during February, and the samples should be processed, scrutinized, and an estimate of  $S_{AW}$  should be made, as soon as possible after each cruise. If the February  $S_{AW}$  estimate during a given year is found to be reliable, the Atlantic layer sampling effort in the following May could be much trimmed, or skipped altogether. Stations N04, N05 and V06 are the most critical stations. Based on our analysis of both the June 1986 data, May and September 1995 data and the new sampling program (2013-2020), it appears that standard station N04 is at the southern limit for providing representative estimates of  $S_{AW}$  and  $N_{AW}$ . The derived time series from stations N04 and N05 should therefore be considered as representing slightly different waters. Our monitoring should - during a limited period - be complemented by sampling at the new station N04a, which is located between N04 and N05. Based on a combination of these stations, a single optimized  $S_{AW}$  and  $N_{AW}$  estimate for the FC should be produced. TS-profiles from the CTD (the 'down profiles'), immediately prior to making the samples, could also be used as a sampling guide.

Station R08/R07 might provide extra information in the question regarding eastern vs. western source for the Atlantic inflow in the FC (see Section 6 below). If rationalizations are required, the R Section stations would be the first one to discontinue. N13 and N14 are not relevant for this question, since Atlantic water does not reach these northerly placed stations.

### 5.5 Seasonal nutrient drawdown

Oceanic nutrient onwelling must depend on the open ocean-to-shelf nutrient gradient through the spring-summer growth season, as well as the exchange rate of water (Holt et al., 2012). Estimation of possible nutrient onwelling must therefore involve both pre-bloom concentrations and spring/summer nutrient drawdown in the open ocean.

The post-bloom nutrient profiles from the Aug/Sept cruise are here analyzed against the pre-bloom concentrations ( $S_{AW}, N_{AW}$ ), each year. The following parameters are derived from this analysis (see Figure 28): 1) The depth influenced by primary production ( $D_{pp}$ ), 2) the water column integrated nutrient reduction ( $S_{Red}, N_{Red}$ ) and 3) the minimum nutrient concentration ( $S_{min}, N_{min}$ ).

In order to include as much data as possible, we here represent the pre-bloom concentrations by either ( $S_{AW}, N_{AW}$ ), calculated as averages over February and May data - or just the value from one of these seasons, if data from the other season are unavailable. For the stations north of the IFF, with no AW (N13 and N14), we use an average over the 10-200 m water column. The average (2013-2020) pre-bloom (February and/or May) nutrients, are, naturally, comparable to the previously presented  $S_{AW}, N_{AW}$  (compare Table 4 against Table 5).

$D_{pp}$  is obtained by interpolating the Aug/Sept profiles onto 10-m bins, and finding the depth where the Aug/Sept profiles equal the pre-bloom values (see Figure 28). The total silicate reduction is estimated by

$$(S_{Red}) = \int_{D_{pp}}^{10m} (S_{AW} - S(z)^{Aug}) dz$$

where  $S(z)^{Aug}$  is the interpolated fall profile (and similarly for nitrate). Assuming that the oceanic growth is independent of location (1-D model), this metric would equal the total consumption of nutrients by primary production. This assumption is, however, not realistic for the dynamic and spatially heterogeneous waters around the Faroes.  $S_{min}, N_{min}$  are simply the lowest values in the vertically interpolated profiles. If few samples are available in the mixed layer, the linear interpolation can render negative nutrient values at the shallowest bin (10 m). In such cases, the minimum value is set to zero.

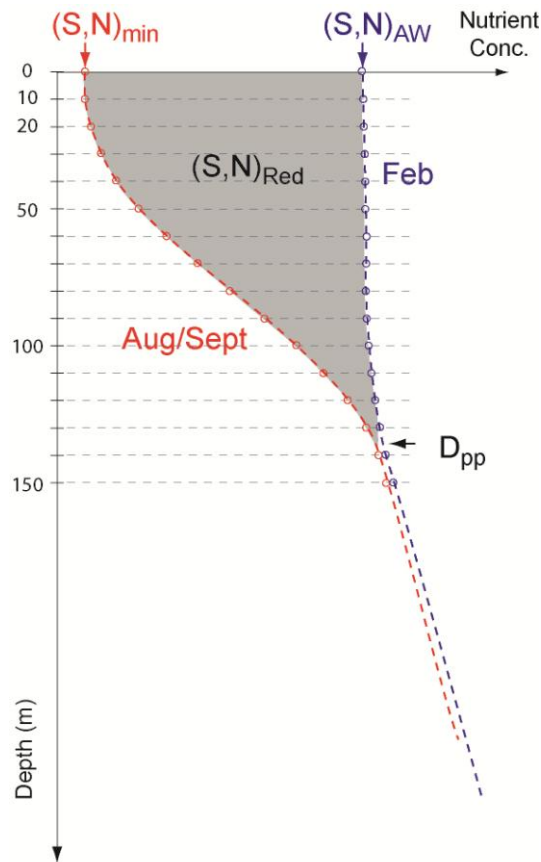


**Figure 28 Sketch of nutrient drawdown parameters**

### 5.5.1 Silicate

The silicate values are highest in the FC core and on the IFR (N04, N05 and R08), and somewhat lower both north of the IFF (N13 and N14) and in the Faroese channels (V06 and S08) (Table 4). All stations, (perhaps except R08) experience silicate limitations in late August ( $[Si] < 1\mu M$ ). The growth-influenced depth,  $D_{pp}$ , is about 200 m for all stations, except N13 and N14, where it is closer to 100 m, likely caused by the low-salinity near-surface layer (See 5.3.1). The integrated silicate reduction,  $S_{Red}$ , is highest in the FC core stations N04 and R08 (270-290  $\mu M \cdot m$  or  $\mu mol m^{-2}$ ), about 230-250  $\mu mol m^{-2}$  in the other AW stations and lower north of the IFF (140-160  $\mu mol m^{-2}$ ).

**Table 5 Average silicate drawdown**

|     | $S_{AW}$ ( $\mu\text{M}$ ) | $S_{min}$ ( $\mu\text{M}$ ) | $D_{pp}$ (m) | $S_{red}$ ( $\mu\text{mol m}^{-2}$ ) |
|-----|----------------------------|-----------------------------|--------------|--------------------------------------|
| N04 | $5.29 \pm 0.18$            | $0.97 \pm 0.32$             | $213 \pm 36$ | $293 \pm 42$                         |
| N05 | $5.03 \pm 0.24$            | $0.71 \pm 0.24$             | $164 \pm 25$ | $229 \pm 25$                         |
| N13 | $4.40 \pm 0.14$            | $0.67 \pm 0.26$             | $84 \pm 10$  | $130 \pm 42$                         |
| N14 | $4.38 \pm 0.13$            | $0.44 \pm 0.36$             | $127 \pm 24$ | $159 \pm 21$                         |
| R08 | $4.84 \pm 0.33$            | $1.48 \pm 0.27$             | $202 \pm 21$ | $267 \pm 38$                         |
| V06 | $4.25 \pm 0.27$            | $0.53 \pm 0.15$             | $187 \pm 27$ | $235 \pm 85$                         |
| S08 | $3.91 \pm 0.49$            | $0.80 \pm 0.51$             | $207 \pm 44$ | $247 \pm 64$                         |

Interannual variability is evident in these metrics. The pre-bloom silicate concentration north of the IFF roughly follows the previously described  $S_{AW}$  changes, relatively high in 2013, dropped abruptly in 2014, increase again until 2018 followed by a subsequent decline (Fig. A52). Considering averages over all standard nutrient stations (Figure 29), the silicate growth depth  $D_{pp}$  was rather deep in 2013, declined until 2016, deepened again to ~220 m in 2018 and became shallower ones more in 2019-2020.

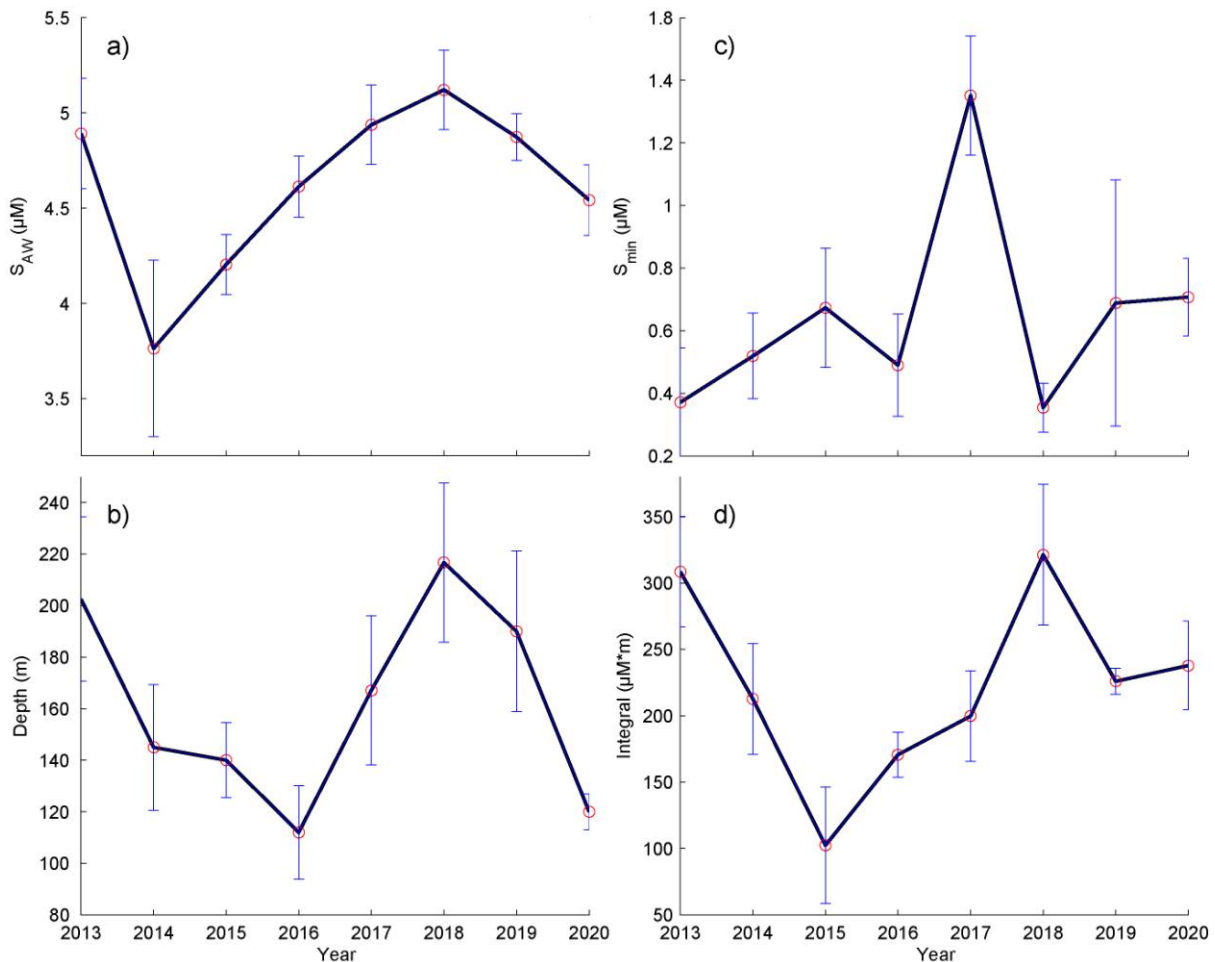


**Figure 29 Averaged silicate drawdown parameters.**

(a) pre-bloom concentrations, (b) growth-influenced depth,  $D_{pp}$  (c) minimum concentration in August,  $S_{min}$  and (d) integrated reduction,  $S_{Red}$ . These have been averaged over all relevant standard stations (N04, N05, R08, V06 and S08), and the associated standard deviations are marked with the vertical blue lines.

This coherent variability resulted in large integrated silicate reduction,  $S_{Red}$ , in 2013 and 2018, and the lowest  $S_{Red}$  in 2015.  $S_{min}$  reveals diatom growth limiting silicate concentrations during all years – except in 2017. During this anomalous year, the concentrations did not go below 1.5  $\mu\text{M}$ , except in the FBC (V06) and in highly stratified waters, far north of the IFF (N14) (Fig. A52).

### 5.5.2 Nitrate

The average pre-bloom nitrate concentrations are  $\sim 12 \mu\text{M}$  near the FC core (R08, N04 and N05),  $\sim 11 \mu\text{M}$  in the Faroese channels (V06 and S08) and 10-11  $\mu\text{M}$  north of the IFF (N13 and N14) (Table 6). Nitrate becomes growth limiting north of the IFF, marginally limiting near FC core ( $N_{min} = 1.8\text{-}2.4 \mu\text{M}$ ), and not limiting on the IFR (R08) and in the Faroese channels ( $N_{min} = 4.5\text{-}5.0 \mu\text{M}$ ). The growth depths for nitrate are 80-180 m, and thus generally shallower than those associated with silicate. The integrated nitrate reduction  $N_{Red}$  is, however, larger than  $S_{Red}$ , caused by the higher pre-bloom nitrate concentrations. The trend in pre-bloom nitrate concentrations was different from the silicate variability these years (cf. Figure 27 and A53, see also Section 5.4). This was, as mentioned, a surprise, since the corresponding data from south Iceland waters ( $S_{FX9}$  and  $N_{FX9}$ , Figure 5) generally co-vary. This leaves open the question, whether we should expect  $S_{AW}$  and  $N_{AW}$  (in Faroese waters) to be correlated or not. Like for silicate, the year 2017 is also characterized by high  $N_{min}$  and thus much residual nitrate after the summer production season (Figure A53). This stands in contrast to the peak in PPI during 2017, which reflects very low summer concentrations of nitrate on the Faroe shelf.

**Table 6 Average nitrate drawdown**

| Mean | $N_{AW}$ ( $\mu\text{M}$ ) | $N_{min}$ ( $\mu\text{M}$ ) | $D_{pp}$ (m) | $N_{red}$ ( $\mu\text{mol m}^{-2}$ ) |
|------|----------------------------|-----------------------------|--------------|--------------------------------------|
| N04  | $11.50 \pm 0.35$           | $2.38 \pm 0.37$             | $122 \pm 49$ | $449 \pm 40$                         |
| N05  | $11.78 \pm 0.30$           | $1.82 \pm 0.69$             | $113 \pm 26$ | $445 \pm 34$                         |
| N13  | $9.81 \pm 0.33$            | $1.21 \pm 0.48$             | $84 \pm 22$  | $341 \pm 48$                         |
| N14  | $10.50 \pm 0.36$           | $0.64 \pm 0.08$             | $76 \pm 12$  | $372 \pm 39$                         |
| R08  | $11.43 \pm 0.14$           | $4.61 \pm 0.23$             | $98 \pm 14$  | $325 \pm 13$                         |
| V06  | $10.93 \pm 0.46$           | $5.06 \pm 0.32$             | $177 \pm 32$ | $396 \pm 68$                         |
| S08  | $10.98 \pm 0.27$           | $4.55 \pm 0.76$             | $145 \pm 22$ | $271 \pm 61$                         |

### 5.5.3 Pre- and post-bloom nutrient concentrations and the PPI

There is only a weak link between the average pre-bloom silicate concentrations (roughly  $S_{AW}$ ) and the PPI, for the period 2013-2020 (Figure 30). The minor PPI peak in 2014 contrasts with a very low  $S_{AW}$  value (as well as with the mentioned low value for  $S_{FX9}$  in 2014, Figure 5, Section 4.1). The generally elevated  $S_{AW}$  (and  $S_{FX9}$ ) during the years 2016-2019 does, however, follow a general elevation in the PPI these years. The only major PPI peak during the 2013-2020 occurred in 2017 – the same year as the post-bloom silicate and nitrate residuals were large (high averaged  $S_{min}$ , Figure 30). Due to this peak, the correlation between  $S_{min}$  and the PPI is significant ( $R = 0.79$ ). If this is a causal link (which our time series are still too short to ascertain), it could be interpreted as follows: In 2013, the high  $S_{AW}$  was followed by deep growth (high  $D_{pp}$ ), efficient removal of silicate from the open ocean waters around the Faroes (high  $S_{Red}$ ), and therefore low post-bloom concentrations  $S_{min}$ . The on-shelf primary production, which typically becomes silicate limited during May-June (Eliassen et al., 2017), could therefore not be efficiently resupplied by nutrient onwelling from the open ocean. Most other years might also have been limited by low  $S_{AW}$  and/or high  $S_{Red}$  and therefore low  $S_{min}$ . The only exception was in 2017, when  $S_{AW}$  was high,  $S_{Red}$  was relatively low, resulting in a high

$S_{min}$ . It is therefore plausible that the waters surrounding the Faroe shelf did not experience nutrient exhaustion this year, and nutrient onwelling could therefore support the onshelf primary production throughout the growth season. In this tentative discussion, we should remember that the PPI is based on nutrient draw down until late June, while the other parameters are based on data in late August.

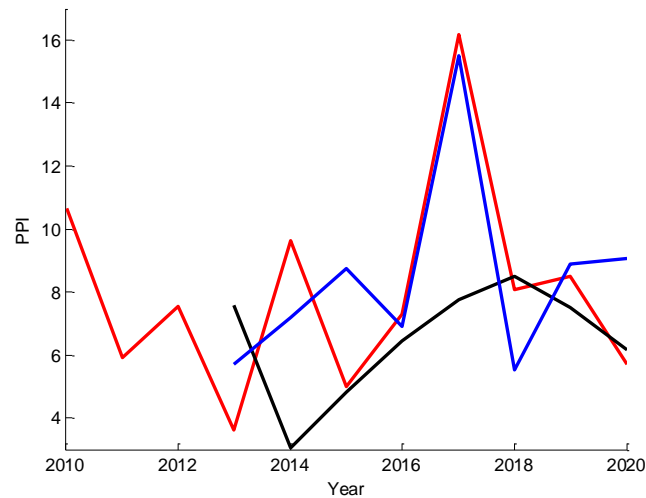


**Figure 30 Open ocean silicate and the primary production index for the Faroe shelf (PPI, red).** Pre-bloom silicate concentration ( $S_{AW}$ , black) and minimum silicate concentration during Aug/Sept ( $S_{min}$ , blue). These latter two records represent averages over all stations, and they are not to scale.

#### 5.5.4 Conclusion and suggestions regarding drawdown

Vertically well resolved near-surface nutrient sampling in Aug/Sept has a potential to provide valuable information – for the open ocean as well as for the Faroe shelf. This sampling effort should therefore continue, at least on the Aug/Sept cruise. If rationalizations are required, the near-surface sampling effort in Feb and May can be reduced, without too much loss of information. To test the robustness of the discussed nutrient profiles, some stations should be revisited several times during a post-bloom season (July-September).

## 5.6 Nutrients at depth

Based on temperature and salinity data, oceanographers often assume that the hydrographic conditions at depth are stable (limited variability). Both the previous nutrient data (from 1986) and the recent data (2013-2020) show – on the contrary – that nutrient concentrations at depth are highly variable. This was the largest surprise, when scrutinizing deep silicate and nitrate records at several locations (different standard stations and depths, Table 7, Figure 2 and Figures. A54-A56). Although some extreme ‘spikes’ are likely due to erroneous samples, the deep signals are not random, and our impression is that most of this deep variability is real. The rather scattered nature of the presented series – in space and time – does not allow for any firm conclusions, but several promising links/hints are evident, as summarized below:

1) Very large and relatively coherent silicate and nitrate variability is observed at 2000 m depth at station N14 (Figures 1 and Figure 31). The most conspicuous event is a nutrient peak in 2015 with more than 14  $\mu\text{M}$  in silicate and nearly 18  $\mu\text{M}$  in nitrate, which in 2016 had dropped to under 6  $\mu\text{M}$  and about 11  $\mu\text{M}$  in silicate and nitrate, respectively. The samples with extreme dips (2015 and 2018) have been scrutinized, and no indication of processing error was identified (pers. Comm. Sólvá Jacobsen). Similar variability (although with weaker fluctuations) is also evident in silicate and nitrate concentrations at 900 m at N14 and at 1300 m and 500 m at station N05. Even nitrate in the FBC (V06 at 500 m, 700 m and 830 m) had a peak in 2015 followed by a decrease in 2016 (Figure 31 and A56). These characteristic inter annual changes are therefore likely real, although the most extreme values should be re-inspected.

2) The silicate and nitrate values at N13 (1300 m) do not show the discussed interannual variability (Fig. A54). Here, the nitrate concentration is about 14  $\mu\text{M}$ , while silicate declined from 12  $\mu\text{M}$  in 2013 to  $\sim 8$   $\mu\text{M}$  during the recent most years. This comes as a surprise, since we, a priori, should expect these to be firmly embedded in NSDW (see Figure 2). At 500 m depths, the silicate and nitrate values at stations N13 and N14 are very similar to each other until 2018, where after the silicate data exhibit rather erratic fluctuations (Fig A54). The most recent silicate data should therefore be re-inspected.

**Table 7 Location from where deep nutrient records are available.**

Abbreviations for the predominant water masses at these locations are also provided (see also Table 1, Table 2 and Figure 2). The upper and lower boundaries of NSAIW are marked as “high” and “low”, respectively.

|     | 500 m           | 700 m         | 830-900 m      | 1050 m         | 1300 m   | 2000 m   |
|-----|-----------------|---------------|----------------|----------------|----------|----------|
| N04 | X (MEIW)        |               |                |                |          |          |
| N05 | X (MEIW)        |               |                |                | X (NSDW) |          |
| N13 | X (NSAIW, high) |               | X (NSAIW, low) |                | X (NSDW) |          |
| N14 | X (NSAIW, high) |               | X (NSAIW, low) |                |          | X (NSDW) |
| V06 | X (MNAW, low)   | X (interface) | X (NSDW)       |                |          |          |
| S08 | X (interface)   | X (interface) |                | X (NSAIW/NSDW) |          |          |

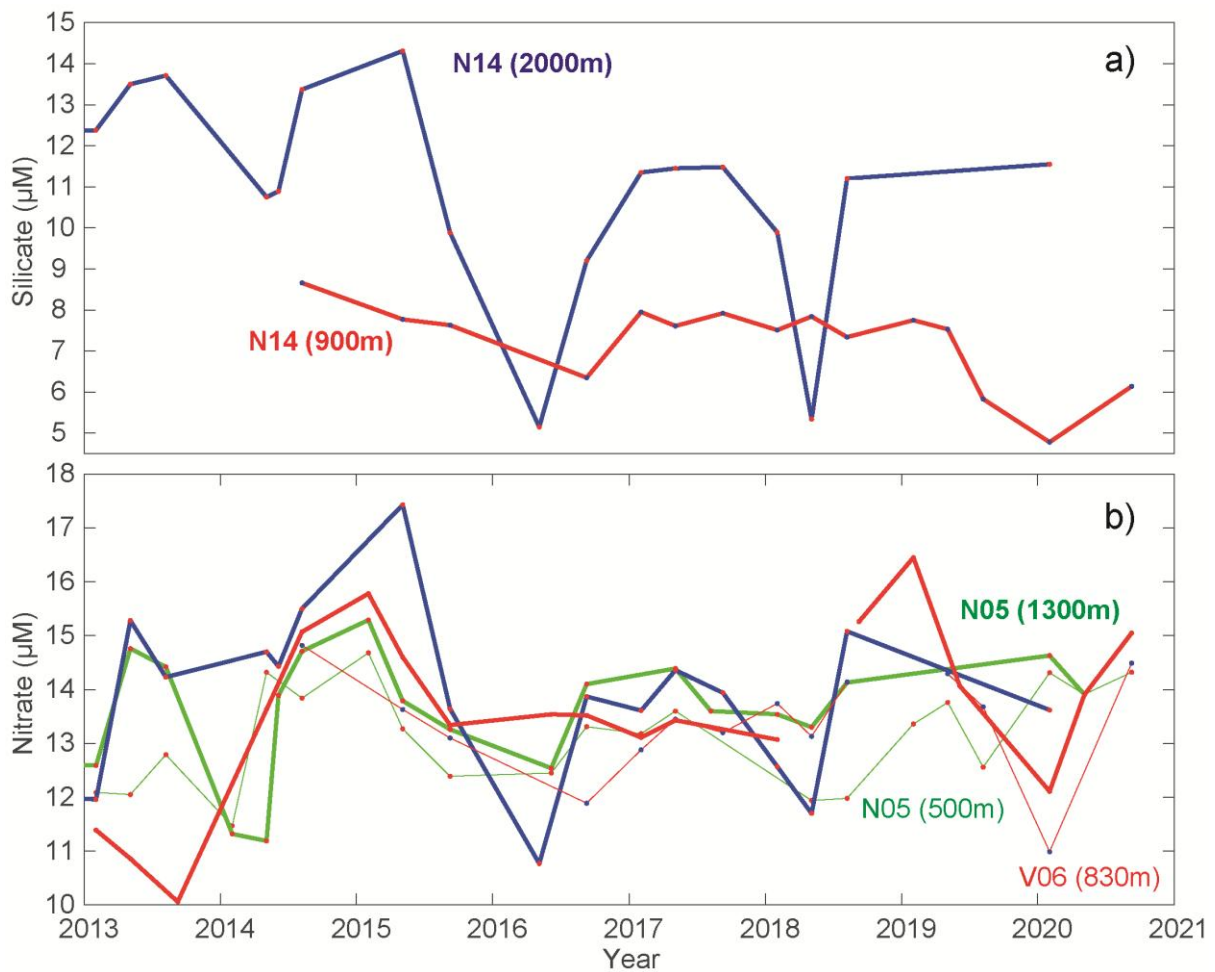


**Figure 31 Principal nutrient signals at depth**

a) Two silicate records and b) selected nitrate records. The sampling locations are presented by the labels in the figure.

3) The nitrate concentrations increased from 2013 to 2020 at several locations [N13 (500 m), N04 and N05 (500 m and 1300 m) and V06 (500 m)], (Figs. A54-A56). Does this suggest that the loss of nitrate in the upper AW accumulated in deeper layers?

4) There was a nutrient drop around 2013-2014, evident in nitrate at stations N04, N05, N14 and V06 and silicate at N05 (Figs. A54-A56).

5) Extremely strong and erratic silicate variability is evident at stations N04 and N05 (500 m), with no correlation between these stations (Fig. A55), while the nitrate signal at these same locations was more coherent. Since this is in the vicinity of the IFSJ, one could speculate if the silicate data capture the intermittent presence of this current jet, while nitrate is less sensitive to these processes.

6) Silicate data at 700 m depth in the FBC render a meaningful interannual signal, while the silicate data at 500 m and 830 m at this location (near the seafloor) do not (Fig. A56). The meaningful silicate variability in the overflow core is, however, dissimilar from all silicate series from north of the Faroe slope. It remains unclear whether this disconnection is due to truly absence of any link, or due to a not optimized sampling strategy.

### 5.6.1 Conclusions and recommendations regarding deep nutrients

The deep nutrient data can provide insight into deep oceanographic processes in the study region, which are not visible in temperature or salinity data. Instead of (or in addition to) making vertical profiles at a few stations (which provides only few deep samples), deep nutrient samples should be taken at 1300 m at all stations on Section N (standard terminal depth of the CTD casts). At the stations where the seafloor is shallower than 1300 m, samples should be taken 50 m over the seafloor. This should be done during every standard hydrographic survey.

## 5.7 Comparison of preservation treatments

In order to address concerns regarding the impact of preservation on nutrient values, we conducted a small method comparison of different preservation protocols on a subset of samples collected during the February hydrographic trip in 2021 (Tur 2106). At five stations we preserved duplicate sets of samples with chloroform, mercuric chloride and freezing at  $-20^{\circ}\text{C}$  on board. Samples were stored for analysis as soon as possible after the cruise (t1: 2 months) and at some interval afterwards (t2: 4 months).

Prior to examining the relative differences in nutrient concentrations as a function of preservative and storage time, we first calculated coefficients of variation (CV) from duplicate measurements determined across all samples included in the comparison ( $n = 30$ ). This was in order to examine the treatment effect relative to the analytical precision of the measurements at the concentrations examined in the study. For nitrate average CV was  $1.7 \pm 1.3\%$  (min: 0.01, max: 5.9). For silicate average CV was  $1.1 \pm 1.0\%$  (min: 0.04, max: 3.4). For phosphate average CV was  $0.5 \pm 0.03\%$  (min: 0.08, max: 1.2).

For nitrate, samples preserved with chloroform were on average 7.6% higher than mercuric chloride and 7.5% higher than freezing, greater than the average CV of  $1.7 \pm 1.3\%$ . The difference between freezing and mercuric chloride was 0.4%, and thus lower than the average CV (Table A1).

For silicate, samples preserved with chloroform were on average 1.7% higher than mercuric chloride and 2.9% higher than freezing, the difference between  $\text{HgCl}_2$  and freezing was 1.1%, thus all values were approximately within the range of analytical precision considering an average CV of  $1.1 \pm 1.0\%$  (Table A2).

For phosphate, samples preserved with chloroform were on average 0.7% higher than mercuric chloride and 1.1% higher than freezing, the difference between  $\text{HgCl}_2$  and freezing was 1.8%, thus all values were approximately within the range of analytical precision considering an average CV of  $0.5 \pm 0.3\%$  (Table A3).

Nitrate values determined after 4 months of sample collection were lower than those determined after two months. Values had decreased by 9.1% for chloroform, 6.4% for  $\text{HgCl}_2$  and 8.2% for frozen samples (Table A4). These differences were all higher than the average CV of  $1.7 \pm 1.3\%$ . Silicate values determined after 4 months were broadly comparable to those determined after 2 months, with differences ranging from -2.4% to 1.9% depending on preservative (Table A5) and within the range of the average CV of  $1.1 \pm 1.0\%$ . Phosphate values determined after 4 months of sample collection were lower than those determined after two months. Values had decreased by 6.1% for chloroform, 6.3% for  $\text{HgCl}_2$  and 8.1% for frozen samples (Table A6). These differences were all higher than the average CV of  $0.5 \pm 0.3\%$ .

## 6 Discussion

Silicate concentration regulates bloom dynamics in the subpolar Atlantic, both in the open ocean (Allen et al., 2005; Henson et al., 2006b) and on shelves (Eliassen et al., 2017a; Holt et al., 2012; Painter et al., 2017; Hátún et al., 2021b). This, in turn influence pelagic fish stocks (Pacariz et al., 2016) and the recruitment to benthic fish stocks on the Faroe shelf (Jacobsen et al., 2019). This, and the fact that silicate concentrations have declined during the last three decades throughout the entire subpolar North Atlantic (Hátún et al., 2021b, 2017a), motivated FAMRI to start regular nutrient monitoring in the open ocean around the Faroe plateau in 2013. The present report is the first description of data from this new nutrient data collection. The monitoring strategy and data quality are assessed in order to evaluate if targets with this monitoring programme are met, and to suggest possible adjustments. Specific conclusions regarding four main topics (pre-bloom nutrient concentrations in the AW, open ocean seasonal nutrient drawdown, ocean-to-shelf nutrient onwelling and nutrients as water mass tracers) have been provided in respective sections (above) and summarized in Section 6.1 below, and will not be reiterated here.

Utilization of nutrient data is more challenging than using conventional temperature and salinity data. Data acquisition using automated electronic instrumentation (like a CTD) are still in its infancy for nitrate and even more so for silicate. Sampling must therefore be done by more cumbersome (time consuming and expensive) methods and the volume of nutrient data is laterally, vertically and temporally much sparser than in TS data collections. The observed nutrient signals are, furthermore, partly induced by water mass variability (physical) and partly by biogenic processes – especially in the near-surface photic zone. Our main *a priori* working hypothesis (before initializing this program in 2013) was that the upper several hundred meter deep water column is well mixed, and thus nutrient enriched, after winter convection, and that this nutrient inventory provides ‘fuel’ for following spring/summer primary production. With this perspective, just a few nutrient samples from the upper ocean would provide ecologically valuable time series, like previously has been done e.g. in the Northern Irminger Sea (Olafsson et al., 2010).

Our 2013-to-present sampling programme has already demonstrated that we can generate meaningful time series of pre-bloom silicate, nitrate and phosphate records for AW around the Faroe Islands ( $S_{AW}$ ,  $N_{AW}$  and  $P_{AW}$ ). There are, however, challenges and uncertainties involved. Winter convection is not as extensive in these waters as it is southwest of Iceland, and we therefore do not have an as deep homogenous water column to sample from around the Faroes. Although the AW (actually MNAW) hydrographic properties are generally considered to be homogenous, there are relatively large nutrient differences between the Faroese channels (FSC and FBC) and the FC north of the Islands – particularly for silicate. Silicate concentrations in the FBC (station V06) are lower than in the FC core (stations N04 and N05), and these latter stations more resemble the nutrient levels in the northern Iceland Basin (Icelandic standard station ST5, (Jacobsen et al., 2019), Figure 26). This suggests that the FC receives much of its water from south of Iceland, which is in compliance with Orvik and Niiler (2002) and Logemann et al. (2013).

The vertically homogenous water column is encountered in the FBC, while the generation of  $S_{AW}$  and  $N_{AW}$  records in the FC is challenged by the variable depth and width of the AW layer (Cisewski et al.,

2021; Hátún et al., 2021a). Care must therefore be taken when choosing samples from stations N04, N04a and/or N05, and the optimal sampling/estimation strategy is yet to be determined. Confluence of the Atlantic source waters to the FC (from the FBC and Icelandic Waters) takes place on the southeastern part of the IFR, and thus near the stations on Section R (R07 and N08, Figure 1). This leads to rather strong lateral gradients in this region, i.e. R07 can be different from R08. Because of this, and since Section R is less frequently occupied compared to section V and N, this region is probably not optimal for providing reliable estimates of  $S_{AW}$  and  $N_{AW}$ . There are, however, other potential benefits from continuing station R08 (assessing the relative contribution of eastern and western AW source waters, seasonal drawdown and nutrients in the IFR overflow). The southern FSC (station V08) is located near the boundary of the European slope current and this region does not develop a deep winter mixed layer. Records of  $S_{AW}$  and  $N_{AW}$ , which are relevant for the Faroe shelf, can therefore probably not be derived from these waters. At all stations, the winter mixed layer is deepest and most homogenous during February, and the influence of primary production is, naturally, least during this season. The February estimates are therefore preferred, but these can be complemented by data from the May cruise, without introducing too much uncertainty.

This report raised some concerns about the quality of especially the silicate data. Rather large differences, both laterally and vertically, are observed. Before plotting, and analysis, clearly erroneous data were removed from the data collection (see Table 3). The long-term and frequently sampled silicate data from station Skopun revealed a marked shift in 2009 (Figure 6), where after they became much 'noisier'. The oceanic data undergo the same processing routines as the Skopun data (see Section 5.1), and it is therefore likely that the increased uncertainty also influences these. A qualitative comparison between our 2013-2020 data collection and the older MH86 and HM86 collections furthermore indicates that the newer data are associated with more noise. The data quality issue must therefore be addressed. Despite this uncertainty, valuable and meaningful results (e.g.  $S_{AW}$ ,  $N_{AW}$  and  $P_{AW}$ ) can, as mentioned, still be extracted.

The high vertical sampling resolution near the surface, made during three seasons (February, May and late August) allows for a tentative assessment of the seasonal nutrient drawdown in the oceanic water around the Faroes. From this we learn that silicate generally becomes exhausted ( $< 2 \mu\text{M}$ ) in all regions during late summer. The only exception was in summer 2017, the year with the highest PPI value during the 2013-2022 period (more on this below). Nitrate is also drawn down to limiting concentrations north of the Faroes, while residual nitrate remains in the Faroese channels throughout the growth season. One viable explanation is that the higher silicate concentrations north of the Faroes allow for more intense primary production, with the capacity to also deplete nitrate, while silicate limitation in the Faroese channels terminates growth before critical nitrate levels are reached.

Does the oceanic nutrient dynamics then influence the Faroe shelf primary production? Interannual variability in the winter nitrate concentrations is identifiable at Skopun, but this is lower than evident in  $N_{AW}$  (at V06 and at both Section N stations). From 2017 and forward, there is a tight link between oceanic and on-shelf concentrations (Figure A57), while the low  $N_{AW}$  values in 2013-2014, and the  $N_{AW}$  peak in 2015 were, however, not observed at Skopun. So is the pre-bloom nitrate concentration around the Faroe shelf as inter-annually variable, as suggested by  $N_{AW}$ ? And does it have a declining trend like south of Iceland Figure 5b, and likely around the Faroe Plateau? If yes,

why is this not observed at Skopun? Possible variability in the oceanic nitrate concentrations and the influence of this on the calculation of the PPI should be considered in the future.

The largest ocean-to-shelf influx likely takes place on the western side of the Faroe shelf (the Western Region) (Eliassen et al., 2017a; Hátún et al., 2013), which suggests that the FBC record should be most relevant for the on-shelf discussion. The FC, however, constitutes the largest nutrient transport, and this current (or its branch the Southern Faroe Current) wraps clockwise around the northern and eastern margin of the plateau, and has a potential to enrich biological production along this margin, and possibly also lead to nutrient onwelling to the central shelf. The winter nutrient concentrations at coastal station Skopun are closer related to the FC stations than to V06 (Figure A57), which suggests the Faroe Current properties have the most direct influence on the Faroe shelf. Interannual variability in the FBC and the FC (as well as the Icelandic stations) is, however, similar (Figure 26).

There are statistically significant correlations between both silicate and nitrate in the south Iceland waters ( $S_{FX9}$  and  $N_{FX9}$ , see Section 4.1) – the main source region for the FC (Logemann et al., 2013), which, as mentioned, likely impacts the Faroe plateau (Figure A57). But this linkage only emerges after linear detrending, since the PPI does not have a long-term trend, which corresponds to the oceanic trends (Figure 5). A general decline in both zooplankton production (Jacobsen et al., 2022), seabird breeding success and populations (Hátún et al., 2017b) and the size of benthic fish stocks (pers. Comm. Petur Steingrund), unfortunately, witness a declining carrying capacity of the Faroe shelf ecosystem during the last several decades. If a revised version of the PPI would reveal a declining trend, then it is possible that the correlation between the oceanic silicate concentrations and the PPI and could be causal. The pre-bloom silicate value ( $S_{AW}$ ) would, however, only enable a rough forecast of the following summer production, since the seasonal oceanic nutrient draw-down must be included in order to explain the most conspicuous peaks in the PPI (Section 5.5.3).

The largest surprise from our initial analysis of the 2013-2020 data collection is the very large nutrient variability at great depths (> 1000 m), where we maybe should expect more quiescent conditions. The first impression was that this extreme variability must be caused by erroneous data, but re-inspection of the data does not suggest this. There is also some coherency in the deep records (Figure 31), which support that this might be a real signal. Large lateral and temporal variability at intermediate depths along Section N could be associated with shifting deep jets, carrying dense nutrient-rich water towards the FSC and the FBC (Chafik et al., 2020; Hátún et al., 2021a; Semper et al., 2020). If this is correct, the nutrient data could complement the conventional TS data in our attempt to better understand the pathways of overflow waters towards the FBC. The even stronger variability at 2000 m depth is an even larger conundrum. The nutrient content is higher in the deep layers of the Norwegian Sea compared to the possible source waters in the Iceland Sea, Greenland Sea and Arctic Ocean, and reasons for this are still not well understood (Onarheim, 2016). If this is associated with geothermally heated and highly silicate rich waters discharged by hydrothermal vents and brought up into the weakly stratified water column by deep overturning cells, it could explain some of the variability. This could, however, not explain why silicate concentrations at 2000 m suddenly should drop below 10  $\mu\text{M}$  (Figure 31). If our deep nutrient data are robust, our perception of the deep layers being occupied by water masses with highly stable nutrient levels must be fundamentally re-considered. Deep sampling and close care with the data quality should be continued in order to clarify this important question.

The method comparison tests between different preservatives did not indicate serious problems with chloroform when compared to mercuric chloride and freezing. In the case of silicate and phosphate, the relative differences in concentration as a function of preservative were in the range of analytical precision of the measurements. However, nitrate values were systematically higher (approx. 8%) with chloroform preservation compared to mercuric chloride and freezing. These differences can be explained either because chloroform is a better preservative for nitrate or due to potential contamination of chloroform with nitrogen. Considering that phosphate values were indistinguishable between preservative treatments, it is possible that chloroform could be contaminated and this should be examined in the future. The comparison of nutrient concentration as a function of storage time revealed that nitrate and phosphate concentrations were systematically lower after four months storage compared to a two- month storage period, whereas silicate values were comparable. In the absence of the possibility to analyse samples on board it is recommended that sample analysis takes place as soon as possible after sample collection, and that the analysis date should be recorded in the database.

## 6.1 Recommendations

Although the nutrient sampling processes are less cumbersome onboard the new R/V Jákup Sverri, compared to R/V Magnus Heinason, there is always a need to optimize the sampling strategy.

We here recommend that:

- All stations should be thoroughly sampled in the Atlantic layer during February, and the samples should be processed, scrutinized, and estimates of  $S_{AW}$  and  $N_{AW}$  should be made, as soon as possible after each cruise.
- If the February  $S_{AW}$  and  $N_{AW}$  estimates during a given year are missing (or found to be unreliable), these can be derived from May data. If the February estimates are found to be reliable, the upper water sampling during May/June shall be reduced to the locations where  $CO_2$  are being taken. High-resolution near-surface sampling in August/September shall continue, on order to address the nutrient draw-down question.
- Key stations for the estimation of  $S_{AW}$  and  $N_{AW}$  are V06, N04, (N04a) and N05.
- The deep nutrient data can provide insight into deep oceanographic processes in the study region, which are not visible in temperature or salinity data.
- Deep nutrient samples should be taken at 1300 m at all stations on Section N (the CTD terminal depth) which are deeper than 1300 m, and 50 m over the seafloor at stations N04 (555 m bottom depth) and N4A (940 m bottom depth).
- Samples should be reinstated at N14 (2000 m) in order to scrutinize the unexpected strong nutrient variability at that location.
- The data quality routines should be carefully scrutinized.
- If the previously occupied November cruise will be reinstated, nutrient samples should also be made during this season (at least once).
- Station S08 should be moved closer to the Shetland slope, in order to capture both overflow water in the Faroe-Shetland Channel Jet (Chafik et al., 2020), and the Atlantic water properties in the slope current (Berx et al., 2013). This should be done on Section E. The positioning of this new FSC standard station could be guided by initial nutrient samples at depth across the FSC (similar to what is suggested for Section N, above).
- Station R08 should be continued.
- Care should be taken to ensure that chloroform is not contaminated with nitrate. This can be achieved by adding chloroform to a blank sample (distilled water or artificial seawater: NaCl solution). Nitrate should be determined on the blank matrix with and without chloroform addition.
- Samples should be analysed as soon as possible after collection and the analysis date recorded in the database.

## 7 Acknowledgements

The authors would like to thank all the scientific and technical staff and all the crew members, who have participated in collecting the nutrient data reported here. Thanks to Ólavur Tyrni Hátún for digitizing data from older reports.

## 8 References

- Allen, J.T., Brown, L., Sanders, R., Moore, C.M., Mustard, A., Fielding, S., Lucas, M., Rixen, M., Savidge, G., Henson, S.A., Mayor, D., 2005. Diatom carbon export enhanced by silicate upwelling in the northeast Atlantic. *Nature* 437, 728–32. <https://doi.org/10.1038/nature03948>
- Aoyama, M., 2018. IOCCP-JAMSTEC 2018 Inter-laboratory Calibration Exercise of a Certified Reference Material for Nutrients in Seawater.
- Aoyama, M., 2015. IOCCP-JAMSTEC 2015 Inter-laboratory Calibration Exercise of a Certified Reference Material for Nutrients in Seawater.
- Berx, B., Hansen, B., Østerhus, S., Larsen, K.M., Sherwin, T.J., Jochumsen, K., 2013. Combining in situ measurements and altimetry to estimate volume, heat and salt transport variability through the Faroe-Shetland Channel. *Ocean Sci.* 9, 639–654. <https://doi.org/10.5194/os-9-639-2013>
- Chafik, L., Hátún, H., Kjellsson, J., Larsen, K.M.H., Rossby, T., Berx, B., 2020. Discovery of an unrecognized pathway carrying overflow waters toward the Faroe Bank Channel. *Nat. Commun.* 11, 1–10. <https://doi.org/10.1038/s41467-020-17426-8>
- Chiswell, S.M., Calil, P.H.R., Boyd, P.W., 2015. Spring blooms and annual cycles of phytoplankton: a unified perspective. *J. Plankton Res.* 37, 500–508. <https://doi.org/10.1093/plankt/fbv021>
- Cisewski, B., Hátún, H., Kristiansen, I., Hansen, B., Larsen, K.M.H., Eliassen, S.K., Jacobsen, J.A., 2021. Vertical Migration of Pelagic and Mesopelagic Scatterers From ADCP Backscatter Data in the Southern Norwegian Sea. *Front. Mar. Sci.* 7. <https://doi.org/10.3389/fmars.2020.542386>
- Cooper, L.H.N., 1955. Deep water movements in the North Atlantic as a link between climatic changes around Iceland and biological productivity of the English Channel and Celtic Sea. *Journal of Marine Research*, 14 (4), 347-362.
- Egge, J.K., Aksnes, D.L., 1992. Silicate as regulating nutrient in phytoplankton competition. *Mar. Ecol. Prog. Ser.* 83, 281–289. <https://doi.org/10.3354/meps083281>
- Eliassen, S.K., Hátún, H., Larsen, K.M.H., Jacobsen, S., 2017a. Faroe shelf bloom phenology – The importance of ocean-to-shelf silicate fluxes. *Cont. Shelf Res.* 143, 43–53. <https://doi.org/10.1016/j.csr.2017.06.004>
- Eliassen, S.K., Larsen, K.M.H., Hansen, B., Rasmussen, T.A.S., 2017b. Phenologically distinct phytoplankton regions on the Faroe Shelf - identified by satellite data, in-situ observations and model. *J. Mar. Syst.* 169, 99–110. <https://doi.org/10.1016/j.jmarsys.2017.01.015>
- Fogelqvist, E., Blindheim, J., Tanhua, T., Østerhus, S., Buch, E., Rey, F., 2003. Greenland-Scotland overflow studied by hydro-chemical multivariate analysis. *Deep. Res.* 50, 73–102.
- Gaard, E., 2000. The plankton community structure on the Faroe Shelf. Dr. philos thesis, University of Tromsø.
- Gaard, E., 1999. Upployst ólívrunnið silikat (No. 3.2, Útgáva 2), Sýnisbókin hjá Umhvørvisdeildini, Umhvørviskannningar.

- Gaard, E., 1996. Phytoplankton community structure on the Faroe shelf. *Fróðskaparrit* 44, 95–106.
- Gaard, E., 1991. Nitrat og Nitrit (No. 3.1, Útgáva 1), *Sýnisbókin hjá Umhvørvisdeildini, Umhvørviskanningar*.
- Gaard, E., Hansen, B., Heinesen, S.P., 1998. Phytoplankton variability on the Faroe Shelf. *ICES J. Mar. Sci.* 55, 688–696.
- Glindø, A.H., 2018. Variability in hydrochemical properties and composition of the dense water in the Faroese Channels. Master Thesis, University of Bergen.
- Grasshoff, K., 1983. *Methods for Seawater Analysis*. Second revised and extended edition. Verlag Chemie.
- Groeger, M., Maier-Reimer, E., Mikolajewicz, U., Moll, A., Sein, D., 2013. NW European shelf under climate warming: implications for open ocean - shelf exchange, primary production, and carbon absorption. *Biogeosciences* 10, 3767–3792.
- Hansen, B., Liljeblad, B., Sjöstedt, S., Sundberg, J., 1987. Report from the cruise with R/V Magnus Heinason to the region north of the Faroe Islands June 1986. No. 17, Gothenburg.
- Hansen, B., Østerhus, S., 2000. North Atlantic–Nordic Seas exchanges. *Prog. Oceanogr.* 45, 109–208. [https://doi.org/10.1016/S0079-6611\(99\)00052-X](https://doi.org/10.1016/S0079-6611(99)00052-X)
- Hátún, H., Azetsu-Scott, K., Somavilla, R., Rey, F., Johnson, C., Mathis, M., Mikolajewicz, U., Coupel, P., Tremblay, J.-É., Hartman, S., Pacariz, S. V., Salter, I., Ólafsson, J., 2017a. The subpolar gyre regulates silicate concentrations in the North Atlantic. *Sci. Rep.* 7, 14576. <https://doi.org/10.1038/s41598-017-14837-4>
- Hátún, H., Chafik, L., Larsen, K.M.H., 2021a. The Norwegian Sea Gyre – A Regulator of Iceland-Scotland Ridge Exchanges. *Front. Mar. Sci.* 8. <https://doi.org/10.3389/fmars.2021.694614>
- Hátún, H., Larsen, K.M.H., Debes, H., 2013. The Western Region, Havstovan Nr.: 13-07, Technical report.
- Hátún, H., Larsen, K.M.H., Eliassen, S.K., Mathis, M., 2021b. Major nutrient fronts in the northeastern Atlantic – from the subpolar gyre to adjacent shelves, in: *Chemical Oceanography of Frontal Zones*. p. Accepted.
- Hátún, H., Olsen, B., Pacariz, S. V., 2017b. The Dynamics of the North Atlantic Subpolar Gyre Introduces Predictability to the Breeding Success of Kittiwakes. *Front. Mar. Sci.* 4. <https://doi.org/10.3389/fmars.2017.00123>
- Henson, S.A., Robinson, I., Allen, J.T., Waniek, J.J., 2006a. Effect of meteorological conditions on interannual variability in timing and magnitude of the spring bloom in the Irminger Basin, North Atlantic. *Deep Sea Res. Part I Oceanogr. Res. Pap.* 53, 1601–1615. <https://doi.org/10.1016/j.dsr.2006.07.009>
- Henson, S.A., Sanders, R., Holeton, C., Allen, J., 2006b. Timing of nutrient depletion, diatom dominance and a lower-boundary estimate of export production for Irminger Basin, North Atlantic. *Mar. Ecol. Prog. Ser.* 313, 73–84. <https://doi.org/10.3354/meps313073>

- Hinrichs, I., Gouretski, V., Pätsch, J., Emeis, K., Stammer, D., 2017. North Sea Biogeochemical Climatology (<https://icdc.cen.uni-hamburg.de/daten/ocean/nsbc/>). World Data Cent. Clim. DKRZ.
- Holt, J., Butenschon, M., Wakelin, S.L., Artioli, Y., Allen, J.I., 2012. Oceanic controls on the primary production of the northwest European continental shelf: model experiments under recent past conditions and a potential future scenario. *Biogeosciences* 9, 97–117.
- Jacobsen, S., Gaard, E., Hátún, H., 2022. Declining Pre-bloom *Calanus finmarchicus* Egg Production Adjacent to Two Major Overwintering Regions in the Northeastern Atlantic. *Front. Mar. Sci.* 9. <https://doi.org/10.3389/fmars.2022.822978>
- Jacobsen, S., Gaard, E., Hátún, H., Steingrund, P., Larsen, K.M.H., Ólafsdóttir, S.R., Poulsen, M., 2019. Environmentally Driven Ecological Fluctuations on the Faroe Shelf Revealed by Fish Juvenile Surveys. *Front. Mar. Sci.* <https://doi.org/10.3389/fmars.2019.00559>
- Jeansson, E., Olsen, A., Jutterström, S., 2017. Arctic Intermediate Water in the Nordic Seas, 1991–2009. *Deep. Res. Part I Oceanogr. Res. Pap.* 128, 82–97. <https://doi.org/10.1016/j.dsr.2017.08.013>
- Johnson, C., Inall, M., Häkkinen, S., 2013. Declining nutrient concentrations in the northeast Atlantic as a result of a weakening Subpolar Gyre. *Deep Sea Res. Part I Oceanogr. Res. Pap.* 82, 95–107. <https://doi.org/10.1016/j.dsr.2013.08.007>
- Kristiansen, I., Gaard, E., Hátún, H., Jónasdóttir, S., Ferreira, A.S.A., 2016. Persistent shift of *Calanus* spp. in the southwestern Norwegian Sea since 2003, linked to ocean climate. *ICES J. Mar. Sci.* 73, 1319–1329. <https://doi.org/10.1093/icesjms/fsv222>
- Kristiansen, I., Hátún, H., Petursdottir, H., Gislason, A., Broms, C., Melle, W., Jacobsen, J.A., Eliassen, S.K., Gaard, E., 2019. Decreased influx of *Calanus* spp. into the south-western Norwegian Sea since 2003. *Deep Sea Res. Part I Oceanogr. Res. Pap.* 149, 103048. <https://doi.org/10.1016/j.dsr.2019.05.008>
- Lalli, C.M., Parsons, T.R., 1993. *Biological oceanography: An introduction*. Pergamon Press, Exeter.
- Larsen, K.M.H., 2009. *Circulation and exchange of water masses on the Faroe Shelf and the impact on the Shelf ecosystem*. PhD Thesis, University of Bergen.
- Larsen, K.M.H., Hátún, H., Hansen, B., Kristiansen, R., 2012. Atlantic water in the Faroe area: sources and variability. *ICES J. Mar. Sci.* 69, 802–808. <https://doi.org/10.1093/icesjms/fss028>
- Liljeblad, B., Sjöstedt, S., Sundberg, J., Østerhus, S., 1987. Report from the cruise with R/V Håkon Mosby to the region north of Faroe Islands June 1986. No. 14, Gothenburg.
- Logemann, K., Ólafsson, J., Snorrason, Á., Valdimarsson, H., Marteinsdóttir, G., 2013. The circulation of Icelandic waters – a modelling study 931–955. <https://doi.org/10.5194/os-9-931-2013>
- Longhurst, A., 2007. *Ecological geography of the sea*. Elsevier.
- Mahadevan, A., D’Asaro, E., Lee, C., Perry, M.J., 2012. Eddy-Driven Stratification Initiates North Atlantic Spring Phytoplankton Blooms. *Science*. 337, 54–58.

<https://doi.org/10.1126/science.1218740>

- Marsland, S.J., Haak, H., Jungclaus, J.H., Latif, M., Roske, F., 2003. The Max-Planck-Institute global ocean/sea ice model with orthogonal curvilinear coordinates. *Ocean Model.* 5, 91–127.
- Nielsdottir, M.C., Moore, C.M., Sanders, R., Hinz, D.J., Achterberg, E.P., 2009. Iron limitation of the postbloom phytoplankton communities in the Iceland Basin. *Global Biogeochem. Cycles* 23, doi:10.1029/2008GB003410.
- Olafsson, J., Olafsdottir, S.R., Benoit-Cattin, A., Takahashi, T., 2010. The Irminger Sea and the Iceland Sea time series measurements of sea water carbon and nutrient chemistry 1983–2008. *Earth Syst. Sci. Data* 2, 99–104. <https://doi.org/10.3334/CDIAC/otg.CARINA.AMS.V1.2>
- Onarheim, T., 2016. Variability in deep water mass properties and mixing in the Norwegian Sea. Master Thesis, University of Bergen.
- Orvik, K.A., Niiler, P.P., 2002. Major pathways of Atlantic water in the northern North Atlantic and Nordic Seas toward the Arctic. *Geophys. Res. Lett.* Vol. 29, doi:10.1029/2002GL015002
- Pacariz, S. V., Hátún, H., Jacobsen, J.A., Johnson, C., Eliassen, S., Rey, F., 2016. Nutrient-driven poleward expansion of the Northeast Atlantic mackerel (*Scomber scombrus*) stock: A new hypothesis. *Elem. Sci. Anthr.* 4, 000105. <https://doi.org/10.12952/journal.elementa.000105>
- Painter, S.C., Hartman, S.E., Kivimäe, C., Salt, L.A., Clargo, N.M., Daniels, C.J., Bozec, Y., Daniels, L., Allen, S., Hemsley, V.S., Moschonas, G., Davidson, K., 2017. The elemental stoichiometry (C, Si, N, P) of the Hebrides Shelf and its role in carbon export. *Prog. Oceanogr.* 159, 154–177. <https://doi.org/10.1016/j.pocean.2017.10.001>
- Pätsch, J., Gouretski, V., Hinrichs, I., Koul, V., 2020. Distinct Mechanisms Underlying Interannual to Decadal Variability of Observed Salinity and Nutrient Concentration in the Northern North Sea. *J. Geophys. Res. Ocean.* <https://doi.org/10.1029/2019JC015825>
- Pätsch, J., Kühn, W., 2008. Nitrogen and carbon cycling in the North Sea and exchange with the North Atlantic—A model study. Part I. Nitrogen budget and fluxes. *Cont. Shelf Res.* 28, 767–787. <https://doi.org/10.1016/j.csr.2007.12.013>
- Pörtner, H.O., Roberts, D., Masson-Delmotte, V., Zhai, P., Tignor, M., Poloczanska, E.S., Mintenbeck, K., Alegría, A., Nicolai, M., Petzold, J., Rama, B., Weyer, N.M., 2019. IPCC Special Report on the Ocean and Cryosphere in a Changing Climate.
- Read, J.F., Pollard, R.T., 1992. Water Masses in the Region of the Iceland Faeroes Front. *J. Phys. Oceanogr.* 22, 1365–1378.
- Rey, F., 2012. Declining silicate concentrations in the Norwegian and Barent Seas. *ICES J. Mar. Sci.* 69, 208–212. <https://doi.org/10.1093/icesjms/fss007>
- Rey, F., Skjoldal, H., 1987. Consumption of silicic acid below the euphotic zone by sedimenting diatom blooms in the Barents Sea. *Mar. Ecol. Prog. Ser.* 36, 307–312. <https://doi.org/10.3354/meps036307>
- Richardson, K., Visser, A.W., Pedersen, F.B., 2000. Subsurface phytoplankton blooms fuel pelagic

- production in the North Sea. *J. Plankton Res.* 22, 1663–1671.
- Sarmiento, J.L., Gruber, N., 2019. Ocean Biogeochemical Dynamics, *Ocean Biogeochemical Dynamics*. <https://doi.org/10.2307/j.ctt3fgxqx>
- Schlitzer, R., 2007. Ocean Data View. <http://odv.awi.de>.
- Semper, S., Pickart, R.S., Våge, K., Larsen, K.M.H., Hátún, H., Hansen, B., 2020. The Iceland-Faroe Slope Jet: a conduit for dense water toward the Faroe Bank Channel overflow. *Nat. Commun.* 11, 1–10. <https://doi.org/10.1038/s41467-020-19049-5>
- Skagseth, Ø., Broms, C., Gundersen, K., Hátún, H., Kristiansen, I., Larsen, K.M.H., Mork, K.A., Petursdóttir, H., Sjøiland, H., 2022. Arctic and Atlantic waters in the Norwegian Basin, between year variability and potential ecosystem implications. *Front. Mar. Sci.* In Press.
- Stainton, M.P., 1974. Simple, Efficient Reduction Column for Use of the Automated Determination of Nitrate in Water. *Anal. Chem.* 46, 1616–1618.
- Steinacher, M., Joos, F., Frölicher, T.L., Bopp, L., Cadule, P., Cocco, V., Doney, S.C., Gehlen, M., Lindsay, K., Moore, J.K., Schneider, B., Segschneider, J., 2010. Projected 21st century decrease in marine productivity: A multi-model analysis. *Biogeosciences* 7, 979–1005. <https://doi.org/10.5194/bg-7-979-2010>
- Strickland, J.D., Parsons, T.R., 1972. *A Practical Handbook of Seawater Analysis*.
- Tanhua, T., Olsson, K.A., Jeansson, E., 2005. Formation of Denmark Strait overflow water and its hydro-chemical composition. *J. Mar. Syst.* 57. <https://doi.org/10.1016/j.jmarsys.2005.05.003>
- Van Aken, H.M., Deboer, C.J., 1995. On the synoptic hydrography of intermediate and deep-water masses in the Iceland Basin. *Deep. Res. Part I-Oceanographic Res. Pap.* 42, 165–189.

## 9 Appendix figures

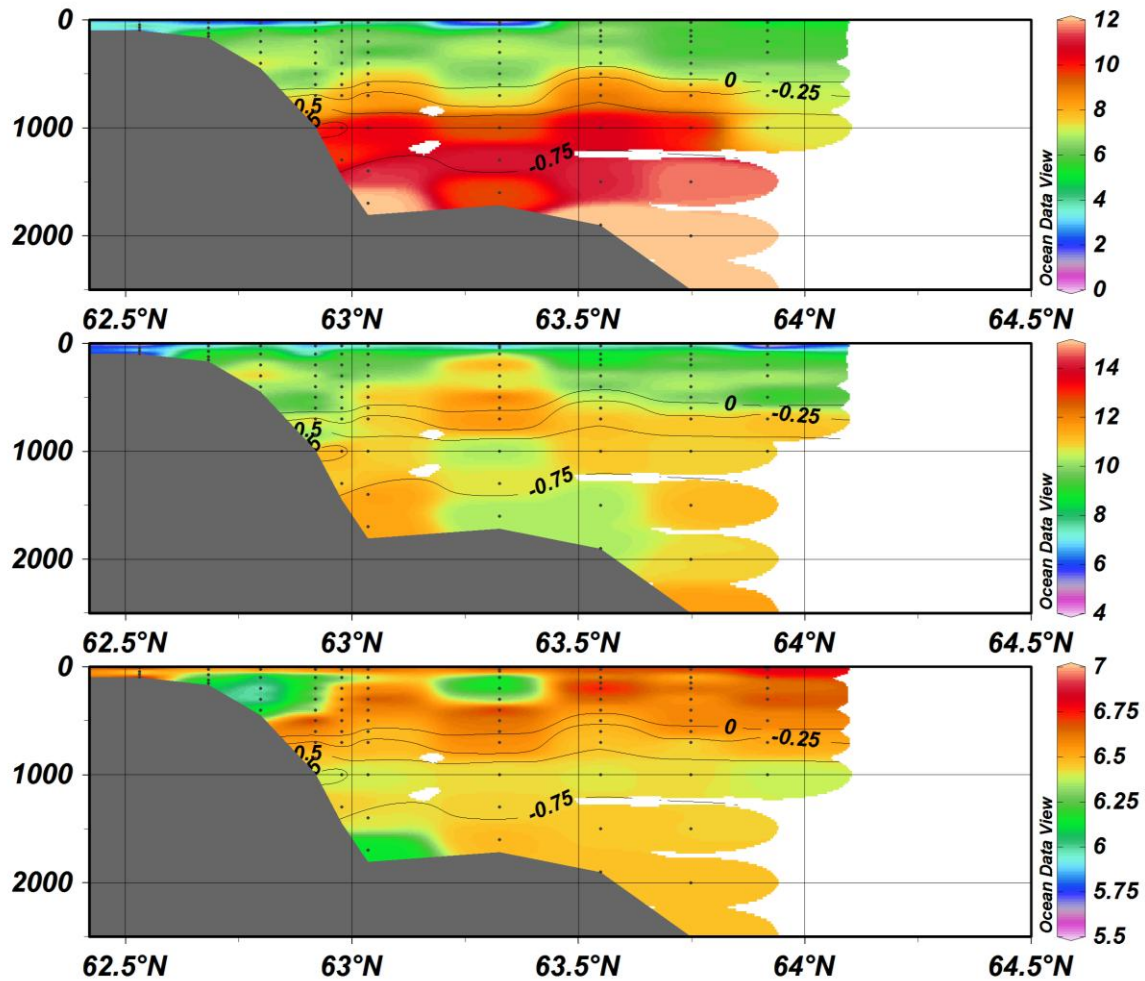


Figure A1 Nutrient transect, roughly along Section N, made by R/S Håkon Mosby in June 1986 (HM86). Upper: silicate ( $\mu\text{M}$ ), middle: nitrate ( $\mu\text{M}$ ), and lower: oxygen ( $\text{ml L}^{-1}$ ). The black lines represent isotherms ( $^{\circ}\text{C}$ ).

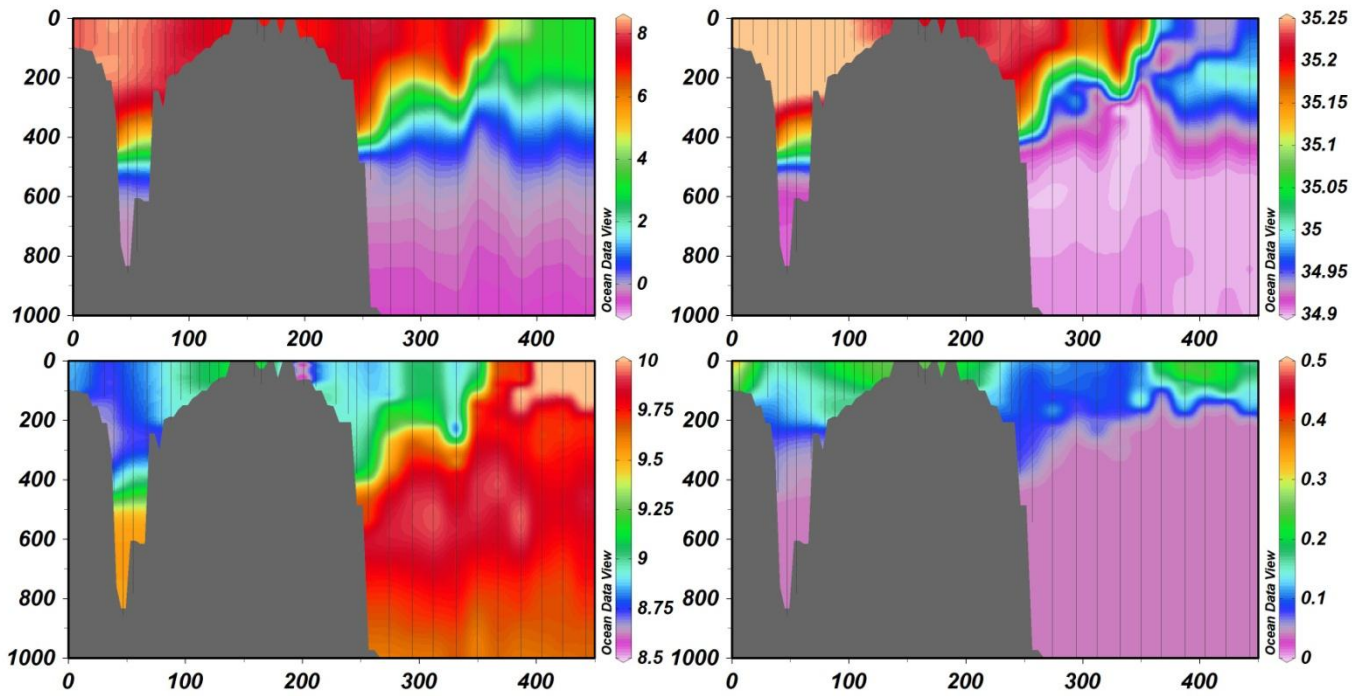


Figure A2 Combined section V-N, February 2013. (a) Temperature ( $^{\circ}\text{C}$ ), (b) salinity (psu), (c) oxygen concentrations ( $\text{mg L}^{-1}$ ) and (d) fluorescence.

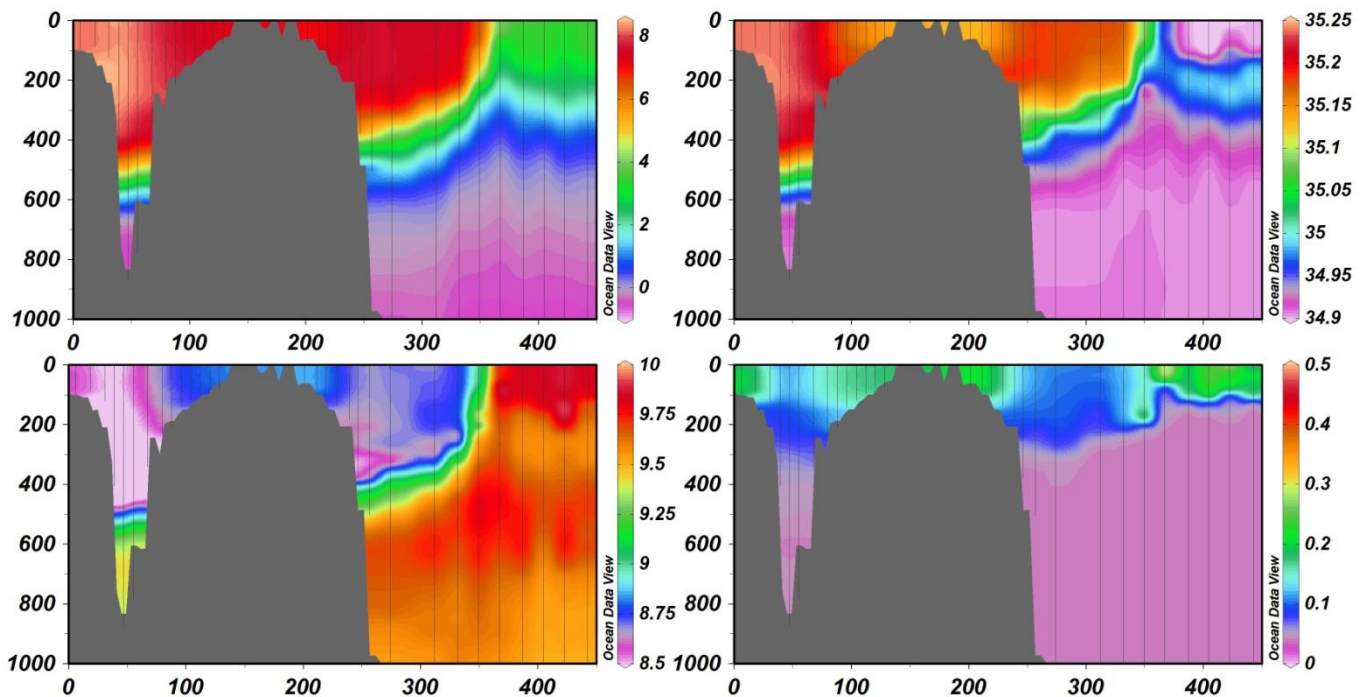


Figure A3 Combined section V-N, February 2014. (a) Temperature ( $^{\circ}\text{C}$ ), (b) salinity (psu), (c) oxygen concentrations ( $\text{mg L}^{-1}$ ) and (d) fluorescence.

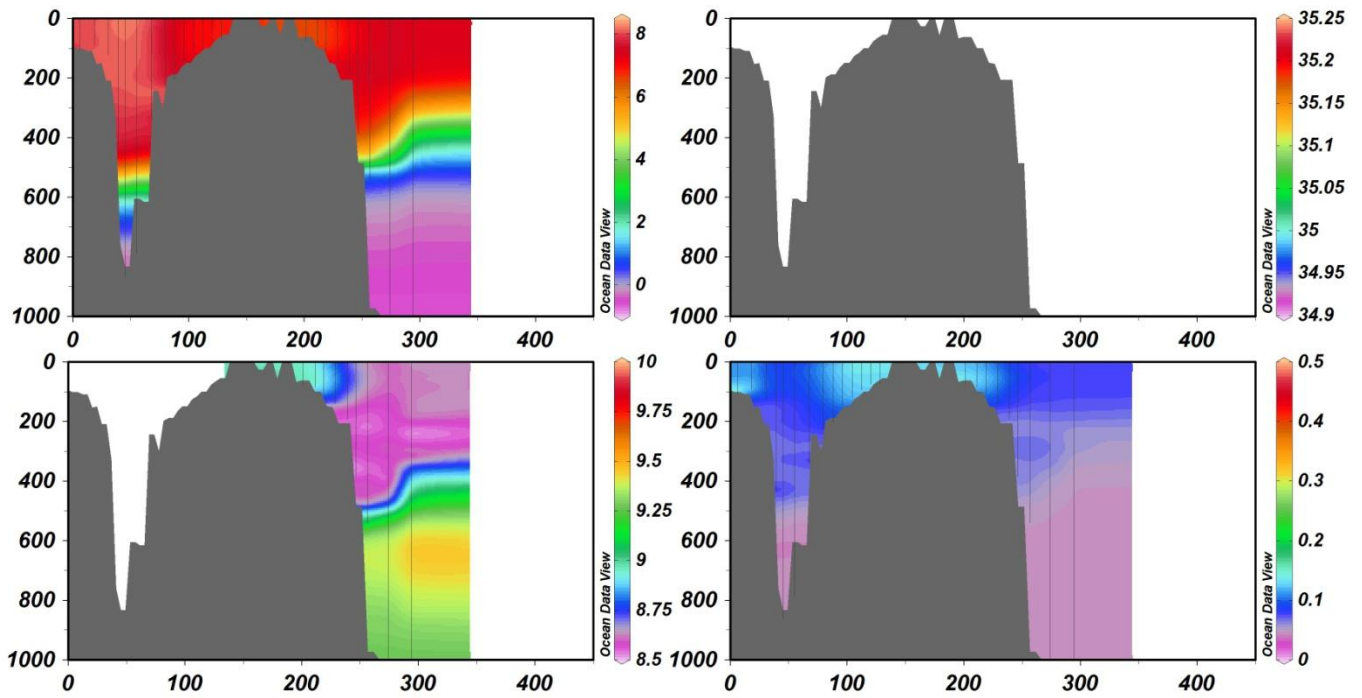


Figure A4 Combined section V-N, February 2015. (a) Temperature ( $^{\circ}\text{C}$ ), (b) salinity (psu), (c) oxygen concentrations ( $\text{mg L}^{-1}$ ) and (d) fluorescence.

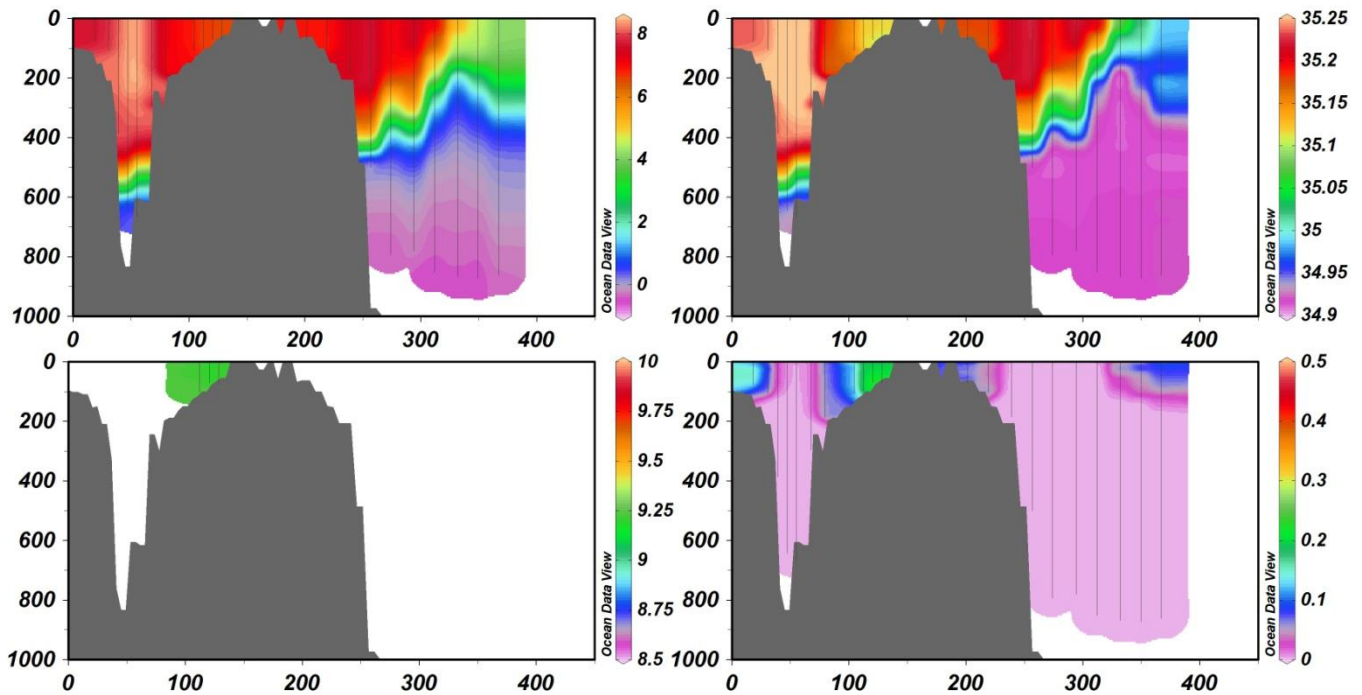


Figure A5 Combined section V-N, February 2016. (a) Temperature ( $^{\circ}\text{C}$ ), (b) salinity (psu), (c) oxygen concentrations ( $\text{mg L}^{-1}$ ) and (d) fluorescence.

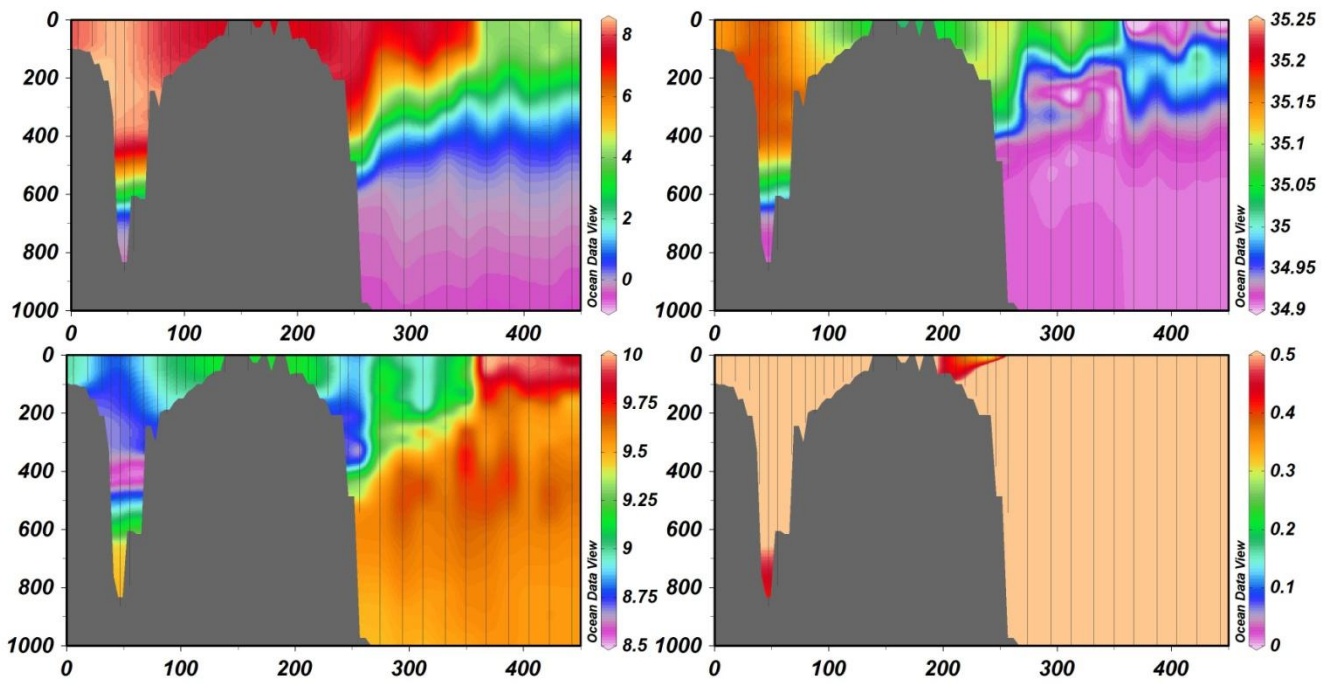


Figure A6 Combined section V-N, February 2017. (a) Temperature ( $^{\circ}\text{C}$ ), (b) salinity (psu), (c) oxygen concentrations ( $\text{mg L}^{-1}$ ) and (d) fluorescence.

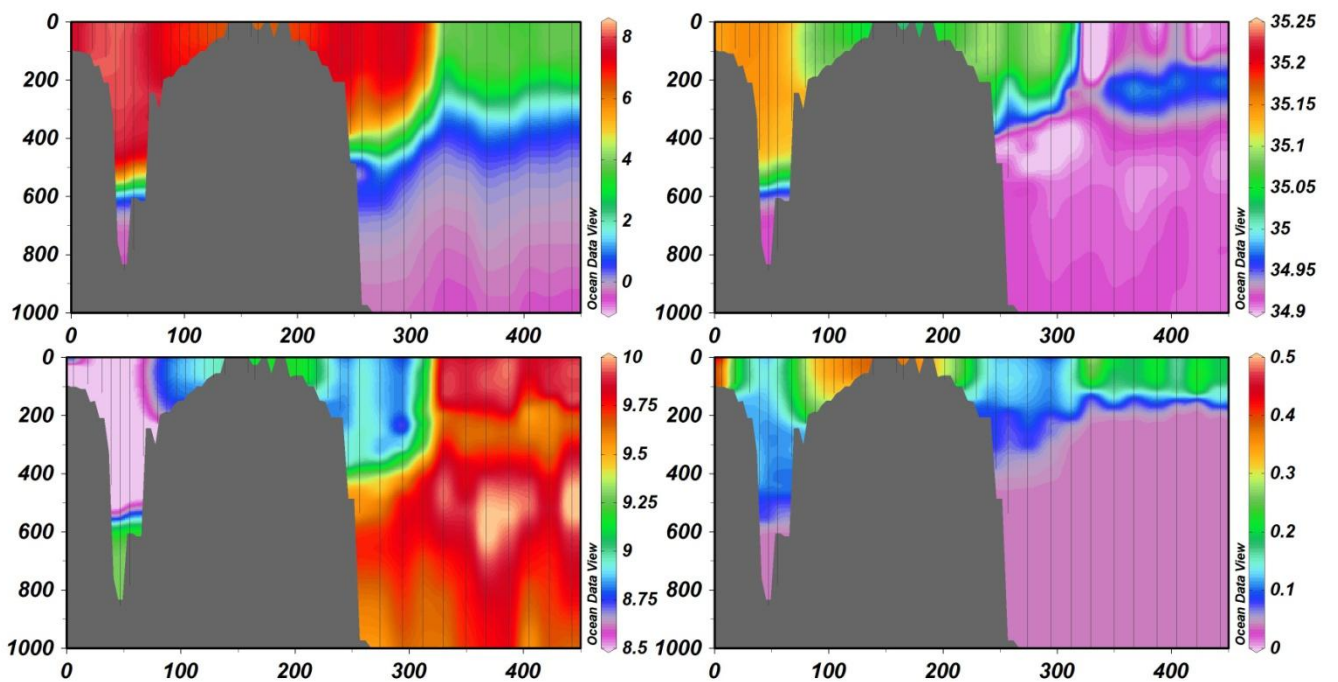


Figure A7 Combined section V-N, February 2018. (a) Temperature ( $^{\circ}\text{C}$ ), (b) salinity (psu), (c) oxygen concentrations ( $\text{mg L}^{-1}$ ) and (d) fluorescence.

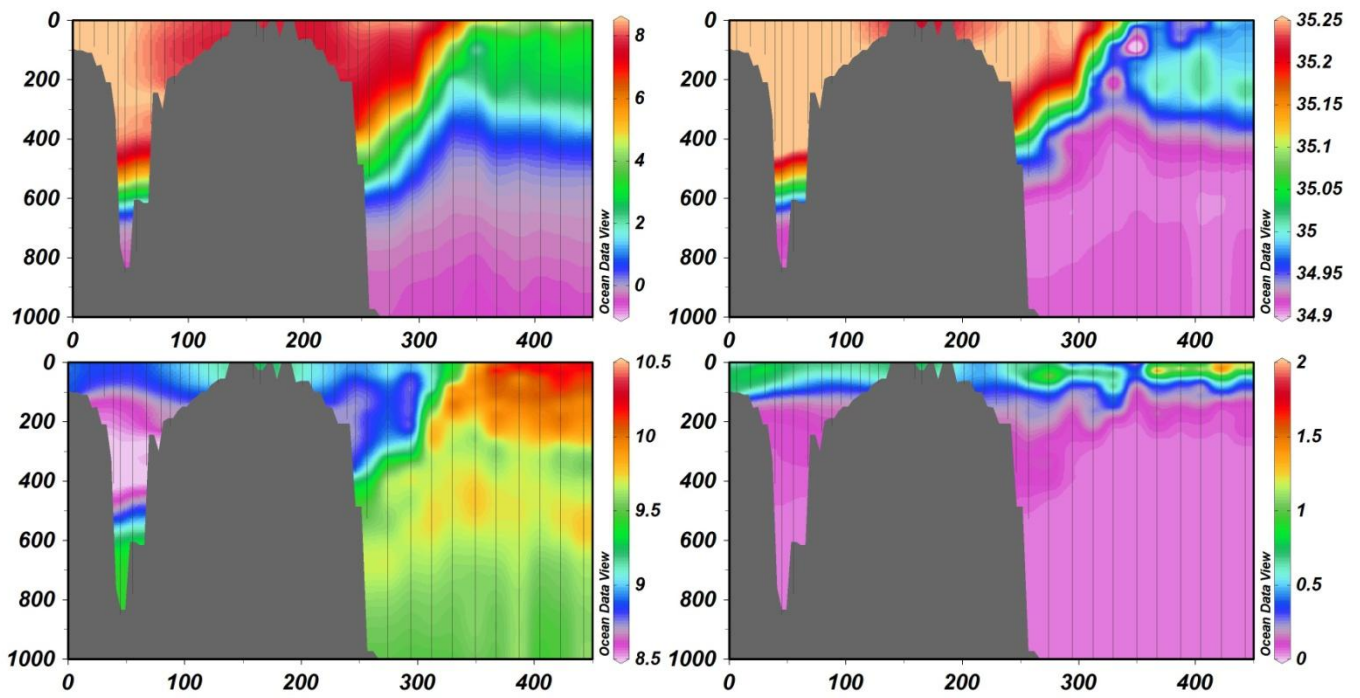


Figure A8 Combined section V-N, May-June 2013. (a) Temperature ( $^{\circ}\text{C}$ ), (b) salinity (psu), (c) oxygen concentrations ( $\text{mg L}^{-1}$ ) and (d) fluorescence.

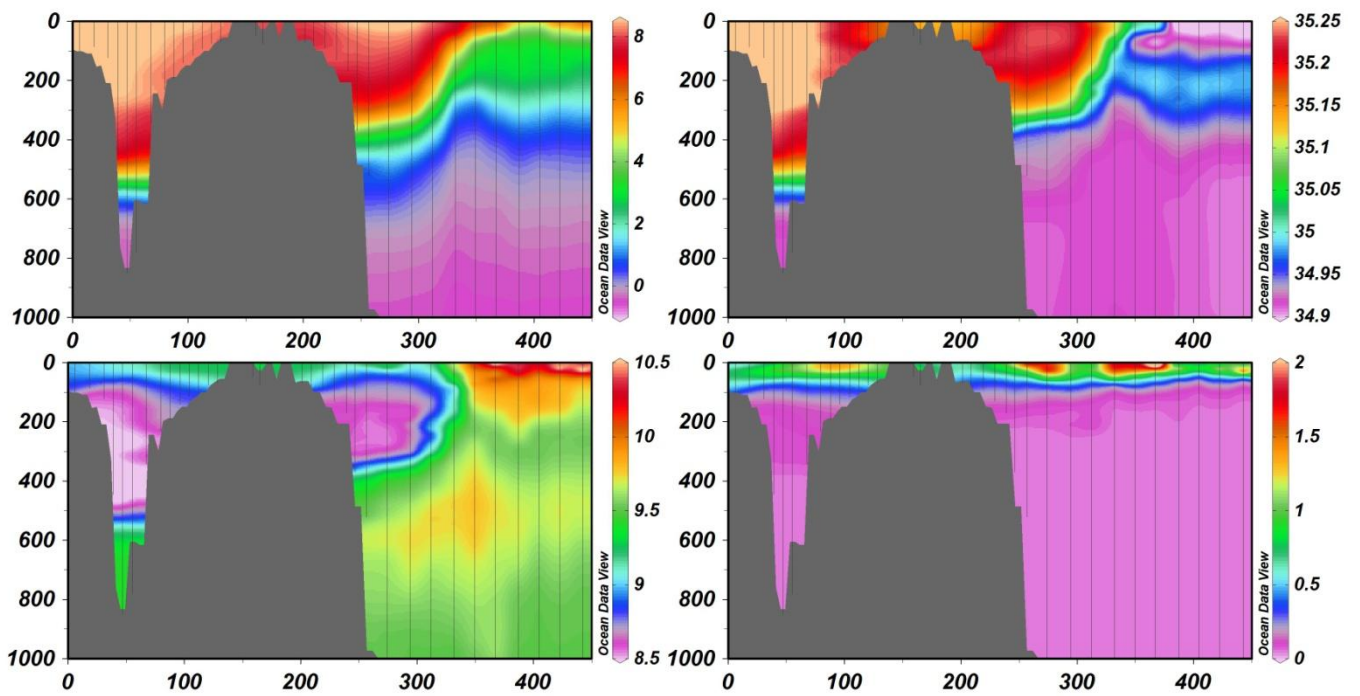


Figure A9 Combined section V-N, May-June 2014. (a) Temperature ( $^{\circ}\text{C}$ ), (b) salinity (psu), (c) oxygen concentrations ( $\text{mg L}^{-1}$ ) and (d) fluorescence.

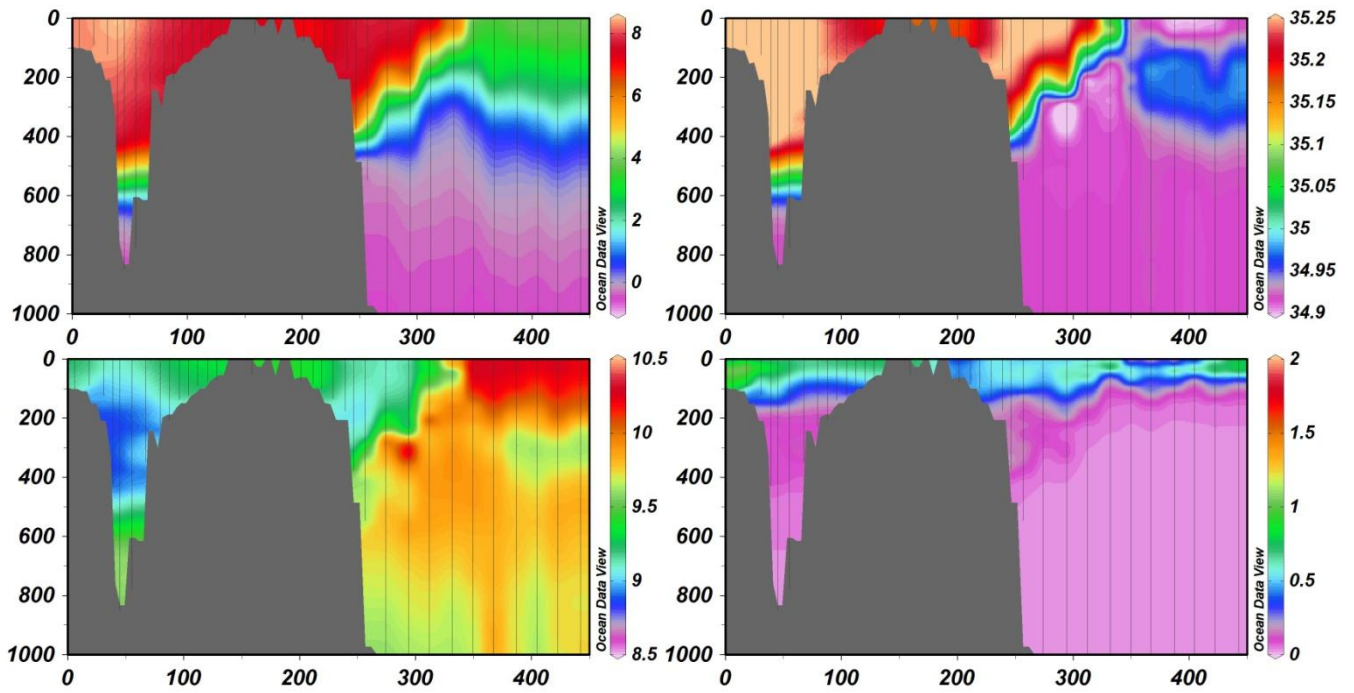


Figure A10 Combined section V-N, May-June 2015. (a) Temperature ( $^{\circ}\text{C}$ ), (b) salinity (psu), (c) oxygen concentrations ( $\text{mg L}^{-1}$ ) and (d) fluorescence.

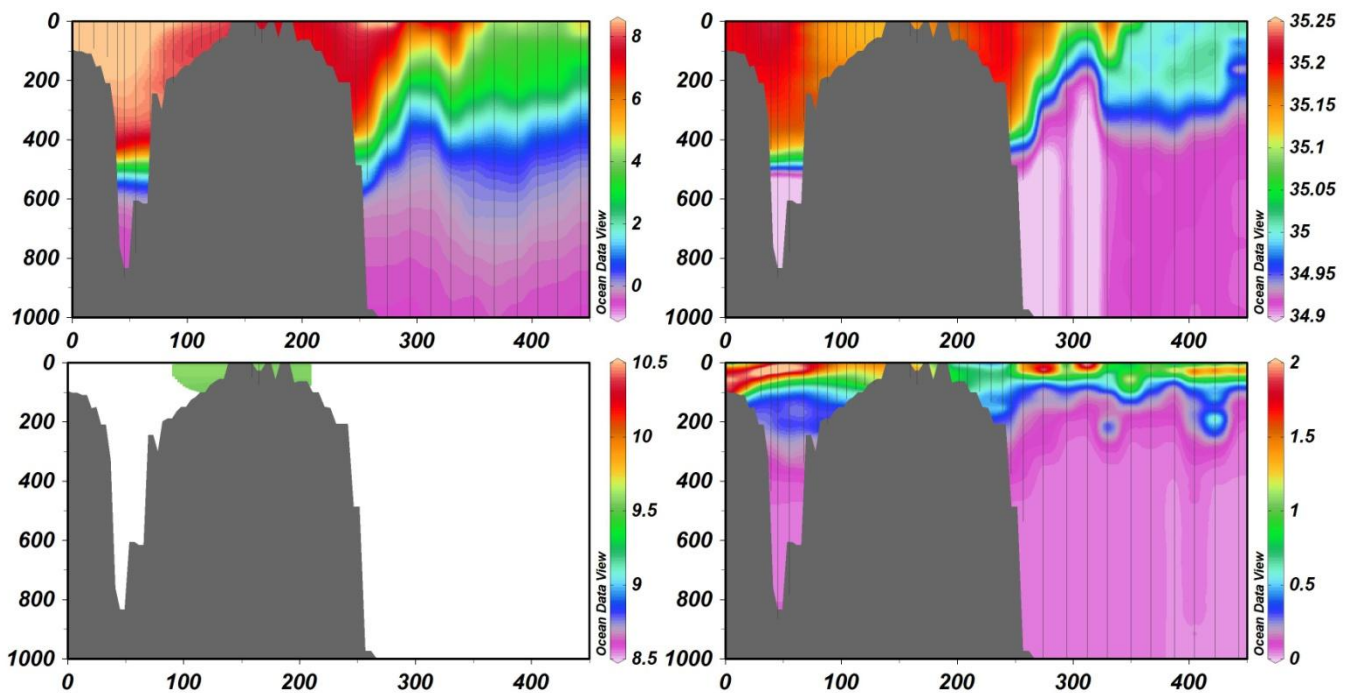


Figure A11 Combined section V-N, May-June 2016. (a) Temperature ( $^{\circ}\text{C}$ ), (b) salinity (psu), (c) oxygen concentrations ( $\text{mg L}^{-1}$ ) and (d) fluorescence.

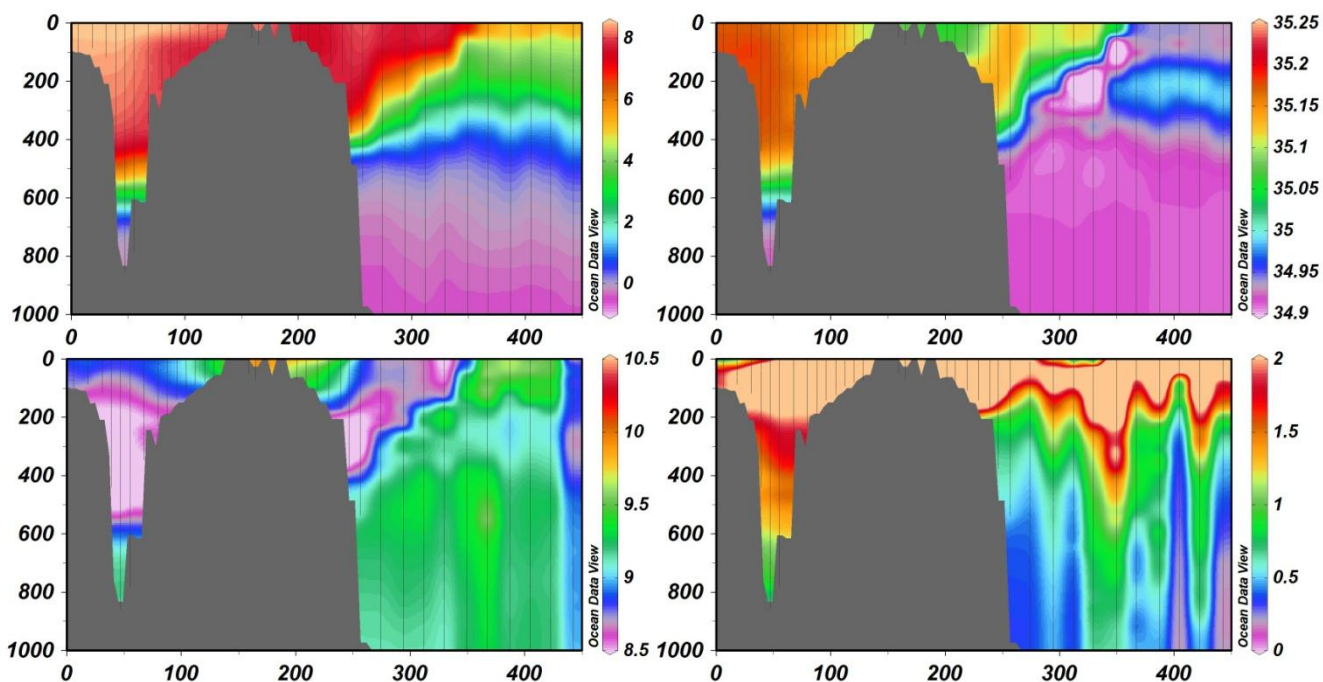


Figure A12 Combined section V-N, May-June 2017. (a) Temperature ( $^{\circ}\text{C}$ ), (b) salinity (psu), (c) oxygen concentrations ( $\text{mg L}^{-1}$ ) and (d) fluorescence.

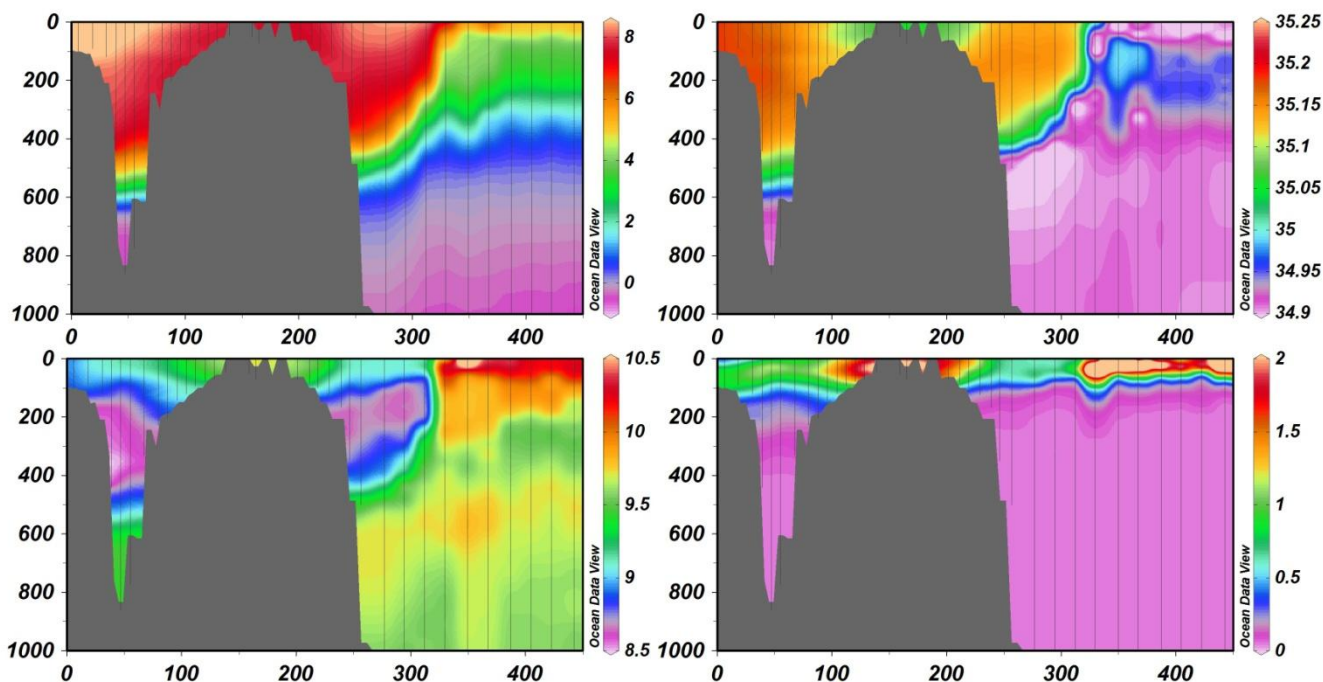


Figure A13 Combined section V-N, May-June 2018. (a) Temperature ( $^{\circ}\text{C}$ ), (b) salinity (psu), (c) oxygen concentrations ( $\text{mg L}^{-1}$ ) and (d) fluorescence.

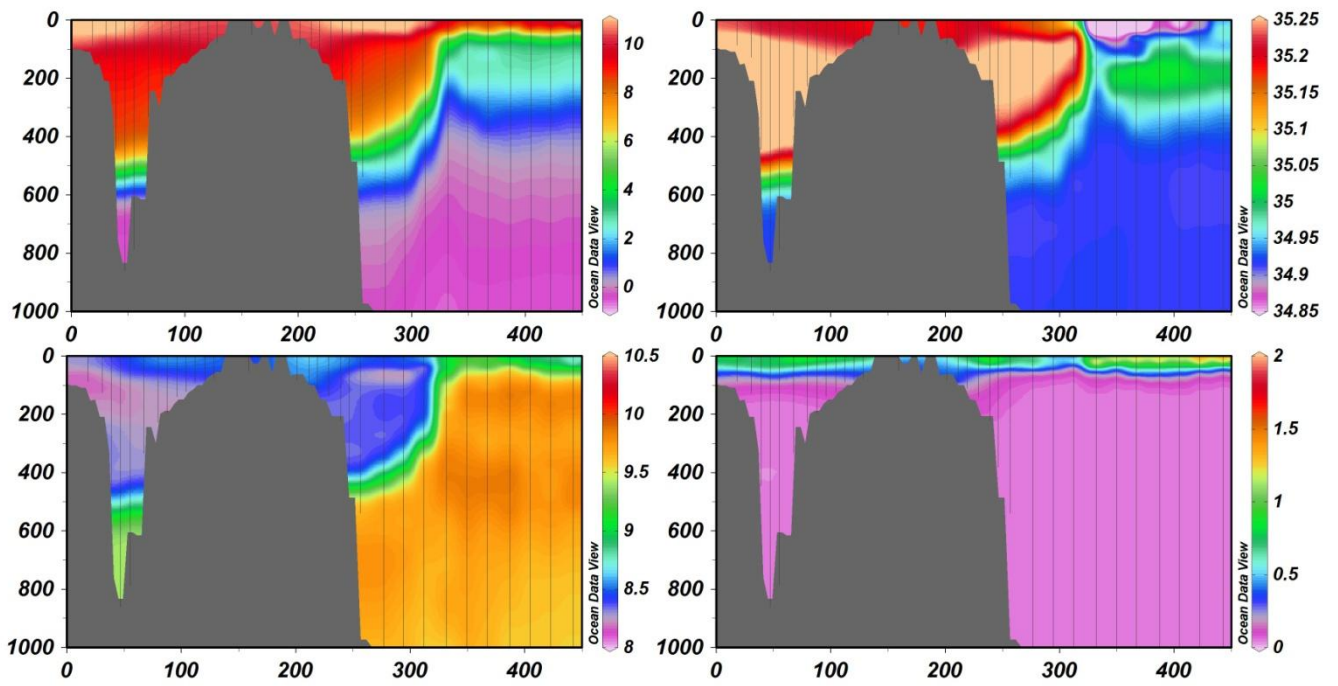


Figure A14 Combined section V-N, August-September 2013. (a) Temperature (°C), (b) salinity (psu), (c) oxygen concentrations (mg L<sup>-1</sup>) and (d) fluorescence.

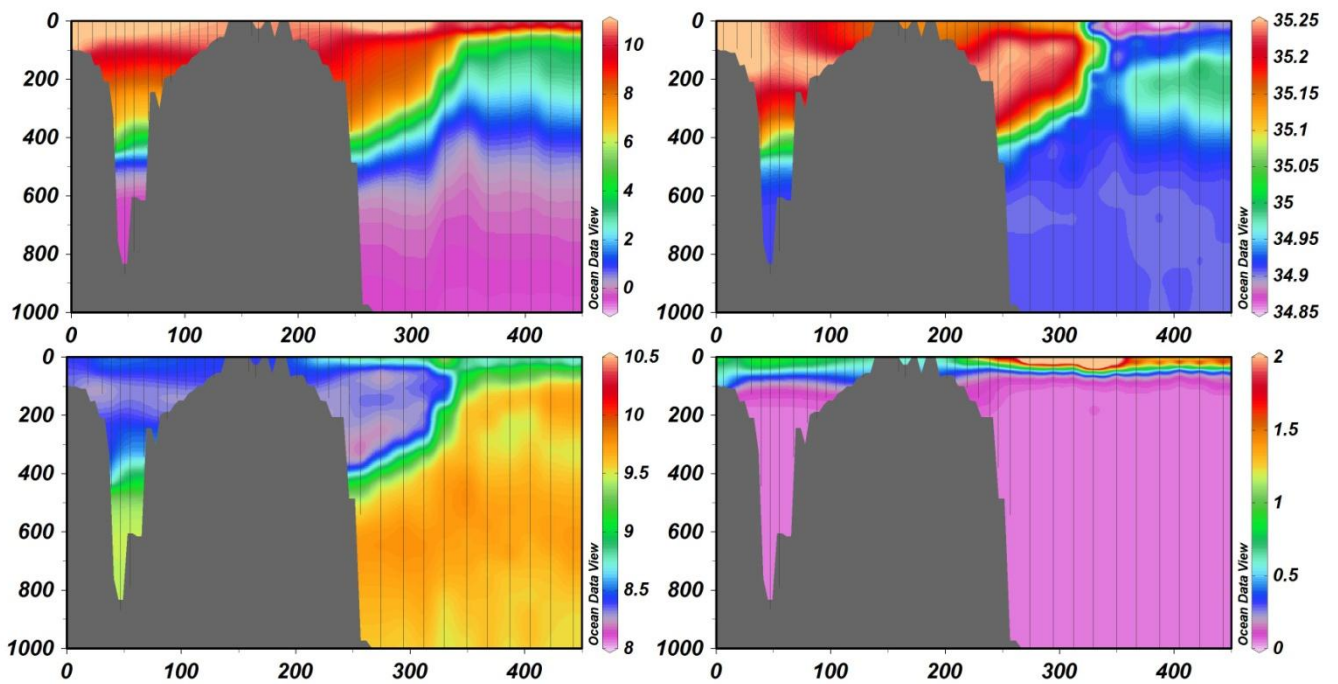


Figure A15 Combined section V-N, August-September 2014. (a) Temperature (°C), (b) salinity (psu), (c) oxygen concentrations (mg L<sup>-1</sup>) and (d) fluorescence.

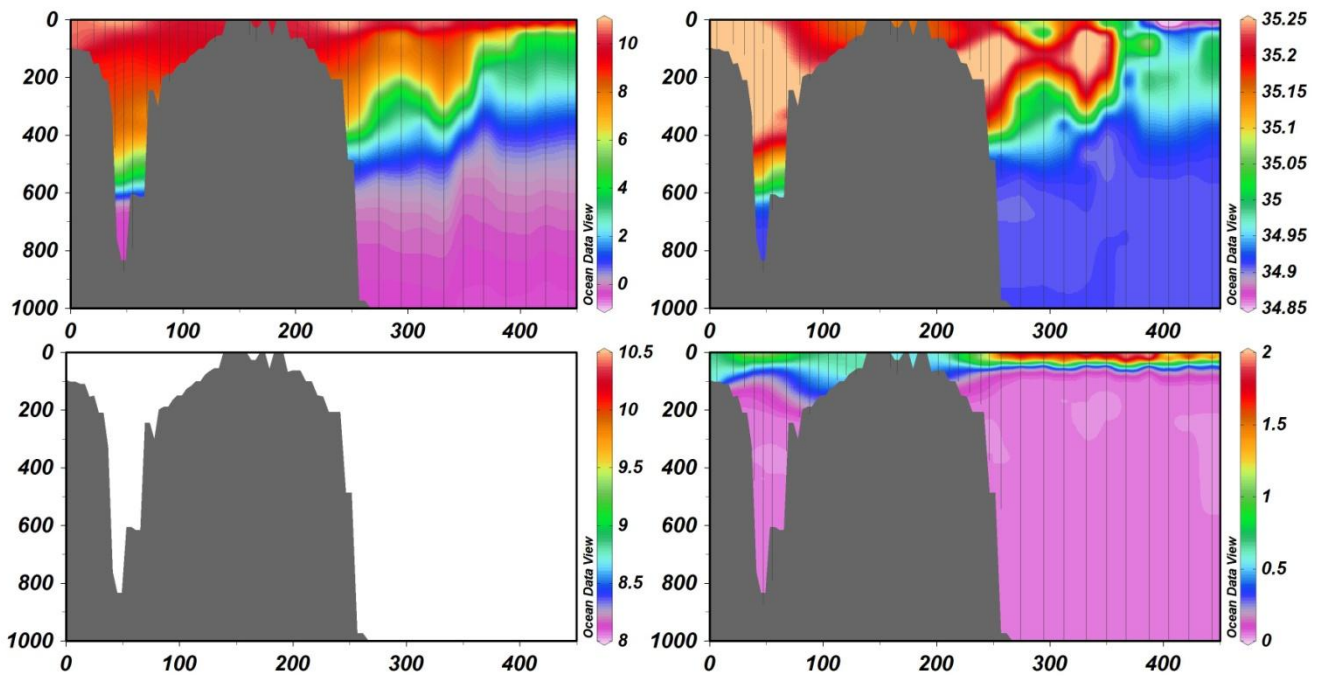


Figure A16 Combined section V-N, August-September 2015. (a) Temperature ( $^{\circ}\text{C}$ ), (b) salinity (psu), (c) oxygen concentrations ( $\text{mg L}^{-1}$ ) and (d) fluorescence.

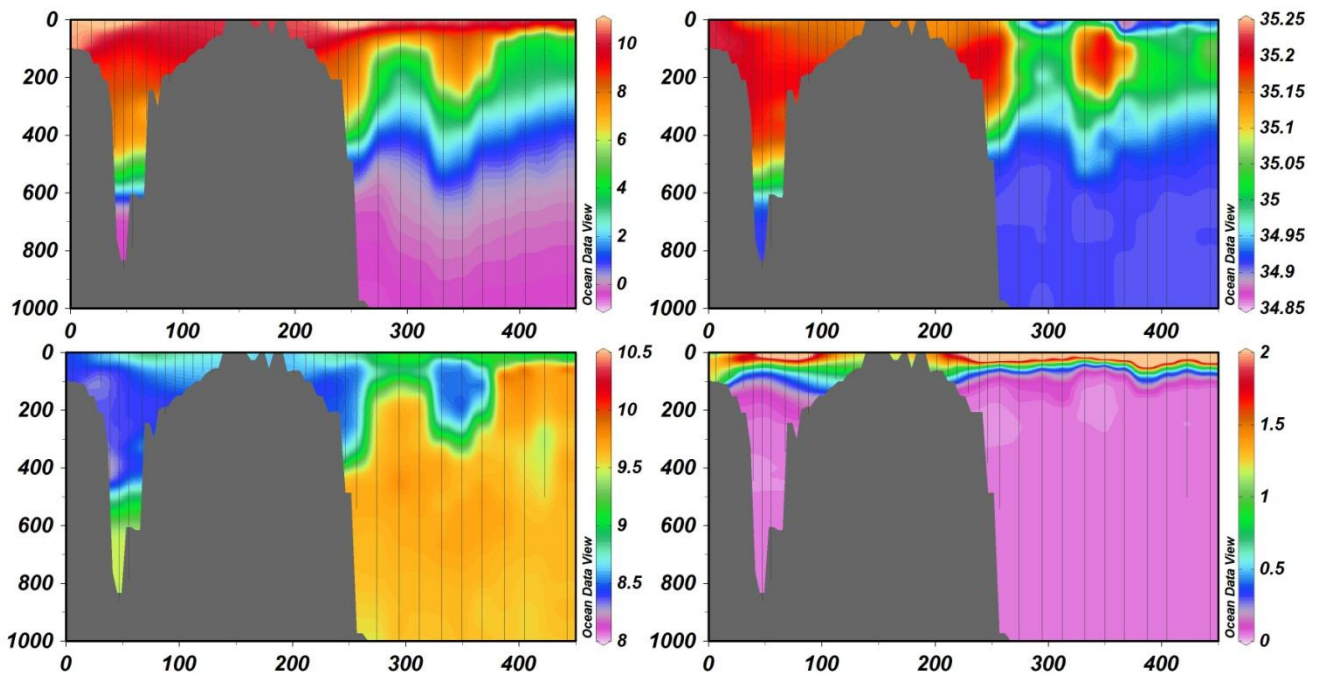


Figure A17 Combined section V-N, August-September 2016. (a) Temperature ( $^{\circ}\text{C}$ ), (b) salinity (psu), (c) oxygen concentrations ( $\text{mg L}^{-1}$ ) and (d) fluorescence.

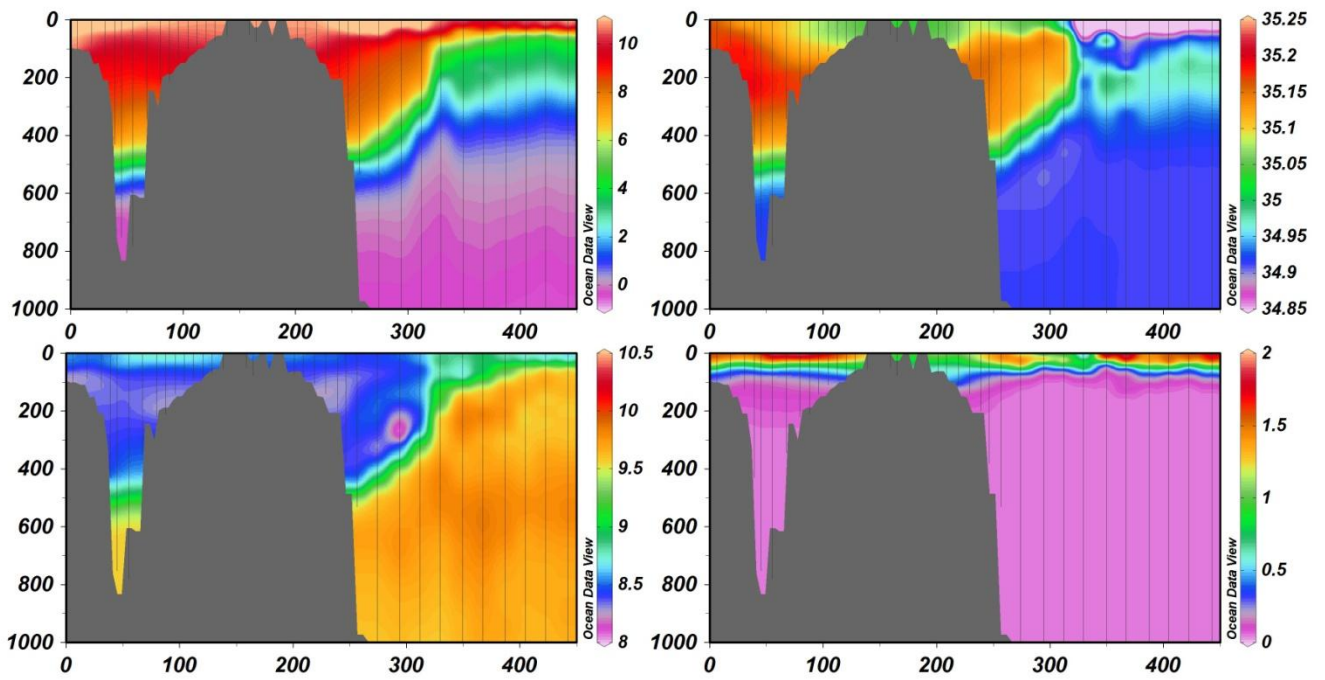


Figure A18 Combined section V-N, August-September 2017. (a) Temperature ( $^{\circ}\text{C}$ ), (b) salinity (psu), (c) oxygen concentrations ( $\text{mg L}^{-1}$ ) and (d) fluorescence.

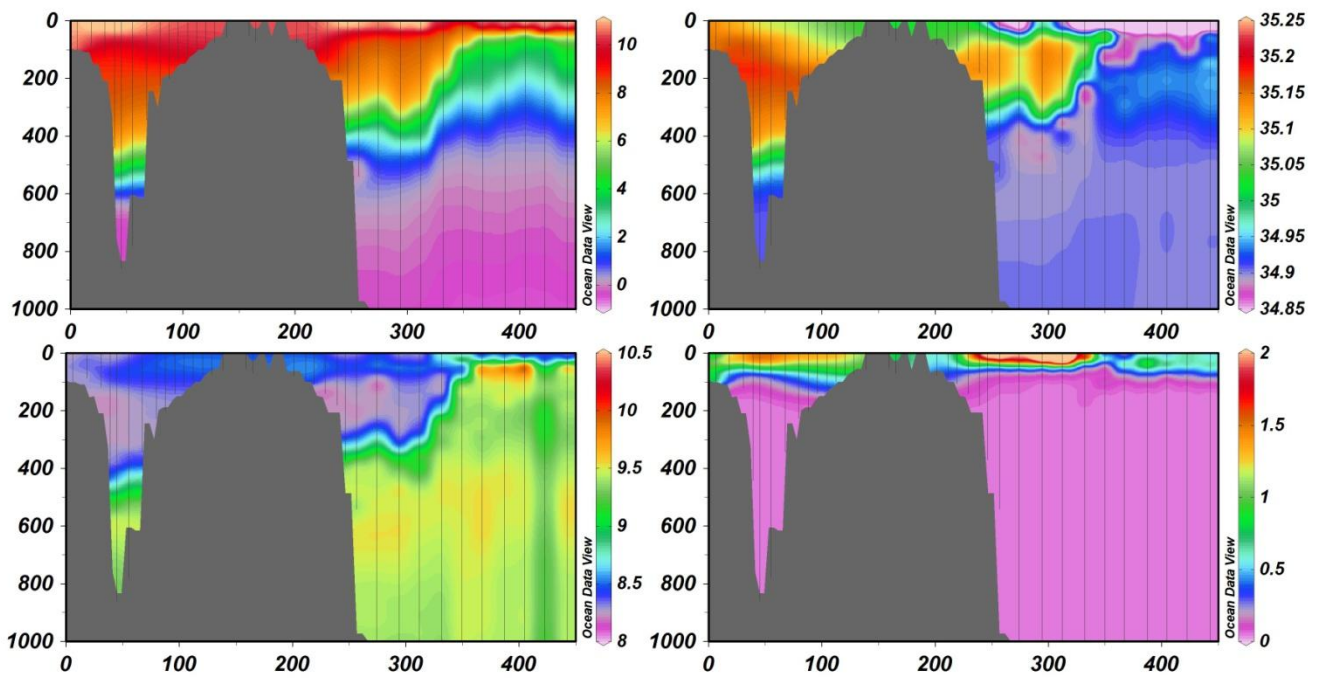


Figure A19 Combined section V-N, August-September 2018. (a) Temperature ( $^{\circ}\text{C}$ ), (b) salinity (psu), (c) oxygen concentrations ( $\text{mg L}^{-1}$ ) and (d) fluorescence.

## 9.1 Section R-S

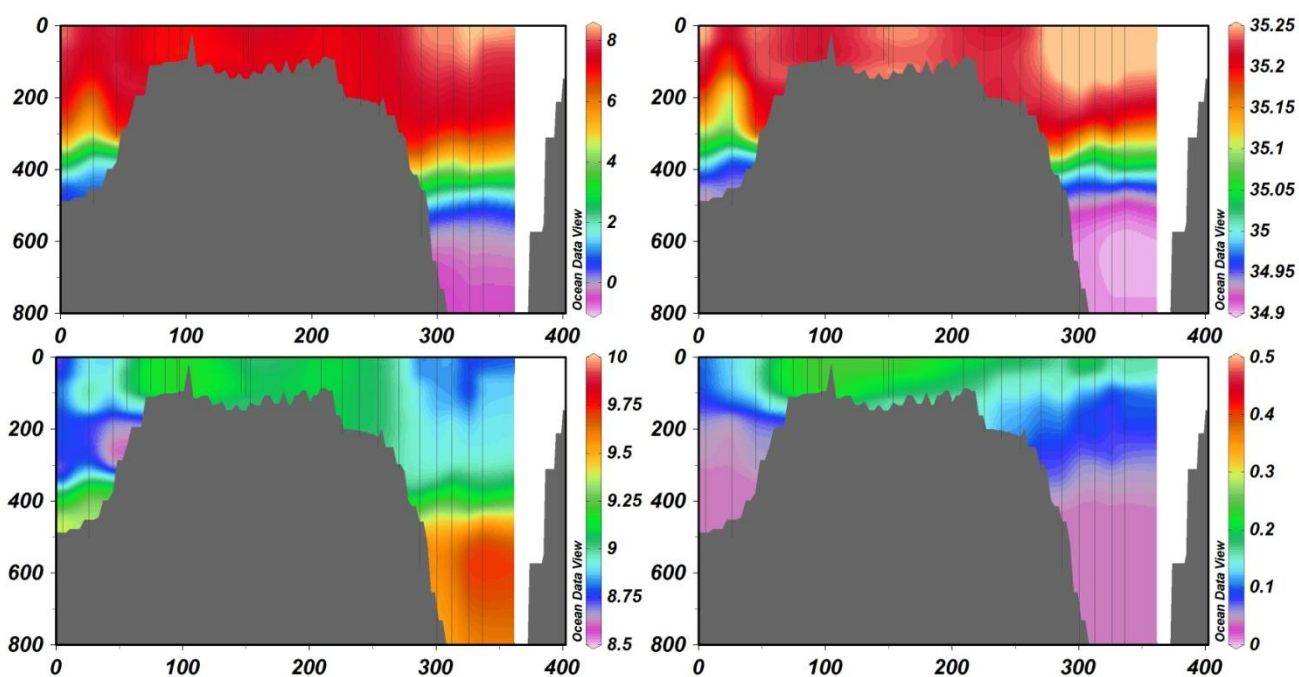


Figure A20 Combined section R-S, February 2013. (a) Temperature ( $^{\circ}\text{C}$ ), (b) salinity (psu), (c) oxygen concentrations ( $\text{mg L}^{-1}$ ) and (d) fluorescence.

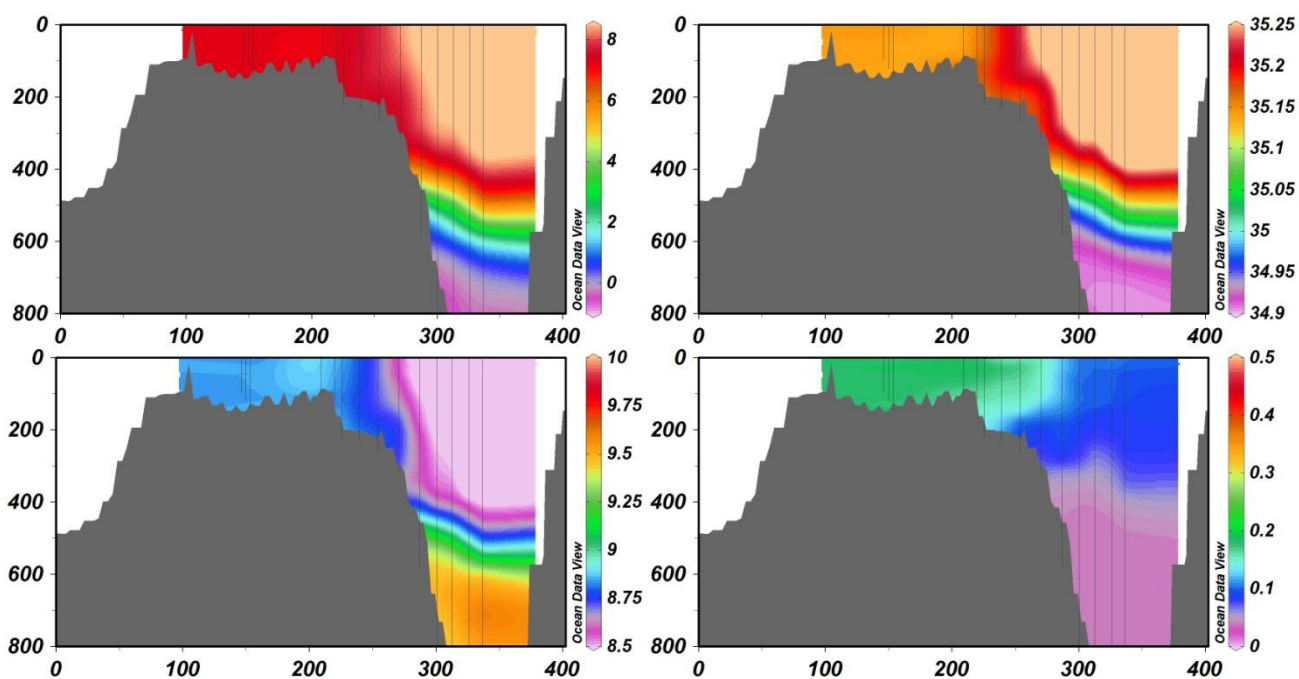


Figure A21 Combined section R-S, February 2014. (a) Temperature ( $^{\circ}\text{C}$ ), (b) salinity (psu), (c) oxygen concentrations ( $\text{mg L}^{-1}$ ) and (d) fluorescence.

R-S February 2015 (No data)

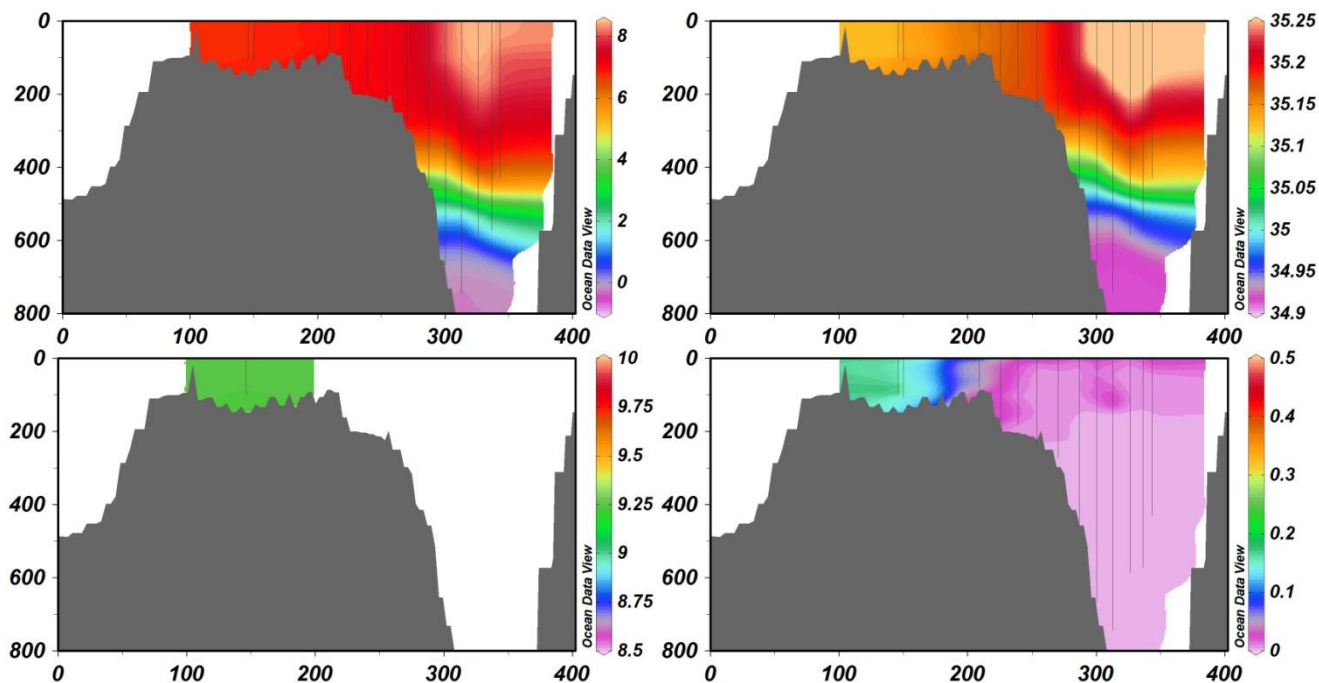


Figure A22 Combined section R-S, February 2016. (a) Temperature (°C), (b) salinity (psu), (c) oxygen concentrations (mg L<sup>-1</sup>) and (d) fluorescence.

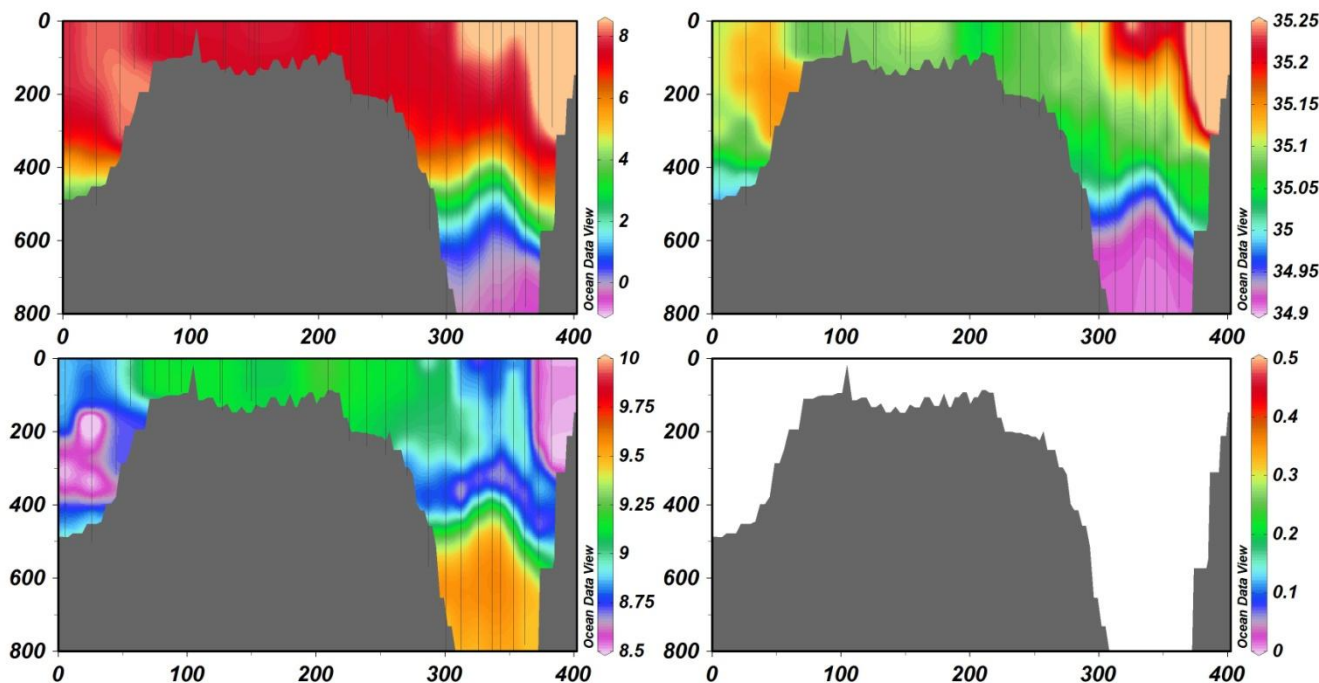


Figure A23 Combined section R-S, February 2017. (a) Temperature (°C), (b) salinity (psu), (c) oxygen concentrations (mg L<sup>-1</sup>) and (d) fluorescence.

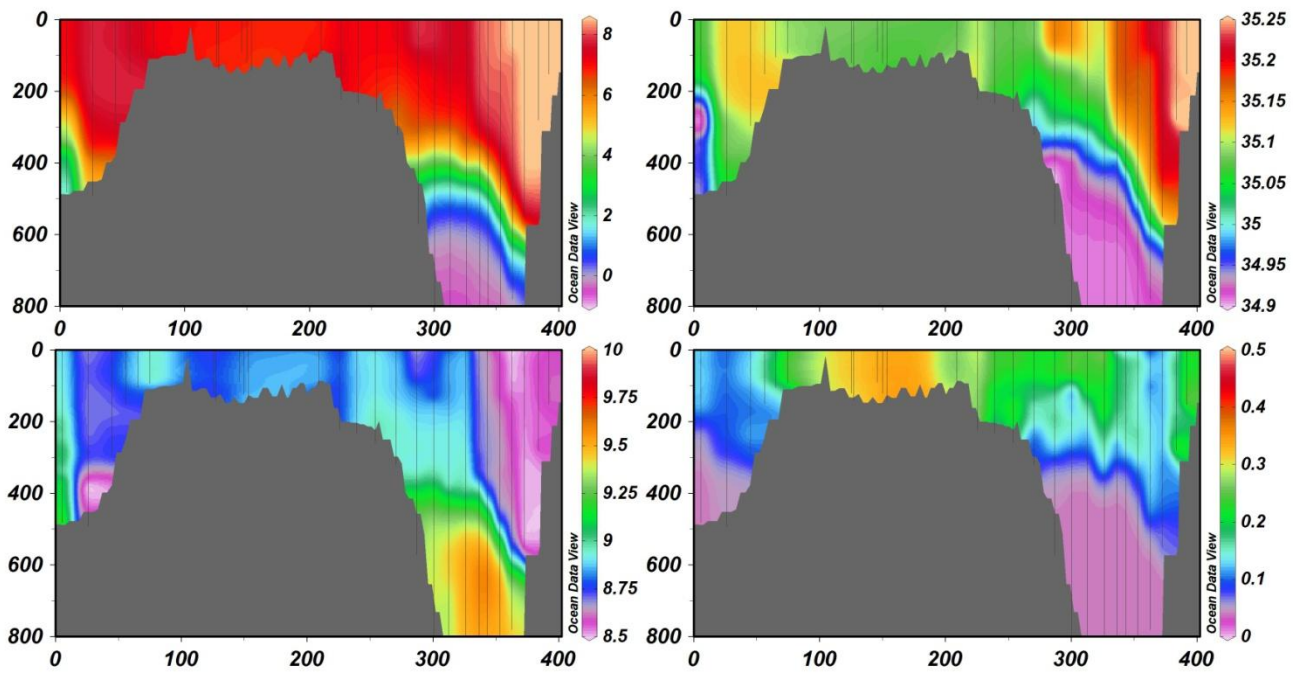


Figure A24 Combined section R-S, February 2018. (a) Temperature (°C), (b) salinity (psu), (c) oxygen concentrations (mg L<sup>-1</sup>) and (d) fluorescence.

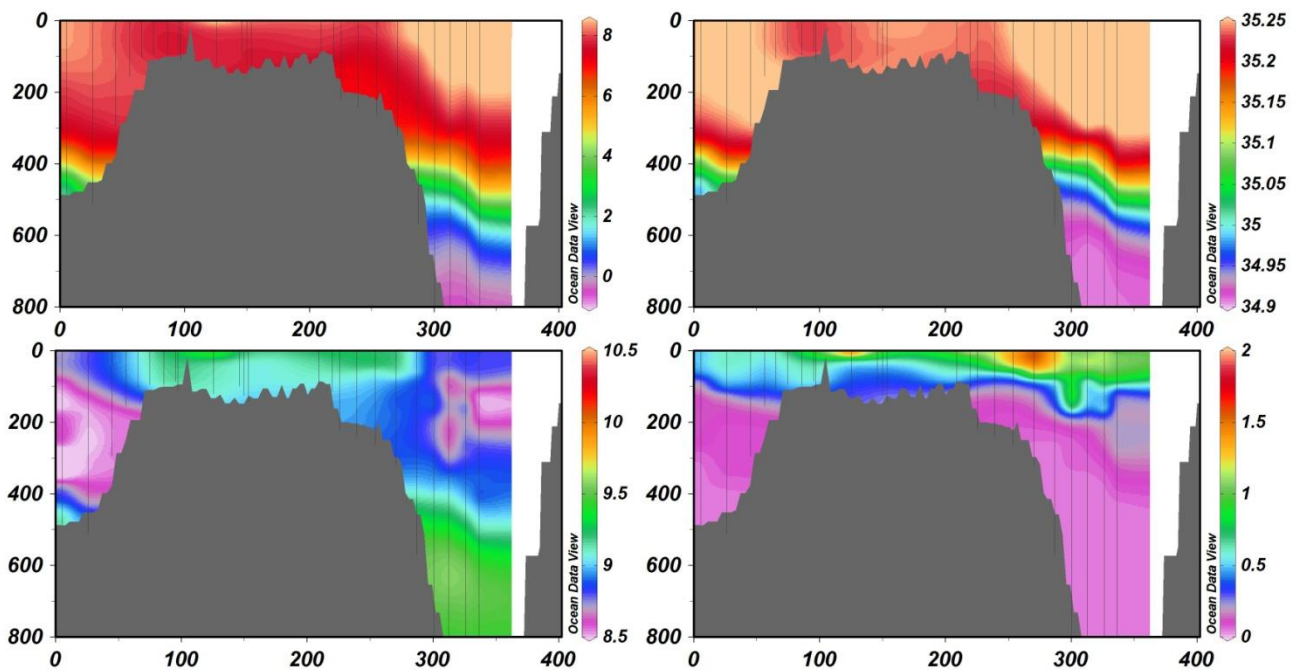


Figure A25 Combined section R-S, May-June 2013. (a) Temperature (°C), (b) salinity (psu), (c) oxygen concentrations (mg L<sup>-1</sup>) and (d) fluorescence.

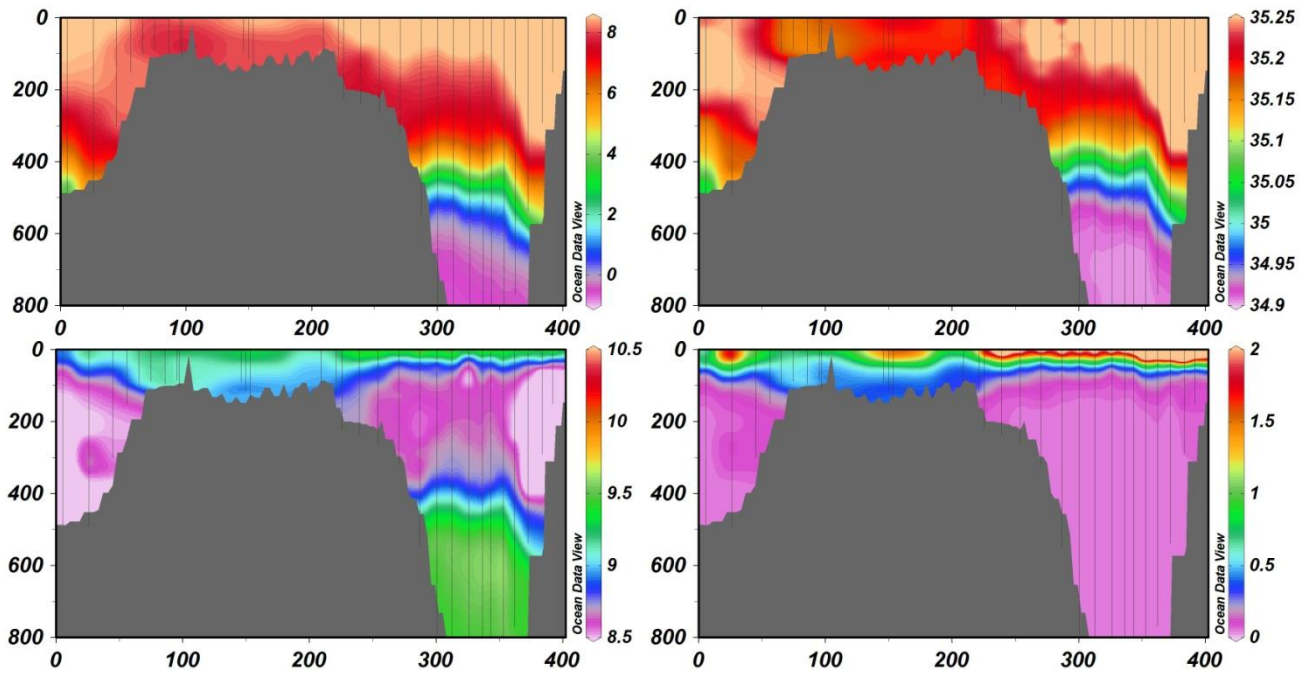


Figure A26 Combined section R-S, May-June 2014. (a) Temperature ( $^{\circ}\text{C}$ ), (b) salinity (psu), (c) oxygen concentrations ( $\text{mg L}^{-1}$ ) and (d) fluorescence.

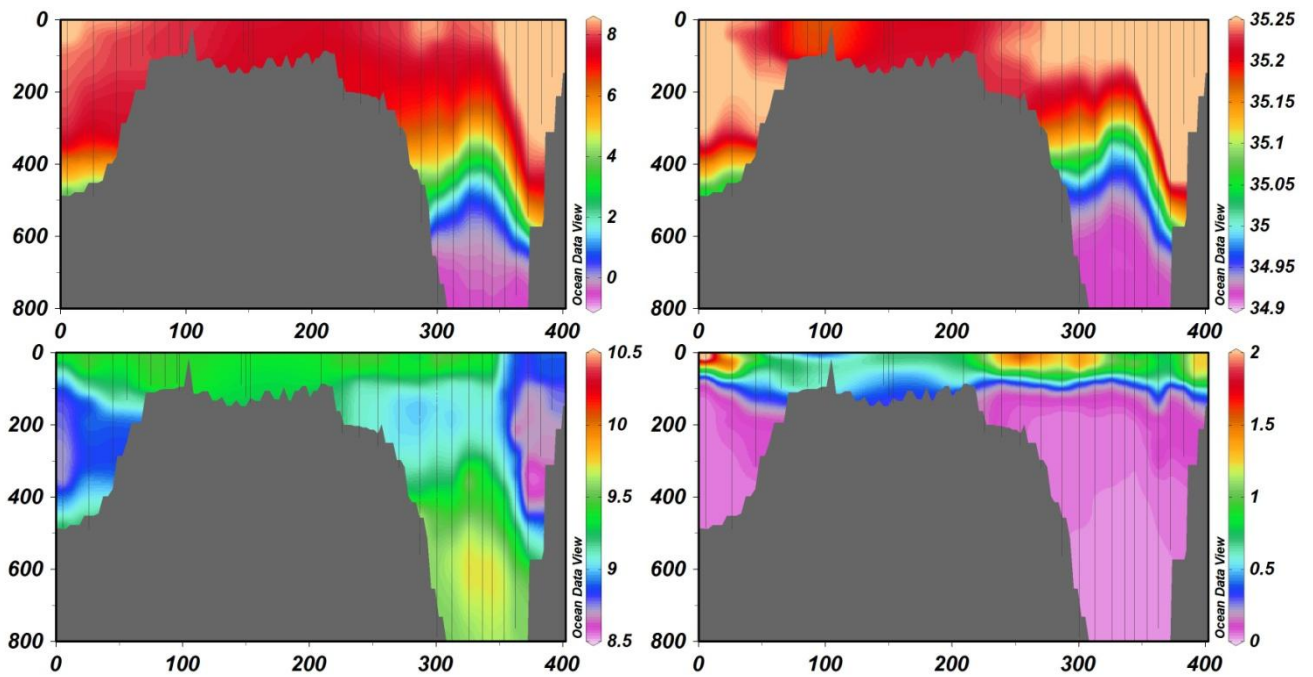


Figure A27 Combined section R-S, May-June 2015. (a) Temperature ( $^{\circ}\text{C}$ ), (b) salinity (psu), (c) oxygen concentrations ( $\text{mg L}^{-1}$ ) and (d) fluorescence.

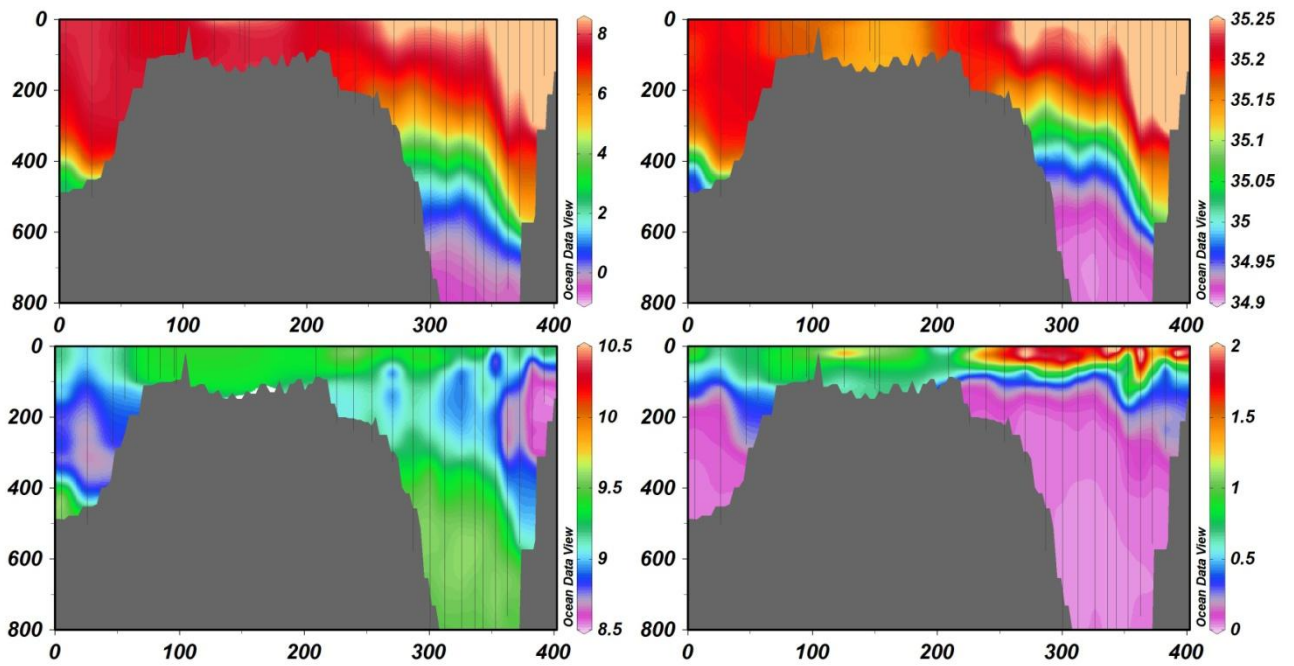


Figure A28 Combined section R-S, May-June 2016. (a) Temperature ( $^{\circ}\text{C}$ ), (b) salinity (psu), (c) oxygen concentrations ( $\text{mg L}^{-1}$ ) and (d) fluorescence.

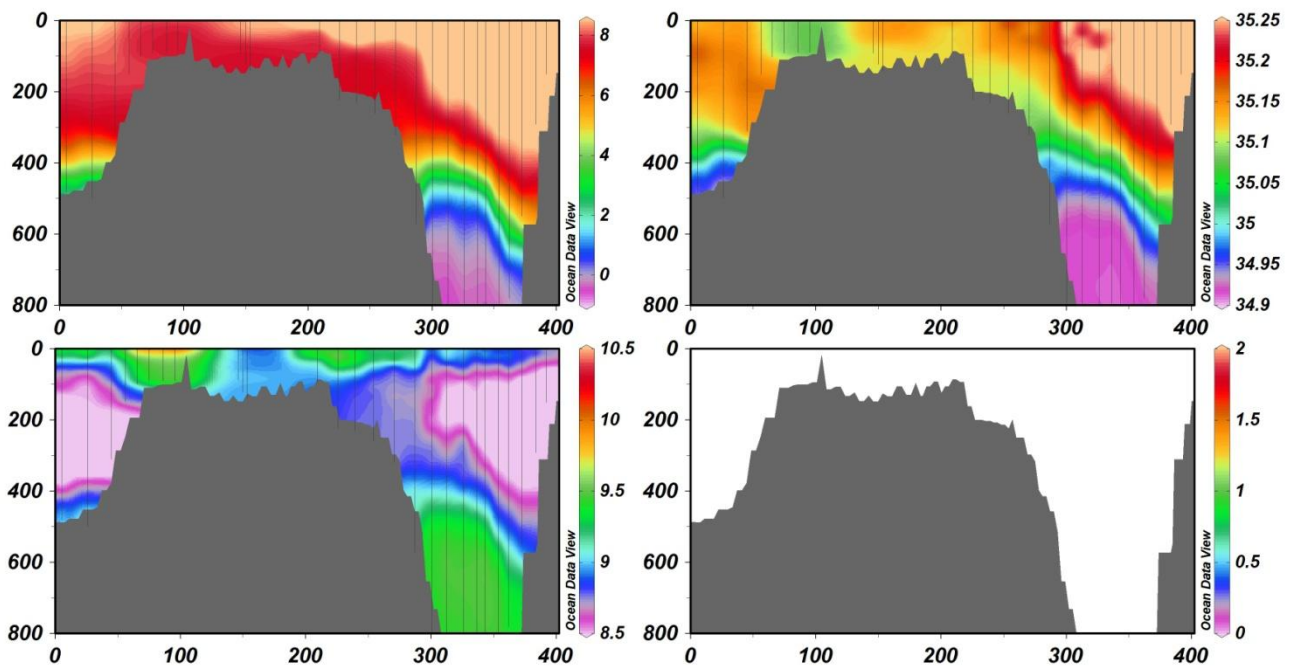


Figure A29 Combined section R-S, May-June 2017. (a) Temperature ( $^{\circ}\text{C}$ ), (b) salinity (psu), (c) oxygen concentrations ( $\text{mg L}^{-1}$ ) and (d) fluorescence.

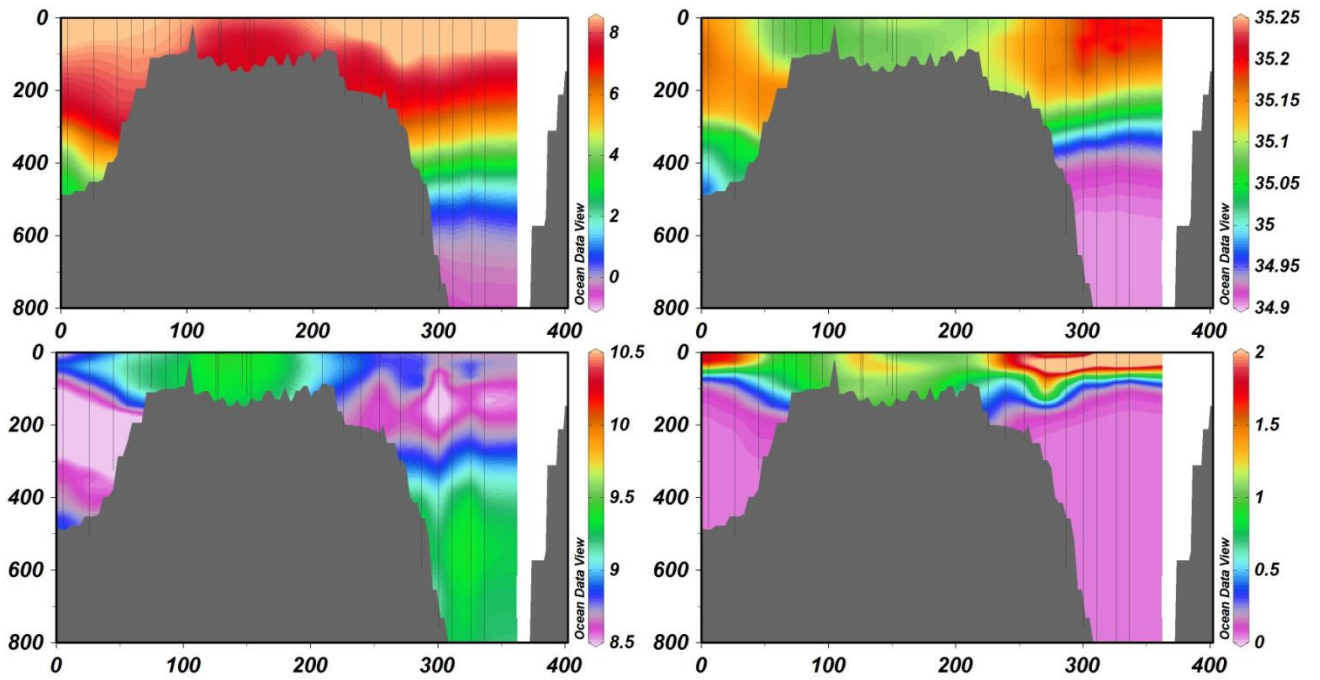


Figure A30 Combined section R-S, May-June 2018. (a) Temperature ( $^{\circ}\text{C}$ ), (b) salinity (psu), (c) oxygen concentrations ( $\text{mg L}^{-1}$ ) and (d) fluorescence.

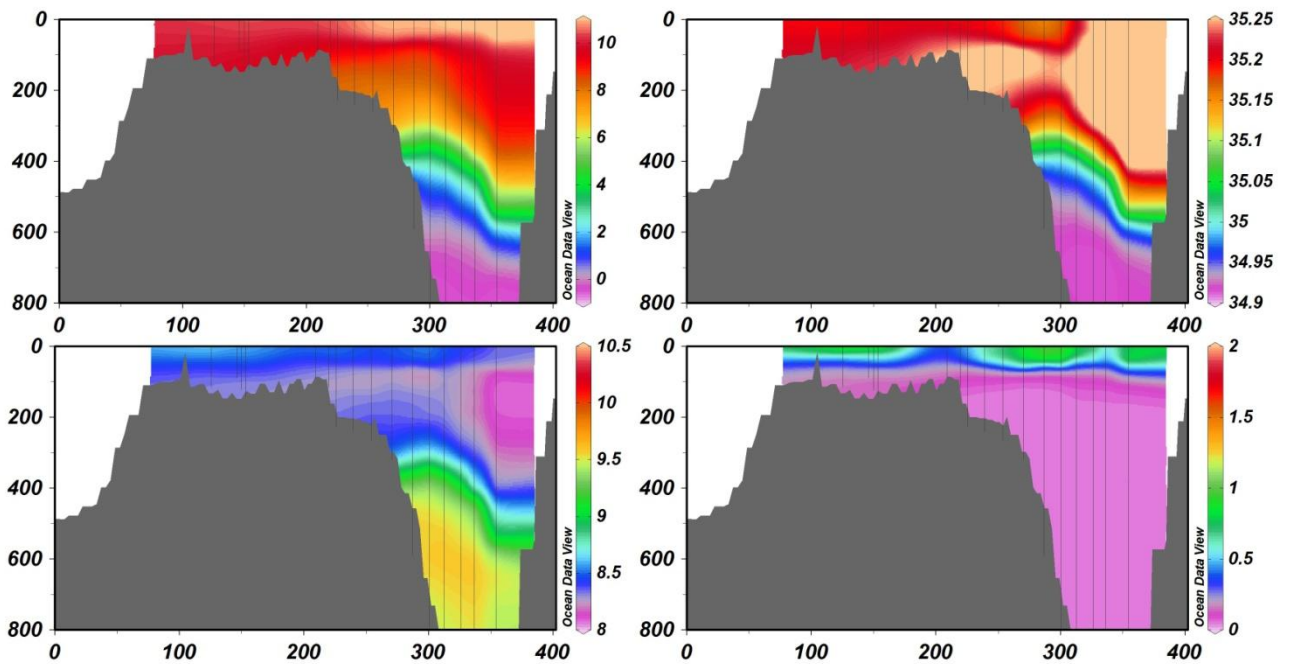


Figure A31 Combined section R-S, August-September 2013. (a) Temperature ( $^{\circ}\text{C}$ ), (b) salinity (psu), (c) oxygen concentrations ( $\text{mg L}^{-1}$ ) and (d) fluorescence.

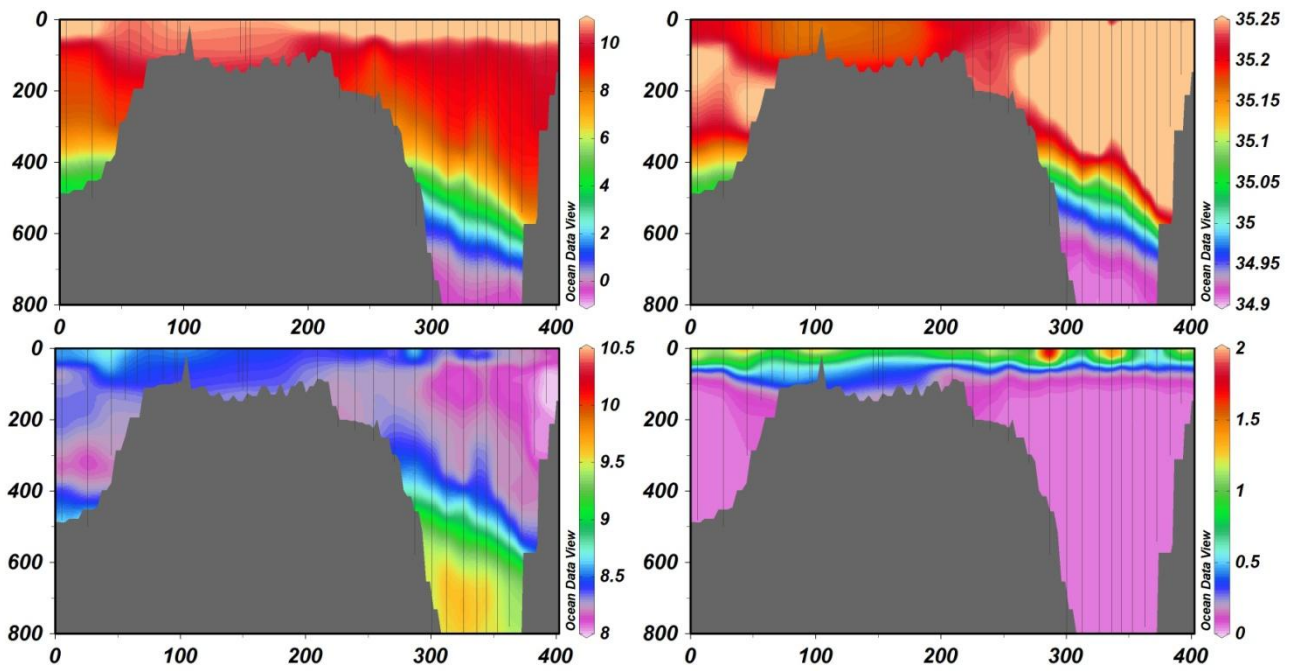


Figure A32 Combined section R-S, August-September 2014. (a) Temperature ( $^{\circ}\text{C}$ ), (b) salinity (psu), (c) oxygen concentrations ( $\text{mg L}^{-1}$ ) and (d) fluorescence.

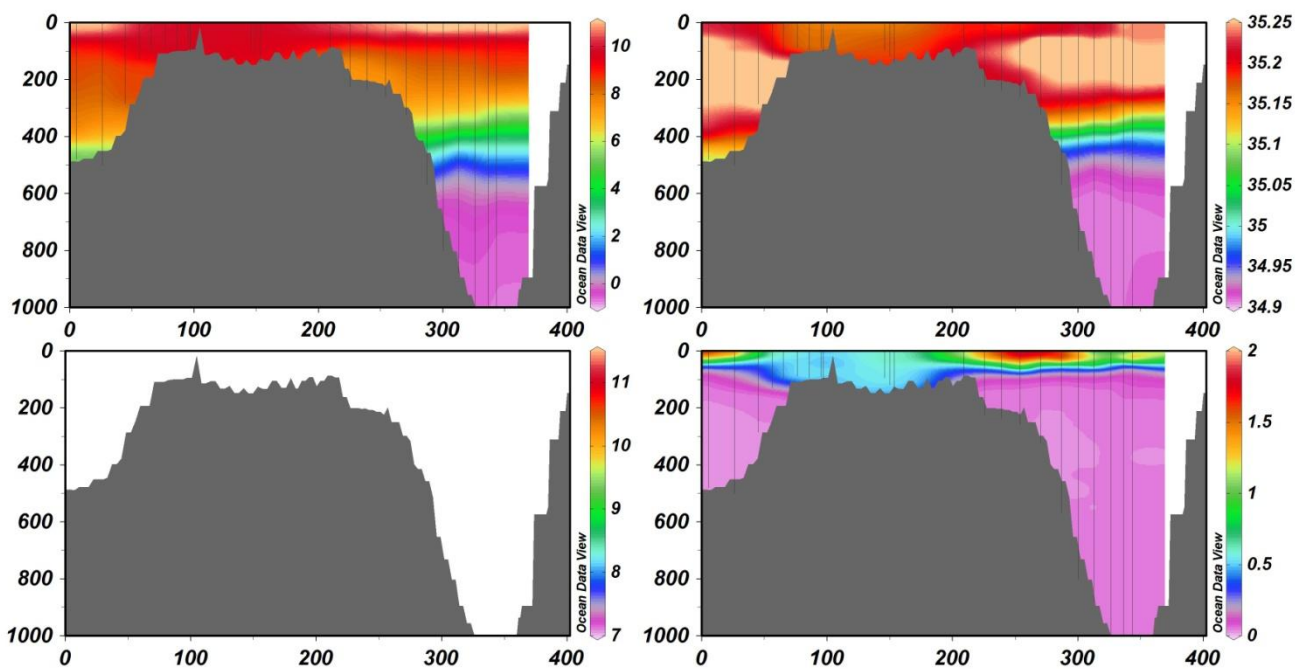


Figure A33 Combined section R-S, August-September 2015. (a) Temperature ( $^{\circ}\text{C}$ ), (b) salinity (psu), (c) oxygen concentrations ( $\text{mg L}^{-1}$ ) and (d) fluorescence.

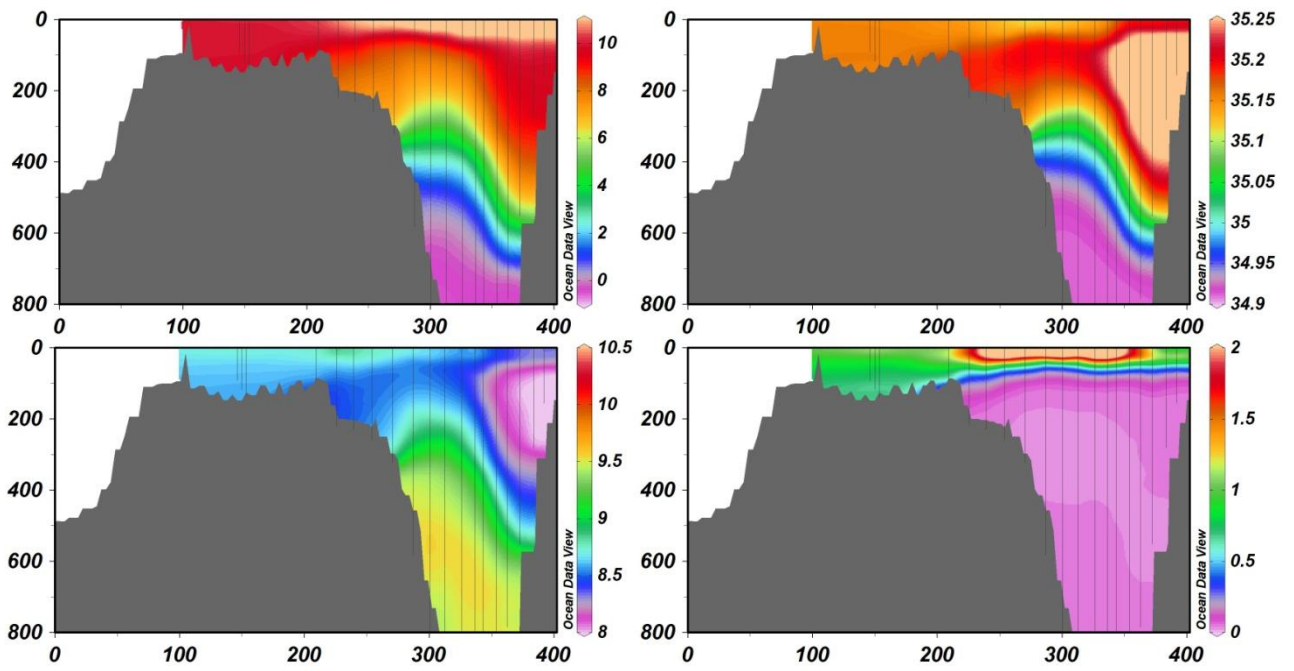


Figure A34 Combined section R-S, August-September 2016. (a) Temperature ( $^{\circ}\text{C}$ ), (b) salinity (psu), (c) oxygen concentrations ( $\text{mg L}^{-1}$ ) and (d) fluorescence.

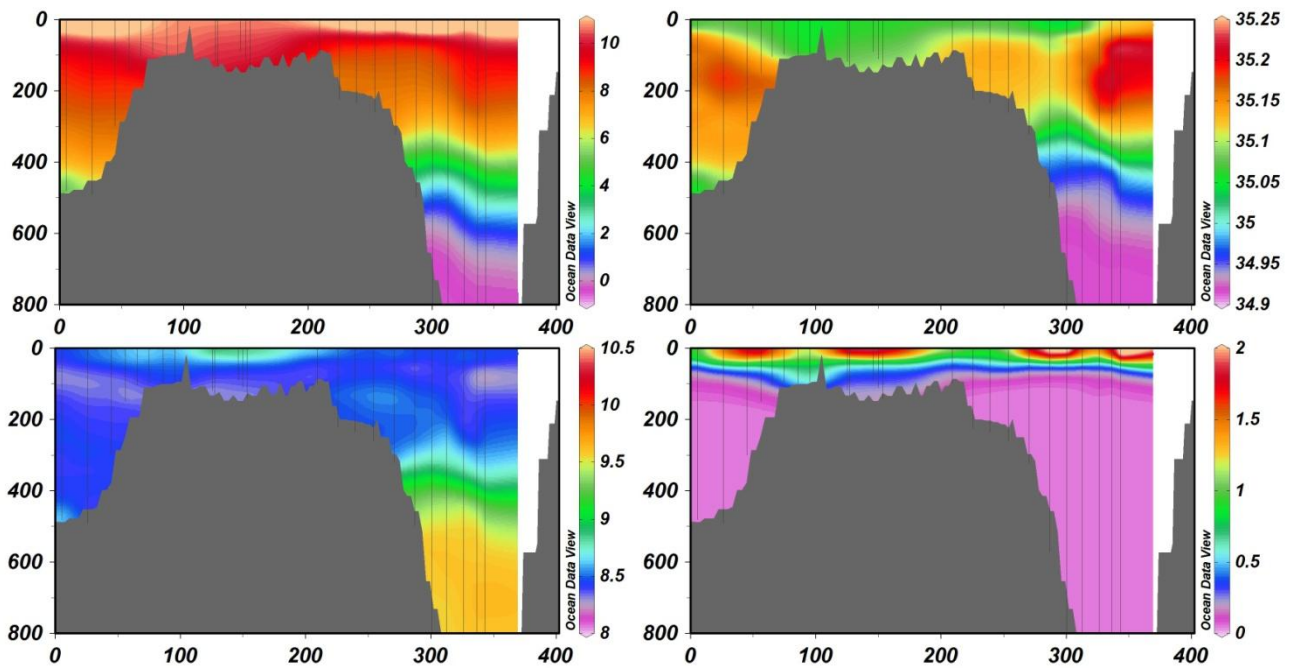


Figure A35 Combined section R-S, August-September 2017. (a) Temperature ( $^{\circ}\text{C}$ ), (b) salinity (psu), (c) oxygen concentrations ( $\text{mg L}^{-1}$ ) and (d) fluorescence.

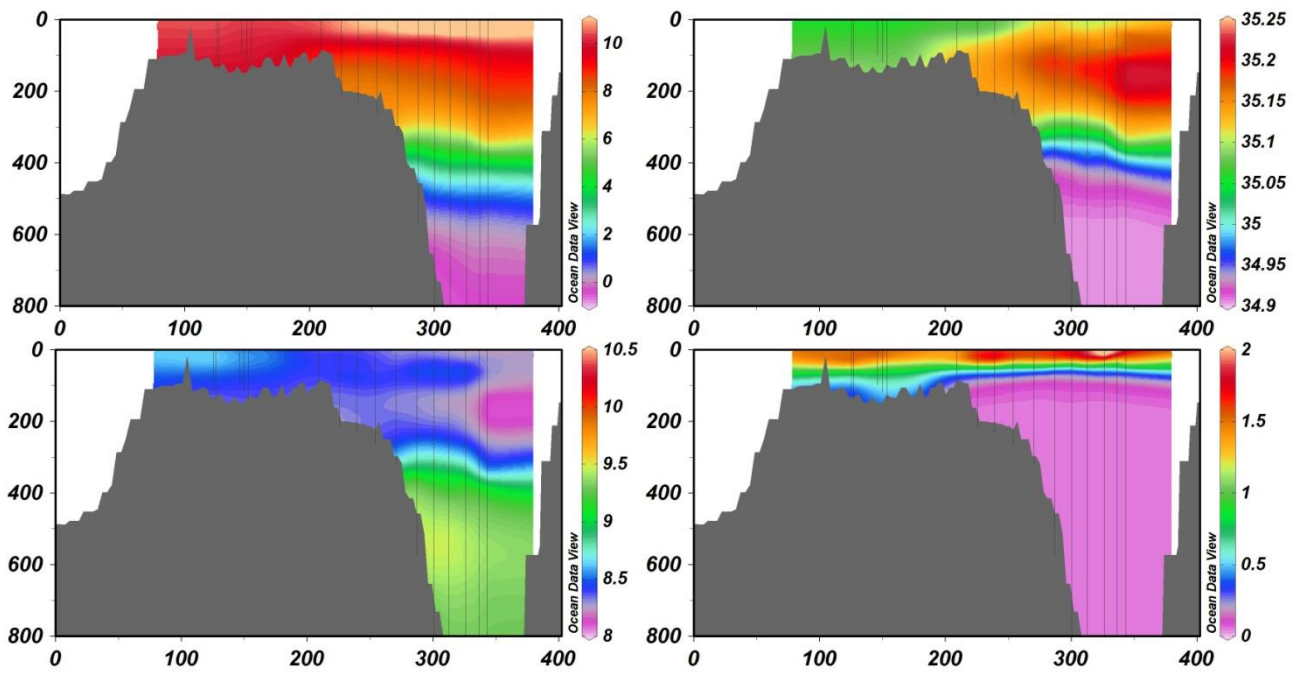


Figure A36 Combined section R-S, August-September 2018. (a) Temperature ( $^{\circ}\text{C}$ ), (b) salinity (psu), (c) oxygen concentrations ( $\text{mg L}^{-1}$ ) and (d) fluorescence.

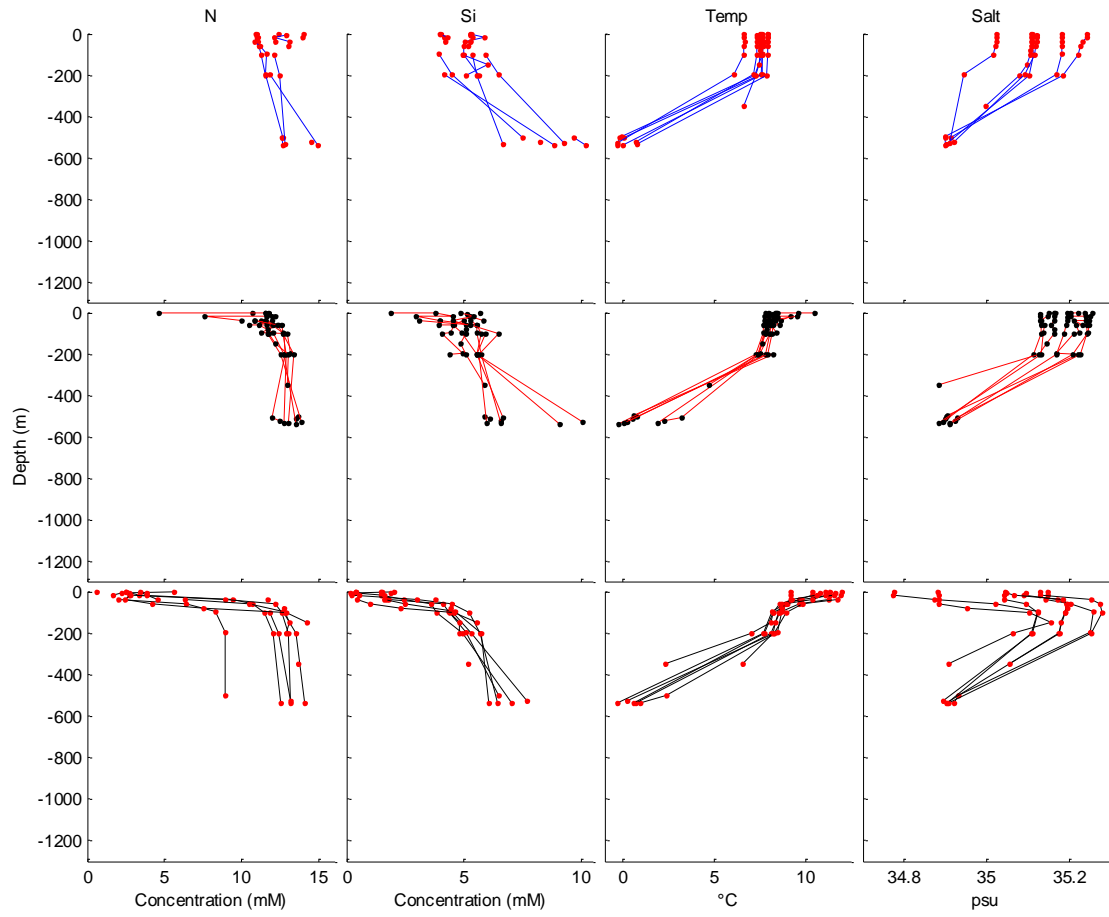


Figure A37 Individual nitrate (N), silicate (Si), temperature (T) and salinity (S) profiles from standard station N04 during the years 2013-2020. Upper row: Mid-February, middle row May-June and lower row: August-September.

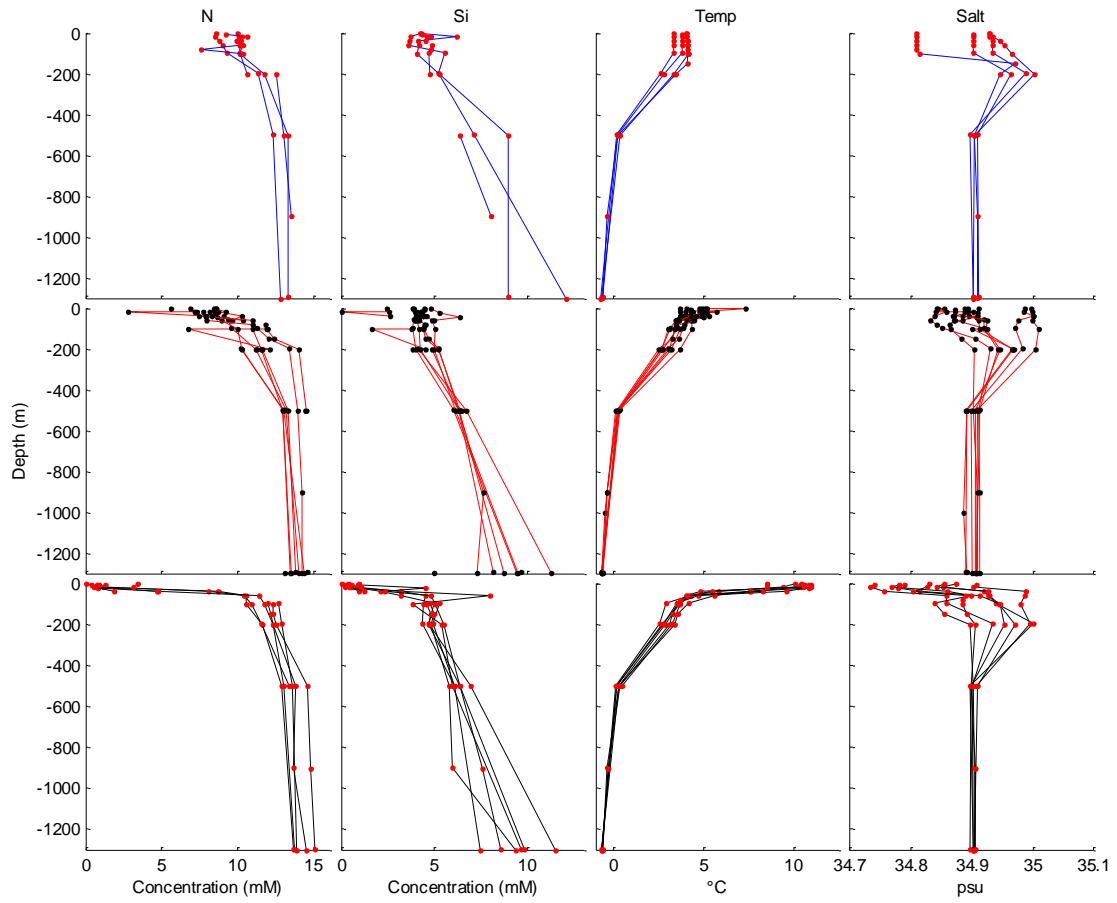


Figure A38 Individual profiles at station N13 (panels as described under Fig. A37)

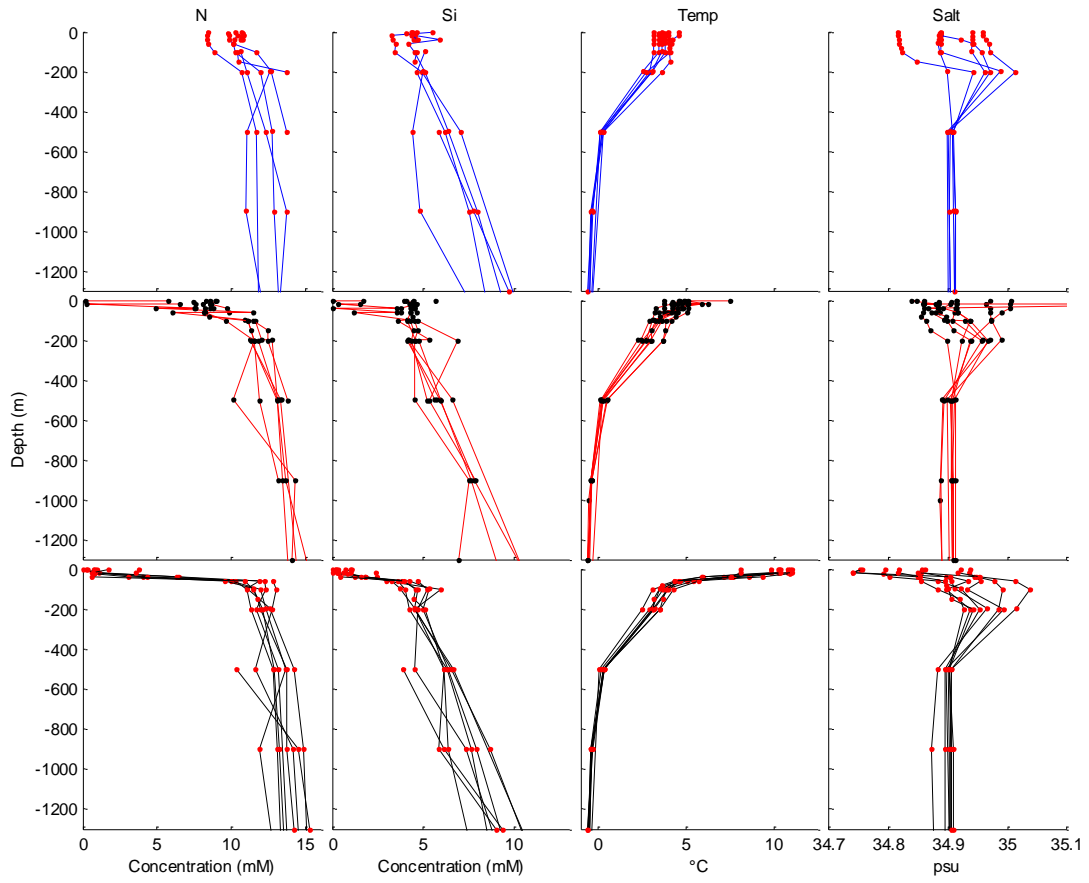


Figure A39 Individual profiles at station N14 (panels as described under Fig. A37)

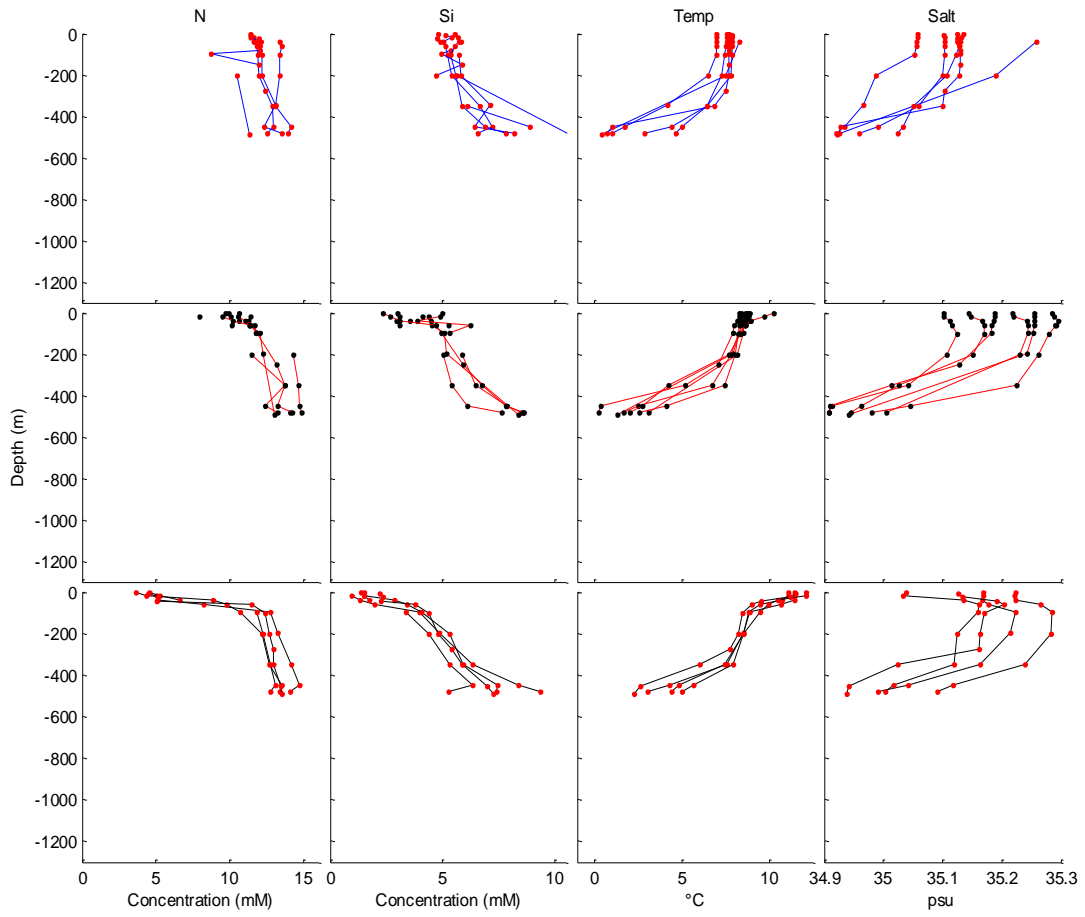


Figure A40 Individual profiles at station R08 (panels as described under Fig. A37)

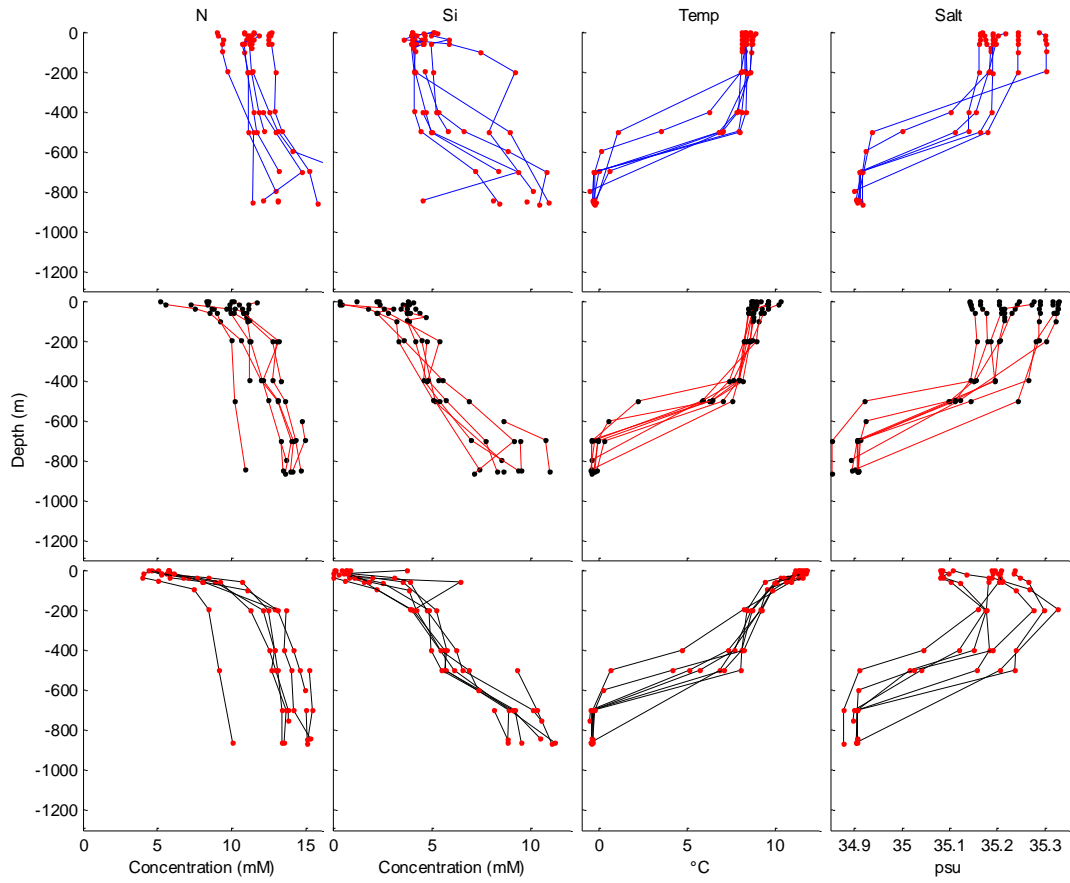


Figure A41 Individual profiles at station V06 (panels as described under Fig. A37)

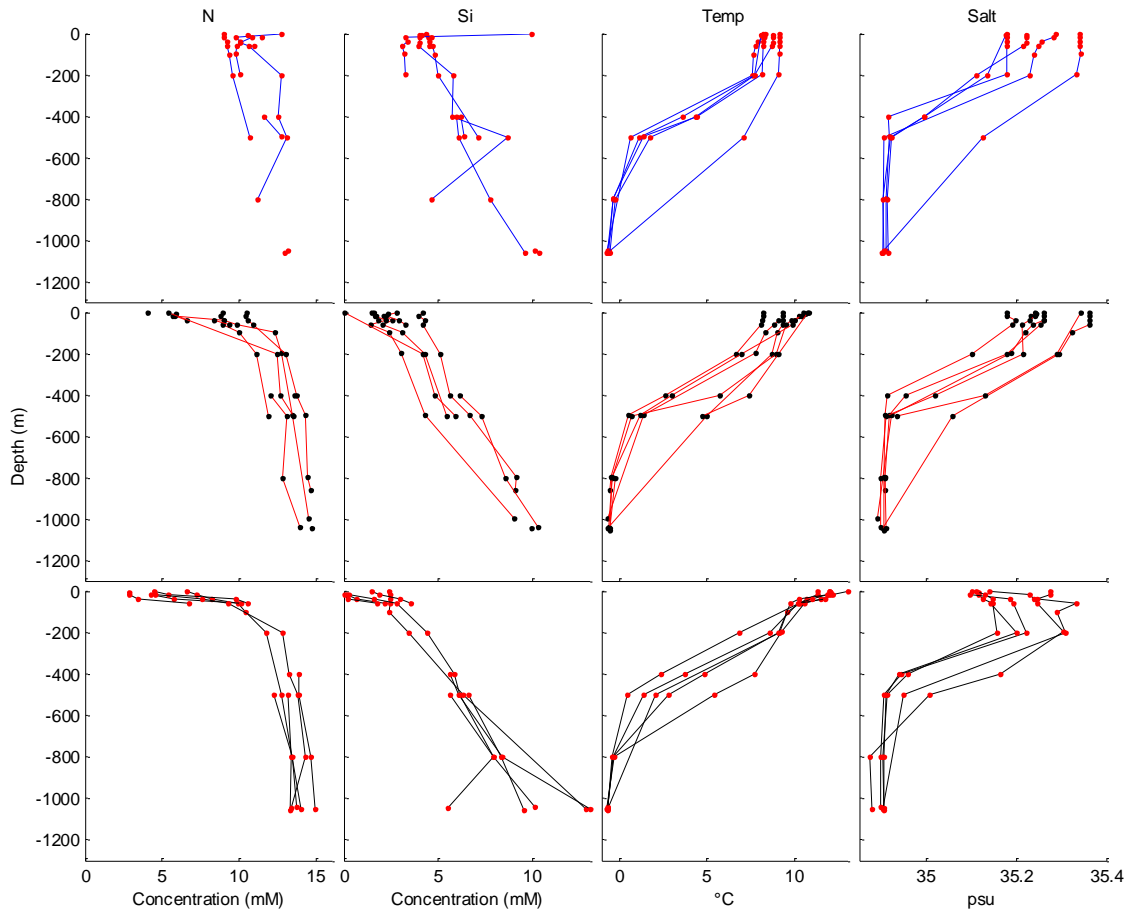


Figure A42 Individual profiles at station S08 (panels as described under Fig. A37)

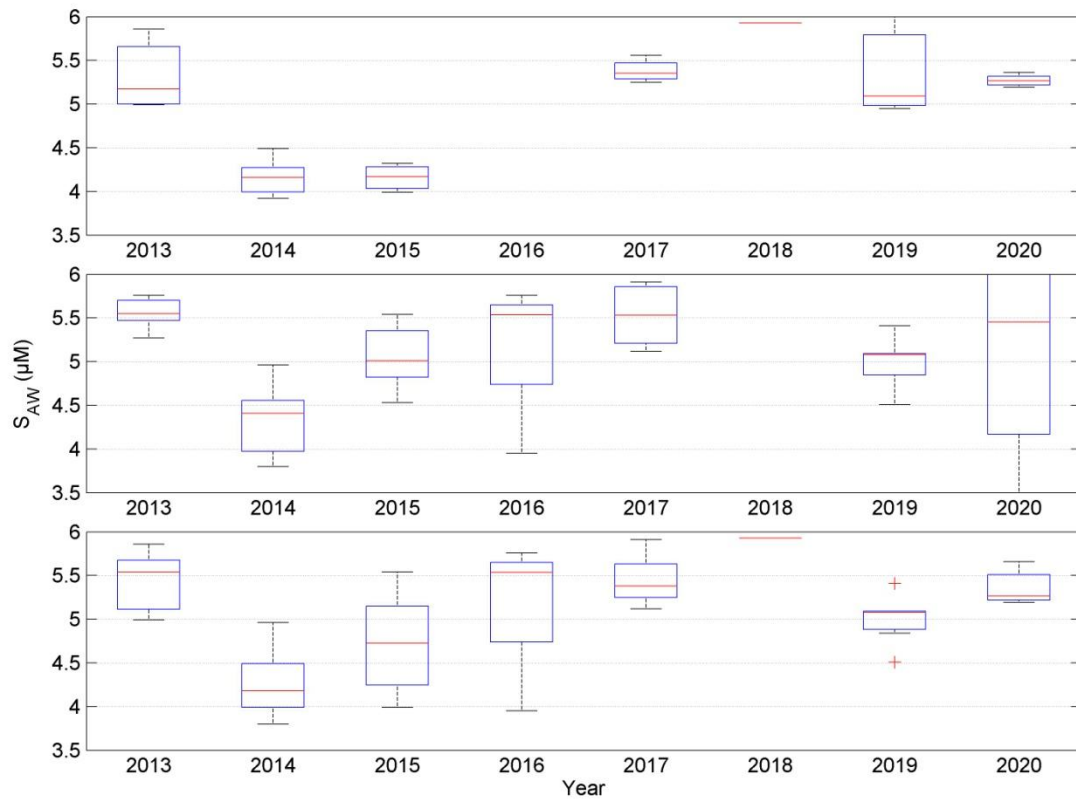


Figure A43 Boxplots for silicate samples taken at station N04. Upper panel: Mid-February, mid-panel: May-June and lower panel: the above seasons combined. The red central mark is the median, the edges of the boxes are the 25th and 75th percentiles, the whiskers extend to the most extreme data points the algorithm considers to be not outliers, and the outliers are plotted individually (from the Boxplot.m routine in Matlab®).

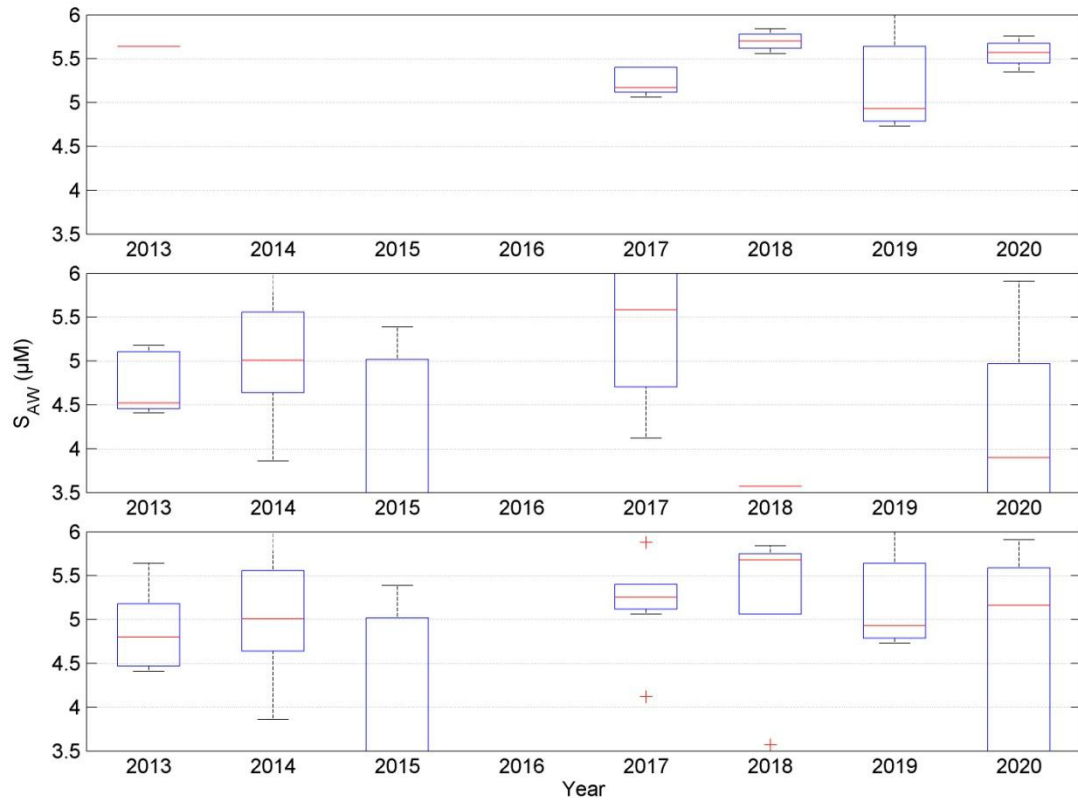


Figure A44 Boxplots for silicate samples taken at station R08 (details as for Fig. A43).

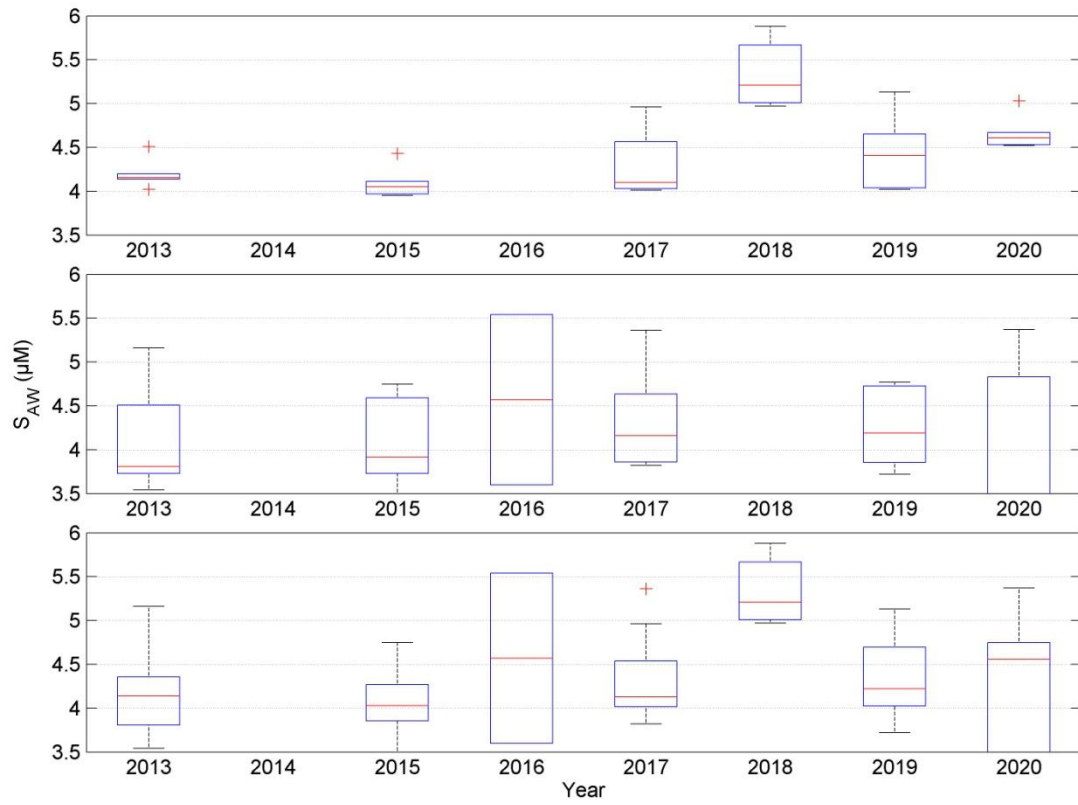


Figure A45 Boxplots for silicate samples taken at station V06 (details as for Fig. A43).



Figure A46 Boxplots for silicate samples taken at station S08 (details as for Fig. A43).

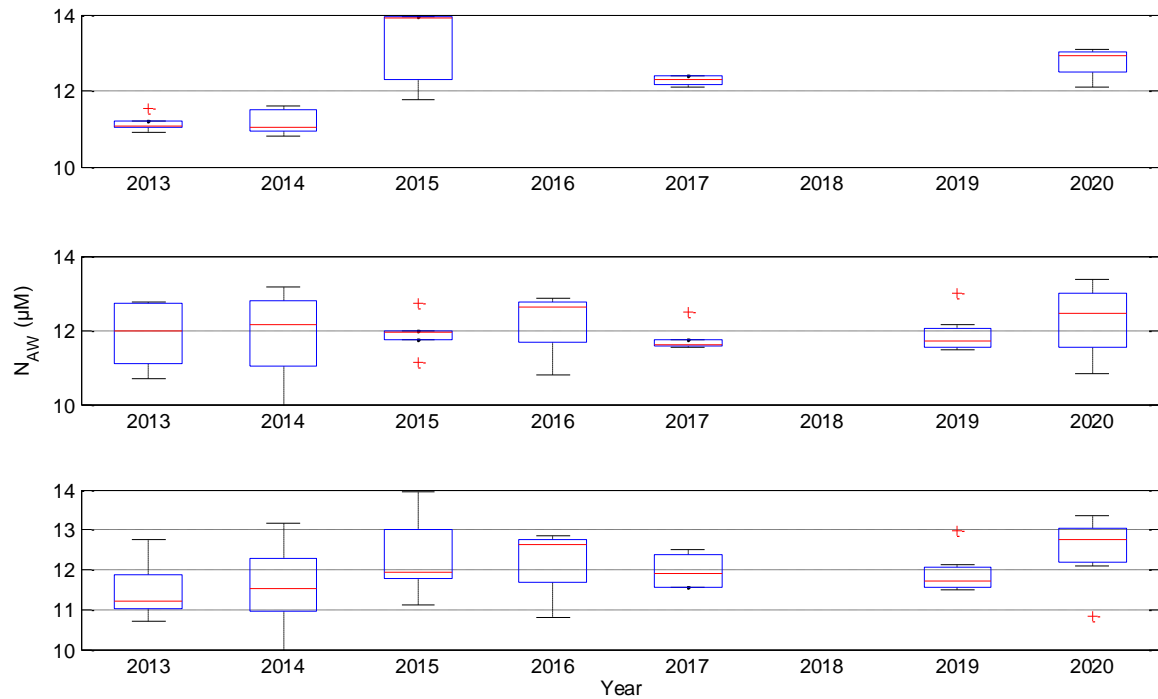


Figure A47 Boxplots for **nitrate** samples taken at station N04 (details as for Fig. A43).

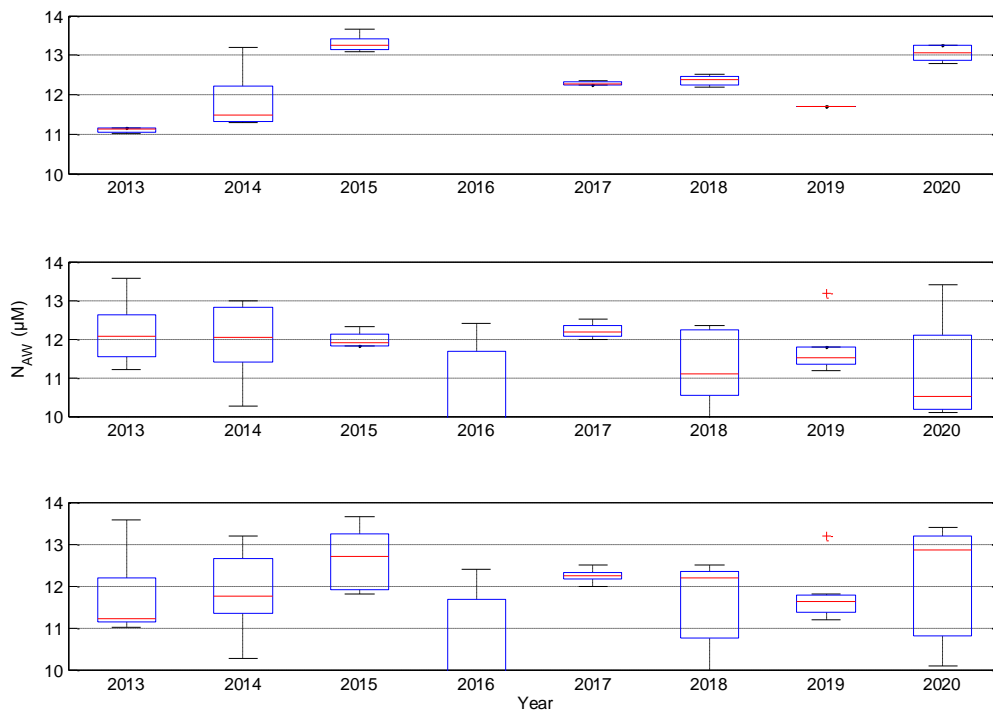


Figure A48 Boxplots for nitrate samples taken at station N05 (details as for Fig. A43).

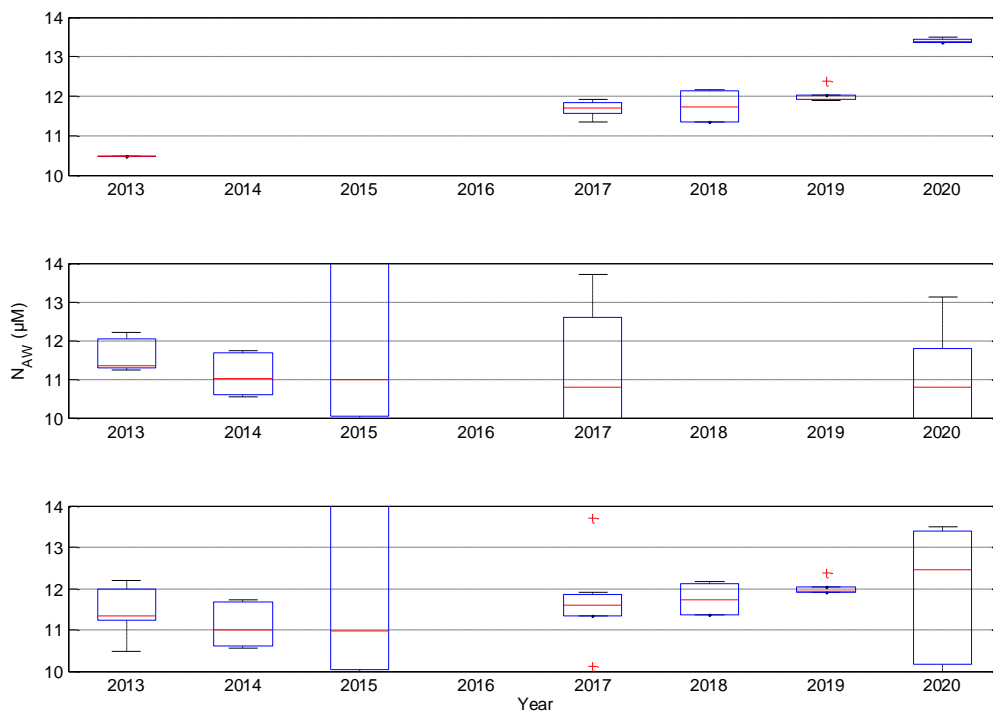


Figure A49 Boxplots for nitrate samples taken at station R08 (details as for Fig. A43).

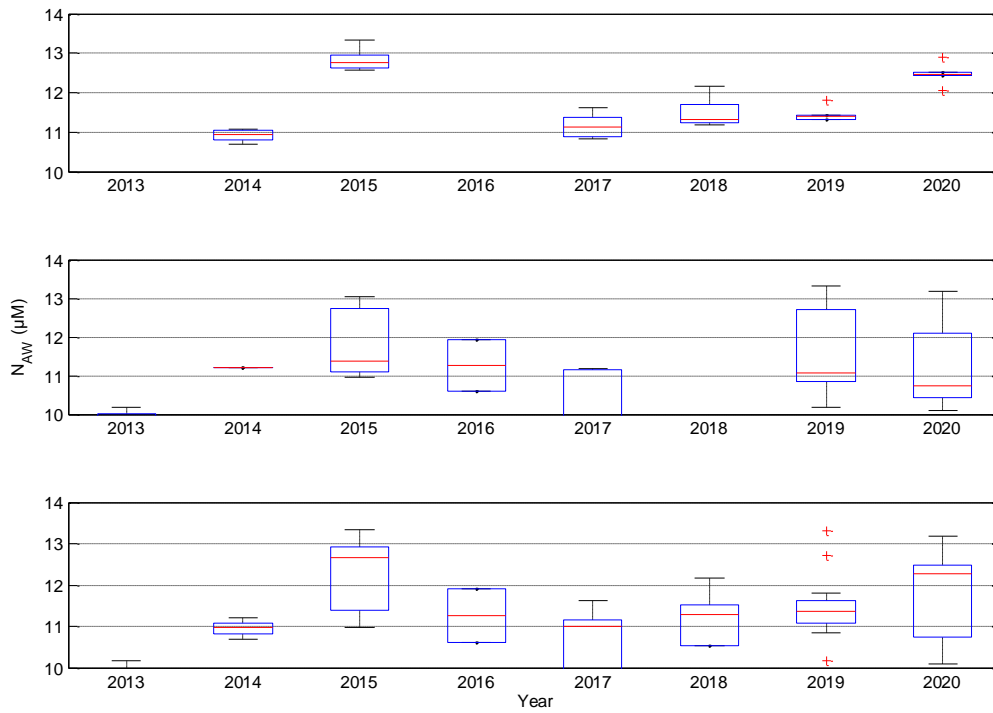


Figure A50 Boxplots for nitrate samples taken at station V06 (details as for Fig. A43).

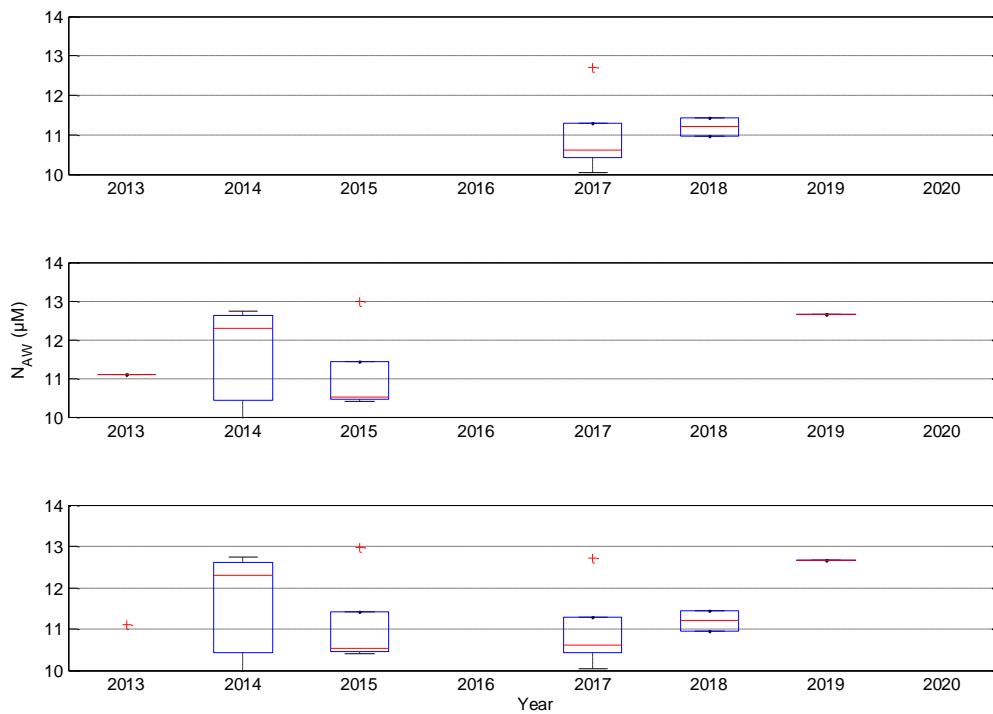


Figure A51 Boxplots for **nitrate** samples taken at station S08 (details as for Fig. A43).

The boxplot for phosphate are not shown.

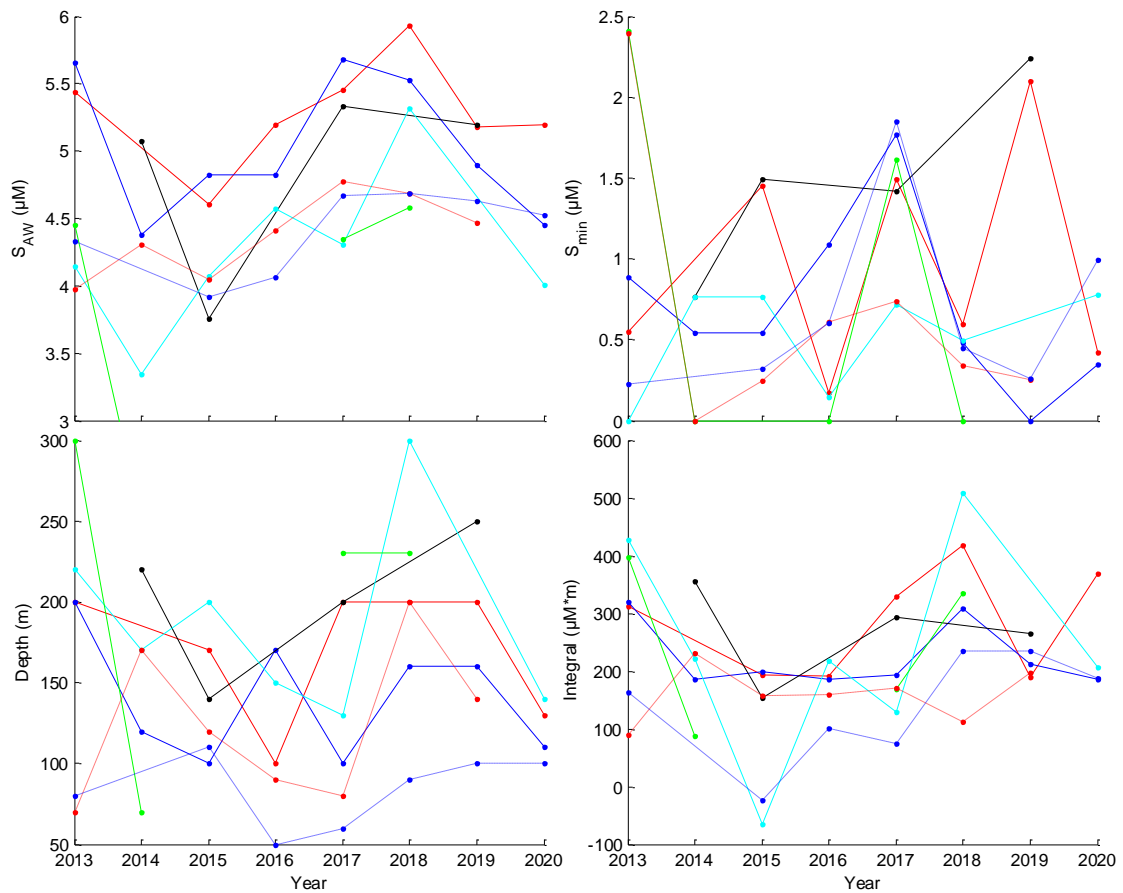
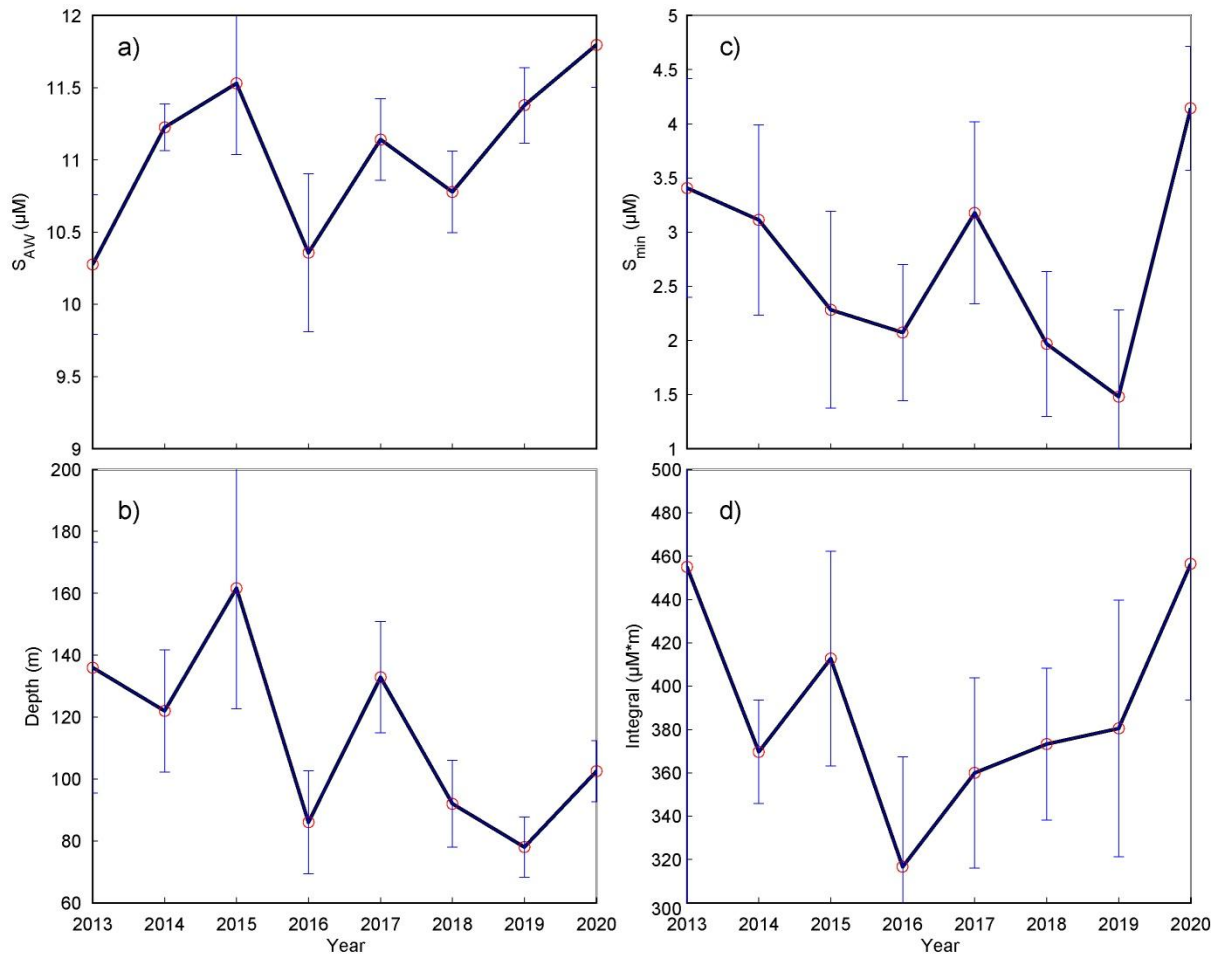
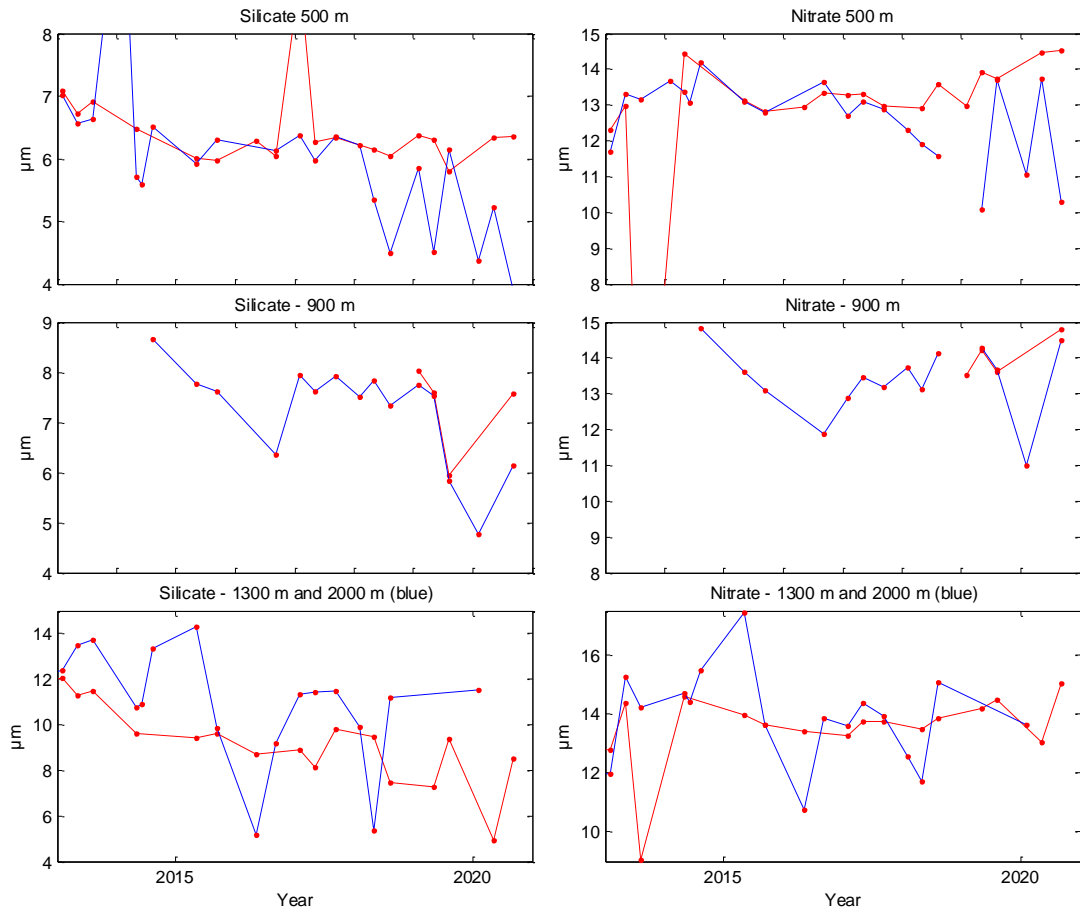


Figure A52 **Silicate drawdown parameters at the individual standard nutrient stations** (a) pre-bloom concentrations, (b) growth-influenced depth,  $D_{pp}$  (c) minimum concentration in August,  $S_{min}$  and (d) integrated silicate reduction,  $S_{Red}$ . The individual standard nutrient stations are colored N04 (red), N05 (blue), R08 (black), V06 (cyan), S08 (green), N13 (dashed blue) and N14 (dashed red).



**Fig. A53 Averaged nitrate drawdown parameters** (a) pre-bloom concentrations, (b) growth-influenced depth,  $D_{pp}$  (c) minimum concentration in August,  $N_{min}$  and (d) integrated reduction,  $N_{Red}$ . These have been averaged over all relevant standard stations (N04, N05, R08, V06 and S08), and the associated standard deviations are marked with the vertical blue lines.



**Fig. A54 Deep nutrient records at depth at station N13 (red) and N14 (blue). Silicate in the left panels and nitrate in the right panels.**

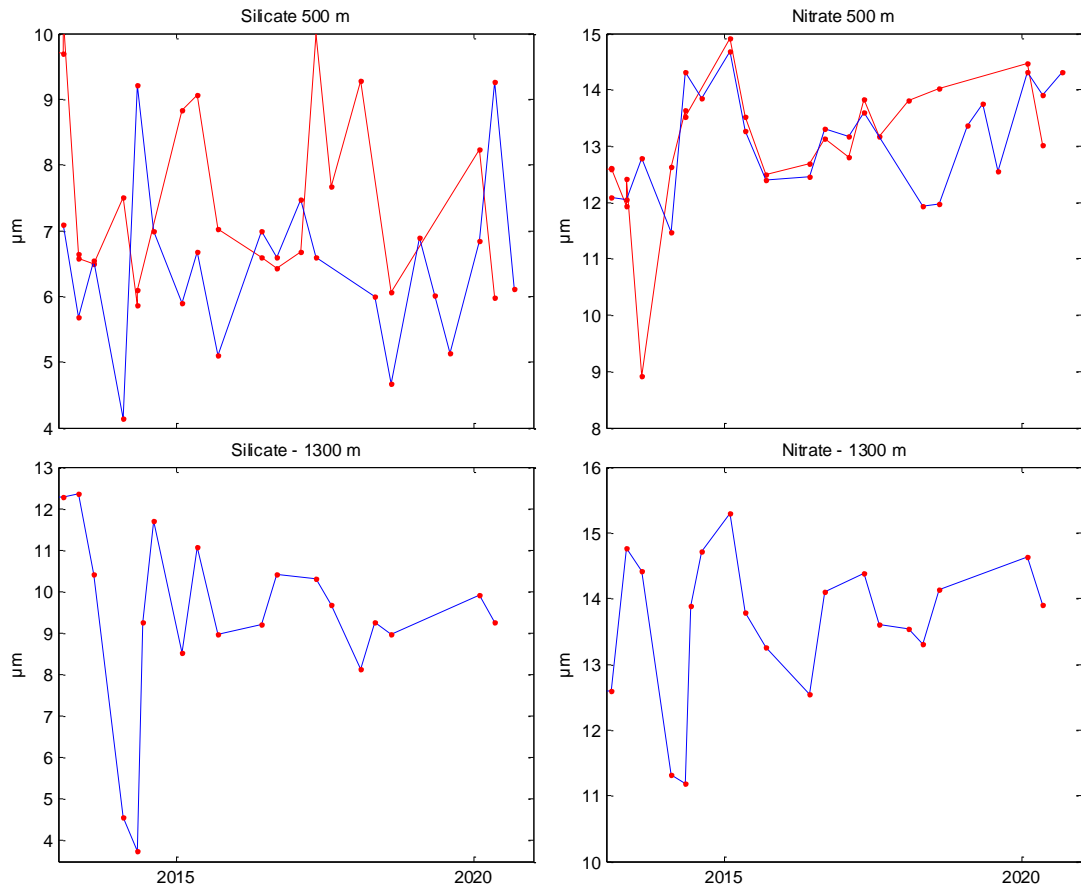


**Fig. A55 Deep nutrient records at depth at station N04 (red) and N05 (blue).** Silicate in the left panels and nitrate in the right panels.

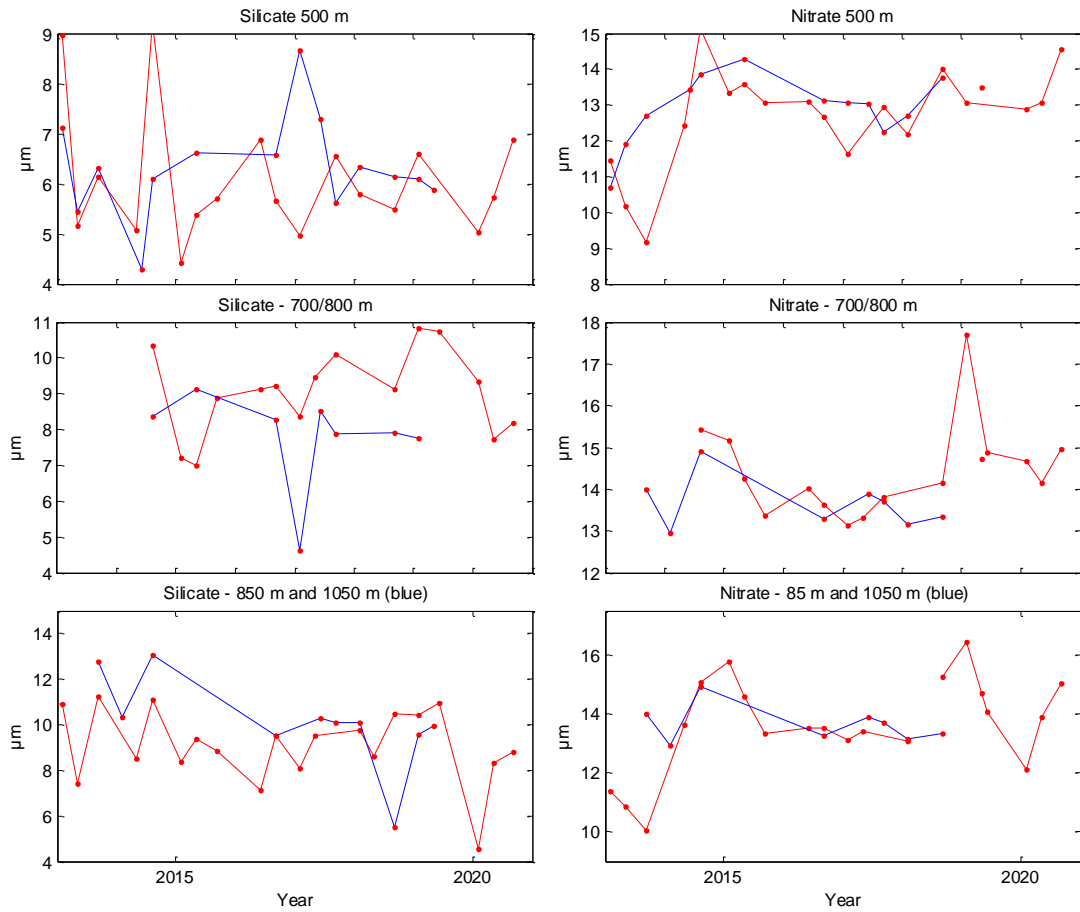


**Fig. A56 Deep nutrient records at depth at station V06 (red) and S08 (blue).** Silicate in the left panels and nitrate in the right panels.

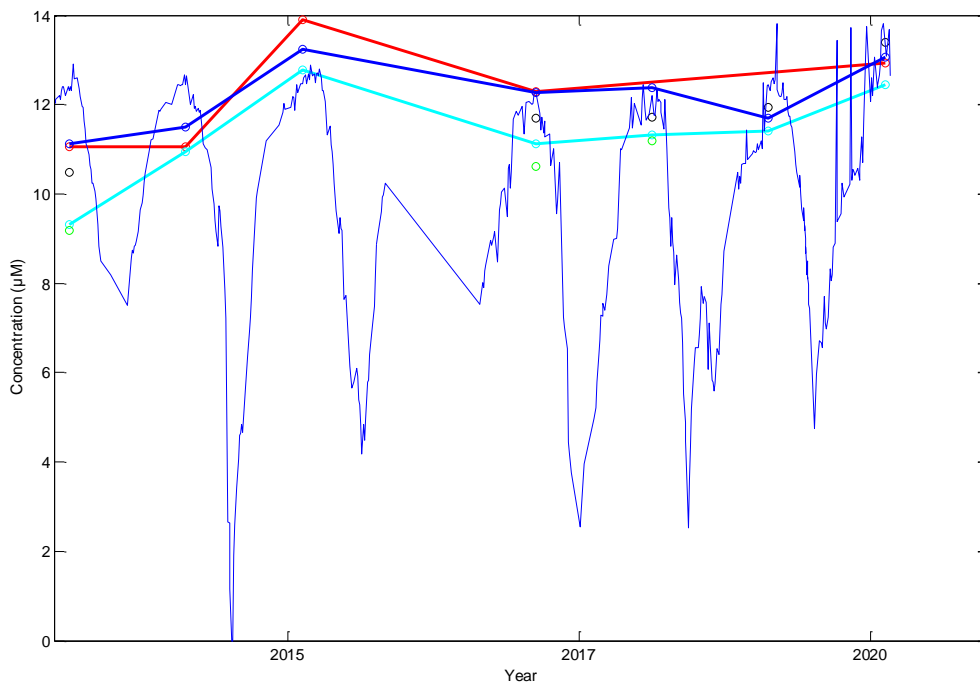
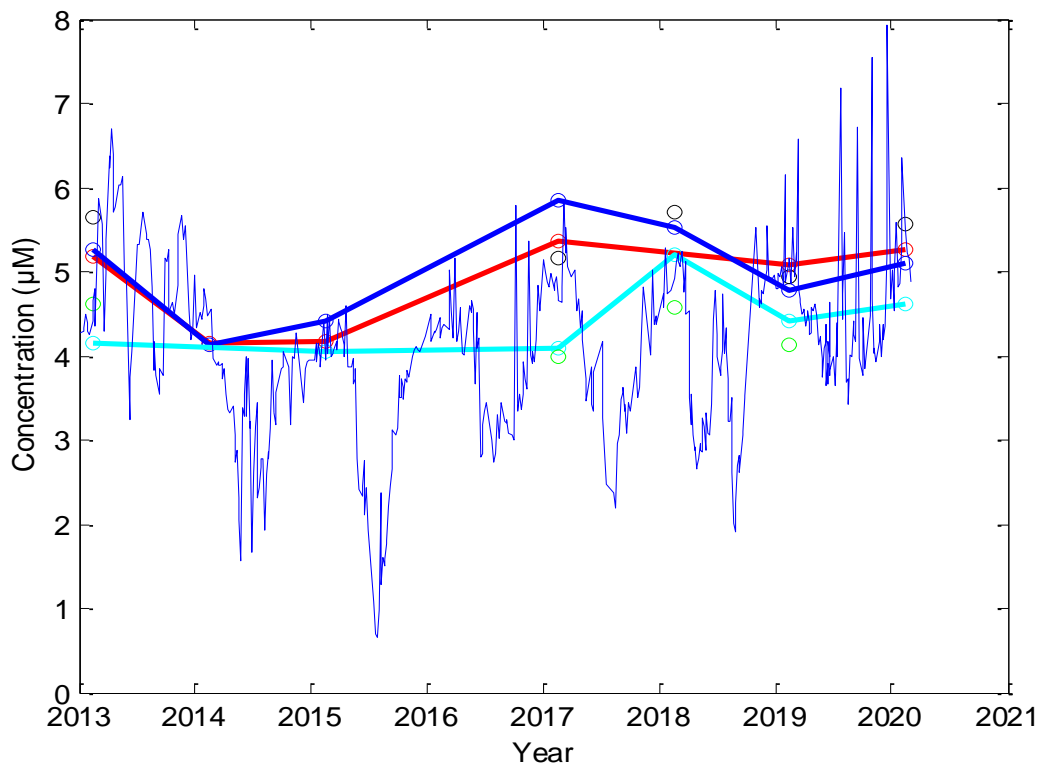


**Fig. A57 Nutrient concentrations at coastal stations Skopun and around the Faroes**

Upper: Silicate and lower: nitrate. The Skopun records are like shown in Figure 6, while the oceanic records ( $S_{AW}$  and  $N_{AW}$ ), obtained from N04 (red), N05 (blue), R08 (black circles), V06 (cyan) and S08 (green circles) are like shown in Figures 26 and 27.

**Table A1** Differences in nitrate concentrations as a function of different preservation methods: Clf = chloroform, HgCl<sub>2</sub> = mercuric chloride, Frozen = -20°C. Values in table are presented as the relative difference between treatments, i.e. for Clf vs HgCl<sub>2</sub> a value of 1.09 implies chloroform values were 9% higher than mercuric chloride values, whereas a value of 0.91 implies they are 9% lower. Averages are calculated from the individual samples and presented as + or – percentages to indicate if a particular treatment exhibits the tendency of being higher or lower. CV is coefficient of variation, i.e. standard deviation / mean (duplicate measurements). Average CV is the average co-efficient of variation for duplicate measurements, Min CV and Max CV are minimum and maximum coefficients of variation. CV was determined from all of the samples included in the preservation comparison (n=30). Note, it is technically incorrect to determine CV from duplicate measurements, but analytical replicates exist as duplicates. CV therefore provides an approximation for the analytical precision of measurements that should be compared with the relative differences between treatments.

| Nitrate |                           | Preservatives            |                  |                             |
|---------|---------------------------|--------------------------|------------------|-----------------------------|
| Depth   | Nitrate                   | Clf vs HgCl <sub>2</sub> | Clf vs Frozen    | Frozen vs HgCl <sub>2</sub> |
| 100     | 14.75                     | 1.09                     | 1.05             | 1.04                        |
| 150     | 13.19                     | 1.11                     | 1.08             | 1.02                        |
| 500     | 16.01                     | 1.08                     | 1.17             | 0.92                        |
| 100     | 13.44                     | 1.03                     | 1.00             | 1.03                        |
| 200     | 13.81                     | 1.02                     | 1.00             | 1.03                        |
|         | <b>Average difference</b> | <b>7.62</b>              | <b>7.46</b>      | <b>0.40</b>                 |
|         | <i>Average CV</i>         | <i>1.7 ± 1.3</i>         | <i>1.7 ± 1.3</i> | <i>1.7 ± 1.3</i>            |
|         | <i>Min CV</i>             | <i>0.01</i>              | <i>0.01</i>      | <i>0.01</i>                 |
|         | <i>Max CV</i>             | <i>5.90</i>              | <i>5.90</i>      | <i>5.90</i>                 |

**Table A2** Differences in silicate concentrations as a function of different preservation methods: Clf = chloroform, HgCl<sub>2</sub> = mercuric chloride, Frozen = -20°C. Values in table are presented as the relative difference between treatments, i.e. for Clf vs HgCl<sub>2</sub> a value of 1.09 implies chloroform values were 9% higher than mercuric chloride values, whereas a value of 0.91 implies they are 9% lower. Averages are calculated from the individual samples and presented as + or – percentages to indicate if a particular treatment exhibits the tendency of being higher or lower. CV is coefficient of variation, i.e. standard deviation / mean (duplicate measurements). Average CV is the average co-efficient of variation for duplicate measurements, Min CV and Max CV are minimum and maximum coefficients of variation. CV was determined from all of the samples included in the preservation comparison (n=30). Note, it is technically incorrect to determine CV from duplicate measurements, but analytical replicates exist as duplicates. CV therefore provides an approximation for the analytical precision of measurements that should be compared with the relative differences between treatments.

| <b>Silicate</b> |                           | <b>Preservatives</b>     |                  |                             |
|-----------------|---------------------------|--------------------------|------------------|-----------------------------|
| Depth           | Nitrate                   | Clf vs HgCl <sub>2</sub> | Clf vs Frozen    | Frozen vs HgCl <sub>2</sub> |
| 100             | 14.75                     | 1.06                     | 1.03             | 1.03                        |
| 150             | 13.19                     | 1.01                     | 1.06             | 0.95                        |
| 500             | 16.01                     | 1.01                     | 1.02             | 0.99                        |
| 100             | 13.44                     | 0.99                     | 1.00             | 0.99                        |
| 200             | 13.81                     | 0.92                     | 0.99             | 0.93                        |
|                 | <b>Average difference</b> | <b>1.71</b>              | <b>2.89</b>      | <b>-1.12</b>                |
|                 | <i>Average CV</i>         | <i>1.1 ± 1.0</i>         | <i>1.1 ± 1.0</i> | <i>1.1 ± 1.0</i>            |
|                 | <i>Min CV</i>             | <i>0.04</i>              | <i>0.04</i>      | <i>0.04</i>                 |
|                 | <i>Max CV</i>             | <i>3.40</i>              | <i>3.40</i>      | <i>3.40</i>                 |

**Table A3** Differences in phosphate concentrations as a function of different preservation methods: Clf = chloroform, HgCl<sub>2</sub> = mercuric chloride, Frozen = -20°C. Values in table are presented as the relative difference between treatments, i.e. for Clf vs HgCl<sub>2</sub> a value of 1.09 implies chloroform values were 9% higher than mercuric chloride values, whereas a value of 0.91 implies they are 9% lower. Averages are calculated from the individual samples and presented as + or – percentages to indicate if a particular treatment exhibits the tendency of being higher or lower. CV is coefficient of variation, i.e. standard deviation / mean (duplicate measurements). Average CV is the average co-efficient of variation for duplicate measurements, Min CV and Max CV are minimum and maximum coefficients of variation. CV was determined from all of the samples included in the preservation comparison (n=30). Note, it is technically incorrect to determine CV from duplicate measurements, but analytical replicates exist as duplicates. CV therefore provides an approximation for the analytical precision of measurements that should be compared with the relative differences between treatments.

| Phosphate |                           | Preservatives            |                  |                             |
|-----------|---------------------------|--------------------------|------------------|-----------------------------|
| Depth     | Nitrate                   | Clf vs HgCl <sub>2</sub> | Clf vs Frozen    | Frozen vs HgCl <sub>2</sub> |
| 100       | 14.75                     | 1.02                     | 1.01             | 1.01                        |
| 150       | 13.19                     | 0.99                     | 1.01             | 0.98                        |
| 500       | 16.01                     | 0.96                     | 0.99             | 0.97                        |
| 100       | 13.44                     | 1.00                     | 1.04             | 0.97                        |
| 200       | 13.81                     | 1.02                     | 1.00             | 1.03                        |
|           | <b>Average difference</b> | <b>-0.74</b>             | <b>1.05</b>      | <b>-1.76</b>                |
|           | <i>Average CV</i>         | <i>0.5 ± 0.3</i>         | <i>0.5 ± 0.3</i> | <i>0.5 ± 0.3</i>            |
|           | <i>Min CV</i>             | <i>0.08</i>              | <i>0.08</i>      | <i>0.08</i>                 |
|           | <i>Max CV</i>             | <i>1.2</i>               | <i>1.2</i>       | <i>1.2</i>                  |

**Table A4** Differences in nitrate concentrations as a function of the interval between the time samples were collected and preserved and the time they were analysed: Clf = chloroform, HgCl<sub>2</sub> = mercuric chloride, Frozen = -20°C. Values in table are presented as the relative difference between samples analysed after 2 months and 4 months for each preservative method, i.e. for Clf a value of 0.92 indicates that nitrate concentrations in 4 month old samples were 8% lower than 2 month old samples. Averages are calculated from the individual samples and presented as + or – percentages to indicate if a particular treatment exhibits the tendency of being higher or lower following increased storage time. CV is coefficient of variation, i.e. standard deviation / mean (duplicate measurements). Average CV is the average co-efficient of variation for duplicate measurements, Min CV and Max CV are minimum and maximum coefficients of variation. CV was determined from all of the samples included in the preservation comparison (n=30). Note, it is technically incorrect to determine CV from duplicate measurements, but analytical replicates exist as duplicates. CV therefore provides an approximation for the analytical precision of measurements that should be compared with the relative differences between treatments.

| <b>Nitrate</b> |                           | <b>Time</b>      |                   |                  |
|----------------|---------------------------|------------------|-------------------|------------------|
| Depth          | Nitrate                   | Clf              | HgCl <sub>2</sub> | Frozen           |
| 100            | 14.75                     | 0.95             | 0.95              | 0.94             |
| 150            | 13.19                     | 0.86             | 0.93              | 0.94             |
| 500            | 16.01                     | 0.89             | 0.93              | 1.04             |
| 100            | 13.44                     | 0.94             | 0.94              | 0.76             |
| 200            | 13.81                     | 0.93             | 0.94              | 0.93             |
|                | <b>Average difference</b> | <b>-9.11</b>     | <b>-6.37</b>      | <b>-8.22</b>     |
|                | <i>Average CV</i>         | <i>1.7 ± 1.3</i> | <i>1.7 ± 1.3</i>  | <i>1.7 ± 1.3</i> |
|                | <i>Min CV</i>             | <i>0.01</i>      | <i>0.01</i>       | <i>0.01</i>      |
|                | <i>Max CV</i>             | <i>5.90</i>      | <i>5.90</i>       | <i>5.90</i>      |

**Table A5** Differences in silicate concentrations as a function of the interval between the time samples were collected and preserved and the time they were analysed: Clf = chloroform, HgCl<sub>2</sub> = mercuric chloride, Frozen = -20°C. Values in table are presented as the relative difference between samples analysed after 2 months and 4 months for each preservative method, i.e. for Clf a value of 0.92 indicates that nitrate concentrations in 4 month old samples were 8% lower than 2 month old samples. Averages are calculated from the individual samples and presented as + or – percentages to indicate if a particular treatment exhibits the tendency of being higher or lower following increased storage time. CV is coefficient of variation, i.e. standard deviation / mean (duplicate measurements). Average CV is the average co-efficient of variation for duplicate measurements, Min CV and Max CV are minimum and maximum coefficients of variation. CV was determined from all of the samples included in the preservation comparison (n=30). Note, it is technically incorrect to determine CV from duplicate measurements, but analytical replicates exist as duplicates. CV therefore provides an approximation for the analytical precision of measurements that should be compared with the relative differences between treatments.

| <b>Silicate</b> |                           | <b>Time</b>      |                         |                  |
|-----------------|---------------------------|------------------|-------------------------|------------------|
| <b>Depth</b>    | <b>Nitrate</b>            | <b>Clf</b>       | <b>HgCl<sub>2</sub></b> | <b>Frozen</b>    |
| 100             | 14.75                     | 0.95             | 1.03                    | 0.98             |
| 150             | 13.19                     | 0.98             | 1.01                    | 1.07             |
| 500             | 16.01                     | 0.96             | 1.01                    | 1.02             |
| 100             | 13.44                     | 1.04             | 1.03                    | 0.83             |
| 200             | 13.81                     | 1.01             | 0.96                    | 1.04             |
|                 | <b>Average difference</b> | <b>-1.57</b>     | <b>1.91</b>             | <b>-2.35</b>     |
|                 | <i>Average CV</i>         | <i>1.1 ± 1.0</i> | <i>1.1 ± 1.0</i>        | <i>1.1 ± 1.0</i> |
|                 | <i>Min CV</i>             | <i>0.04</i>      | <i>0.04</i>             | <i>0.04</i>      |
|                 | <i>Max CV</i>             | <i>3.40</i>      | <i>3.40</i>             | <i>3.40</i>      |

**Table A6** Differences in phosphate concentrations as a function of the interval between the time samples were collected and preserved and the time they were analysed: Clf = chloroform, HgCl<sub>2</sub> = mercuric chloride, Frozen = -20°C. Values in table are presented as the relative difference between samples analysed after 2 months and 4 months for each preservative method, i.e. for Clf a value of 0.92 indicates that nitrate concentrations in 4 month old samples were 8% lower than 2 month old samples. Averages are calculated from the individual samples and presented as + or – percentages to indicate if a particular treatment exhibits the tendency of being higher or lower following increased storage time. CV is coefficient of variation, i.e. standard deviation / mean (duplicate measurements). Average CV is the average co-efficient of variation for duplicate measurements, Min CV and Max CV are minimum and maximum coefficients of variation. CV was determined from all of the samples included in the preservation comparison (n=30). Note, it is technically incorrect to determine CV from duplicate measurements, but analytical replicates exist as duplicates. CV therefore provides an approximation for the analytical precision of measurements that should be compared with the relative differences between treatments.

| <b>Phosphate</b> |                           | <b>Time</b>      |                         |                  |
|------------------|---------------------------|------------------|-------------------------|------------------|
| <b>Depth</b>     | <b>Nitrate</b>            | <b>Clf</b>       | <b>HgCl<sub>2</sub></b> | <b>Frozen</b>    |
| 100              | 14.75                     | 0.96             | 0.94                    | 0.92             |
| 150              | 13.19                     | 0.92             | 0.90                    | 0.93             |
| 500              | 16.01                     | 0.98             | 0.97                    | 0.95             |
| 100              | 13.44                     | 0.90             | 0.93                    | 0.87             |
| 200              | 13.81                     | 0.92             | 0.95                    | 0.92             |
|                  | <b>Average difference</b> | <b>-6.12</b>     | <b>21150.00</b>         | <b>1334.89</b>   |
|                  | <i>Average CV</i>         | <i>0.5 ± 0.3</i> | <i>0.5 ± 0.3</i>        | <i>0.5 ± 0.3</i> |
|                  | <i>Min CV</i>             | <i>0.08</i>      | <i>0.08</i>             | <i>0.08</i>      |
|                  | <i>Max CV</i>             | <i>1.2</i>       | <i>1.2</i>              | <i>1.2</i>       |

